Universitat Politècnica de Catalunya
Departament de Matemàtica Aplicada I

Dynamical Analysis of Lower Abdominal Wall in the Human Inguinal Hernia

PhD. Thesis by: **Gerard Fortuny Anguera**

Departament d'Enginyeria Informàtica i Matemàtiques
Universitat Rovira i Virgili

Advisor: **Antonio Susín Sánchez**

Memòria presentada per a aspirar al grau de Doctor en Matemàtiques per la Universitat Politècnica de Catalunya.

Programa de doctorat de Matemàtica Aplicada

Certifico que la present memòria ha estat realitzada per en Gerard Fortuny Anguera i dirigida per mi.

Barcelona, 16 de Febrer de 2009

Dr. Antonio Susín Sánchez

A Susanna

Contents

Acknowledgements

En primer lloc vull agraïr a en Toni Susín la extremada paciència que ha demostrat al llarg de tot aquest temps, on els seus coneixemets i la seva empenta han estat essencials per dur a terme aquest treball. En segon lloc també vull donar les gràcies a en Manuel López Cano, que sens dubte ha estat una peça essencial durant tot el procès de realització d'aquesta tesi.

Abstract

This PhD thesis aims to build a numerical simulator of the inferior abdominal wall, in order to determine the genesis and causes of the inguinal hernia. Thus, a model with real data on the region of human body (properly discretized) has been built that reproduces the dynamic properties of the various elements of the region allowing the simulation of the moment at which the hernia occurs.

Muscular simulation in general, has became a secondary subjec regarding numerical simulation, because on many occasions the interest has been concentrated in the general properties of the muscle (so that the muscle is considered a single element) and not in a detailed study of each of the parts of the muscle. The field where simulation has possibly been more productive is the cardiac simulation because of the constant interest in creating models of the cardiac muscle and it is for this reason that the only detailed models that exist are those related to the cardiac muscle.

The muscular fibre contraction was simulated using the Hill-Maxwell rehologic model presented by J. Bestel [10] which it regulates the contraction and recovery by means of potential activation function $u(t)$. This model is the first dynamic model in dimension one of a microscopic muscle level.

Currently, there is much varying conjecture regarding the causes of hernias, despite this however, a detailed study of their genesis, has not been possible. This is because on the one hand, it is impossible to catch the moment in which a hernia is generated, and, on the other, there is a lack of sufficiently detailed models of the muscles involved.

We present a dynamic model of the inferior abdominal wall with the active elements (the muscles) and the passive elements (fascias, ligaments and other tissues), so that a study can be made of the various physical and chemical aspects that generate hernias. The model reproduces the real dynamic of the area, as A. Keith and W.J. Lytle conjectured at the beginning of the past century and commonly accepted by surgery community.

This is the first model which reproduces the real dynamic in the inguinal area, so that we can

prove the existence of the two defence mechanisms (the shutter mechanism and the sphincter mechanism in the inguinal ring). With this muscular contraction model we can study several parameters that have an important role in the inguinal hernia genesis and we can do an accurate study about risk elements in the hernia inguinal. This parameters (Young's modulus, Poison's coefficient or intraabdominal pressure, for instance) have an hypothetical and no proved effect in the genesis of inguinal hernias. This work, evaluate the real effect of several parameters in the lineal model and propose a non linear model for the muscular simulation.

Part I

Contents

Chapter 1

Introduction

The etiology of adult inguinal hernias seems to be based on the loss of structural integrity and the mechanical function of the tissue elements of the inguinal region [23]. This can be justified at a molecular and cellular level (abnormal metabolism of the collagenous [63], it changes in the function of the tissue fibroblasts within weaves submissive tensional forces [75]) and at macroscopic level with a malfunction of the anatomical inguinal protection against hernia [2].

The anatomical region where inguinal hernias occur (figure 1.7) is the miopectineous orifice [24], which is divided by the inguinal ligament into an upper area and a lower area. In the upper area or suprainguinal space, the shutter mechanism [40] and the sphincter of the internal inguinal ring [45], are principal anatomical protection mechanisms against hernia. Different anatomical variations in the structures responsible for these mechanisms have been documented (mainly of the shutter mechanism), and these variations, can facilitate the appearance of an hernia. The origin of the internal oblique muscle in the inguinal ligament away from the pubic tubercle and the lack of cover of the internal inguinal ring by the inferior fibres of this inguinal muscle have been suggested as being involved in the genesis of hernias [4]. Different degrees of atrophy of the internal oblique muscle in the inguinal region and its relation to direct inguinal hernias [88] and other factors that include a low pubic arc [43] and an increase in the size of the Hessert's triangle (suprainguinal space) [1]. Although the defence mechanisms are based on the operation of anatomical structures (basically the internal oblique muscle) little is known about the way they really work since all the conclusions on their movement and function have been extracted from static studies. At the moment there are some mathematical models that explain the dynamic behaviour of the muscle with applications in biomechanics, biomedicine or simulation of the movement in general. They are, on the one hand, models that explain the movement of the muscle as a whole and in general without considering the influence of the microscopic level on their contraction and dynamics([85], [77] and [52]), and on the other hand,

models that study the muscular movement at cellular level, such as Hill-Maxwell proposed by J. Bestel [10].

1.1 Motivation

The collaboration between Dr. Antonio Susín, from the Department Applied Mathematics I at Polytecnic University of Catalonia (UPC) and Dr. Manuel Lopez Cano from the Abdominal Wall Unit of the General Surgery Service at the Vall d'Hebron University Hospital of the Autonomous University of Barcelona (UAB) , starts in 2003 with the objective of building a dynamic model of inguinal hernias. Initially this collaboration had docent aspects, as a learning tool for anatomy and surgery training. Initially this collaboration was two fold, a teaching tool for new surgeons for learning anatomy and surgery training, and a research tool for simulation of the dynamic behavior of this region. An initial part of this project was carried out by Carlos Encinas, Javier Rodriguez, Antonio Susín and Manuel Lopez Cano [44] and it led to a dynamic model of the region using a mass-spring method and real anatomic data of the region. The dynamic simulation of the inguinal region to explain the genesis of human hernias, is the main goal of my research and I present in this document the results obtained in this direction.

The inguinal hernia pathology is essentially masculine (dominant in men, 19:1). It is very common at level I hospitals (local hospital) , it represent 46% of interventions, at level II hospital (regional hospital) of 40% and at level III hospital (state hospital) 32% of the interventions. As an example the Vall d'Hebron University Hospital makes 700 to 800 operations a year and around the world some 20 million [1] interventions are made annually. The inguinal hernias increase in prevalence according to age: up to 25 years 24%, up to 65 years 40% and up to 70 47%.

1.2 Objectives

The main objective of this research project is to simulate numerically the human lower abdominal wall, taking into account the different role played by the various active and passive parts. The model should be quite accurate for both to reproduce the natural movement of the various parts of the region, so as to obtain specific answers regarding which physical or chemical may be involved in the genesis of inguinal hernias. Thus the model should reproduce in sufficient detail the various elements in the region, their properties must be dynamic and responsive to changing conditions.

[1] Kingsnorth A., J. World Surg 2005

This model must be able to replicate to the maximum extent the dynamic properties of the active parts (the muscles), because of that, why we will need to generate reticular structures with a distinctive direction that will actually correspond to the direction of the muscle fibre. Being the other directions just a passive deformation elements, it seems natural to simulate first only the the one dimensional direction associated to the muscle fiber. The dynamics of the 3D elements must be controlled for this main direction.

Likewise, the precision in the simulation of the muscular behavior must be related with two factors: the geometrical and the dynamic ones. Therefore, spatial discretization and numerical algorithms must play a central role in this project.

For building a coherent geometrical model, real data from the region is needed. On the one hand, we will have data from measurements of the elements of the abdominal wall, from which we can set our initial conditions, on the other hand have actual hernia data that we will use for validation of our results ([54], [82], [16], [59]).

One of the main objectives that we can afford with an accurate model is to confirm or reject hypotheses about the current dynamic phenomena taking place in this area such as *the shutter mechanism* (see subsection 1.5.4) which are still the subject of conjecture. Our results are the first simulation results that confirms the importance of the shutter mechanism and we are able to relate biochemical and mechanical factors that are accepted as the main factors involved in the genesis of inguinal hernias.

1.3 Principles for Simulation

In this section we present the first fixed image of the area whose dynamics we aim to study. This is intended to provide information rather than be a rigorous exposition of the topic. However, first, we must briefly outline the problem at hand, describe the complexity of its formulation and discuss what repercussions there may be from studying it.

The section is divided into three sections. These reflect the topics that need to be covered in greater detail when we begin our study of the simulated region:

- **The muscle**
- **The inferior abdominal wall**
- **Inguinal hernias**

For a detailed and precise understanding of the muscles of the human body (their structure,

their composition, and how they function at both the cellular level and at their natural size), and specifically the muscles of the inferior abdominal wall, the reader is referred to the the bibliography [8], [9], [21], [27] and [42]. For a full and accurate study of hernias in general and inguinal hernias in particular, also see the bibliography [1], [2], [4], [23], [24], [40], [43], [45], [54], [63], [82] and [88].

1.3.1 The Muscles

The word "muscle" derives from the Latin diminutive term musculus—mus (mouse) and culus (small)—because the Romans thought that the shape of the muscle when contracted resembled a small mouse. Muscles, which are the set of contractile organs in humans and other animals, are made up of muscular tissue.

Muscles can be divided into three types:

- **The skeletal muscle**, also called voluntary muscles, are striated and controlled voluntarily. They are in direct contact with some part of the skeleton by means of tendons.
- **The smooth muscle** are not striated and are controlled involuntarily. Examples of these muscles are those of the walls of the digestive system and those of the urinary system, blood vessels and uterus (for instance).
- **The cardiac muscle** are striated and are not controlled voluntarily.

Since the inguinal region is made up of only skeletal muscles, in this study we will focus on this type of muscle.

Skeletal muscles are in contact with other tissues which, though dynamically passive, deserve a mention. On one hand, they are linked to bones via highly rigid tendons. On the other hand, they are surrounded by fascia—tissues that are only slightly rigid (or not rigid at all) located between the muscles or between the muscles and other organs of the body (figure 1.1).

The functional and structural unit of the muscle is generally the muscular fibre (figure 1.2), which is grouped in fascicles and forms the muscular mass. In this context, provided that the muscles studied here are skeletal muscles, they are made up of a large number of muscular fibres (270,000 in the case of the femoral biceps). The muscular fiber is grouped in fascicles (or fasciculus) that constituted all the muscular mass.

The muscle is a tissue made up of fusiform cells surrounded by the sarcolema, which is the cellular membrane (figure 1.3 (a)) and by the sarcoplasma that it contains the cell nucleus. The

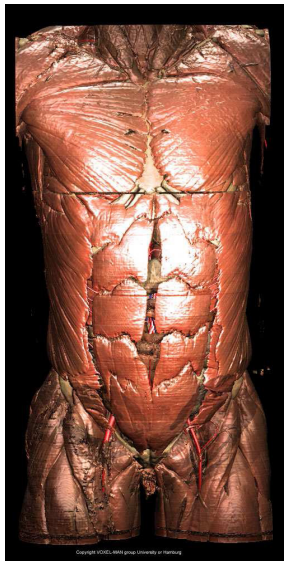

Figure 1.1: The muscular system

Figure 1.2: Picture of the skeletal muscle

sarcolema also receives the nerve ends, which send out the order to activate the muscle. The sarcoplasma is made up of myofibres. Myofibres comprise **sarcomeras**, which are the action units for skeletal muscles. Being grouped together, the sarcomeres clearly delimit a series of easily identifiable bands or lines (figure 1.3 (b)). The Z line is the contact region between two series of sarcomeres (figure 1.3 (b)). The A band comprises the set of proteins responsible for contraction. The M line and the H band are the border between the two regions of the sarcomere in which the proteins responsible for contraction are located. These bands are responsible for the striated appearance of the muscles.

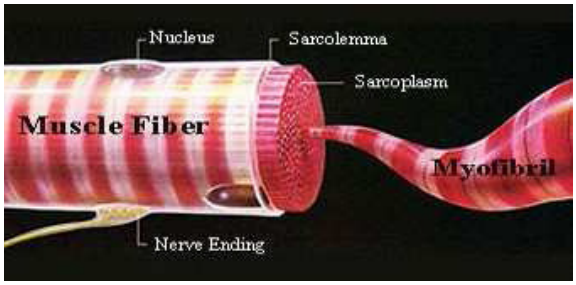

(a) Muscular fiber

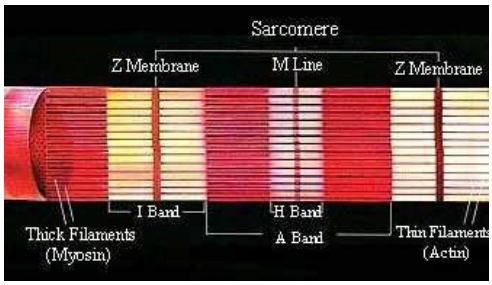

(b) Sarcomera distribution

Figure 1.3: Muscular structure

The main property of the complex protein framework of fibres called actin and myosin is their contractibility, i.e. their ability to shorten when subjected to a chemical or electrical stimulus. These proteins (figure 1.4(a)) are helicoidal and, when activated, they bind and rotate, thus shortening the fibre. Just one movement produces several processes of binding and unbinding of the actin-myosin fibres. Such processes are generically called **activation potential**.

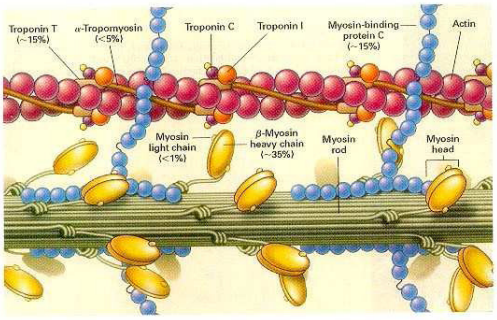

(a) Picture of actin and myosin

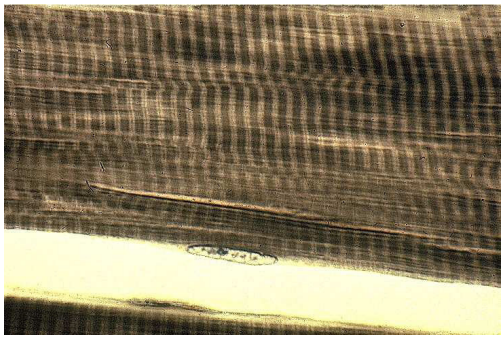

(b) Sarcomeras with a cellular nucleus

Figure 1.4: Muscular composition

1.3.2 Muscular Activity: Activation Potential

Activation potential refers to the intracellular changes that lead to variation in the concentration of calcium ions. Muscular movement is produced at the intracellular level when the sarcoplasmic reticulum causes a change in the concentration of calcium inside the sarcomeres. Relaxation occurs when this concentration is reduced, mainly because the sarcoplasma re-absorbs the calcium and then eliminates it by diffusion. This process is called the *sliding filaments mechanism* (figure 1.5). The following stages have been reported for the sliding filaments:

- **Initial position**. At the beginning of the cycle a layer of myosin binds firmly to an actin

filament in a rigour configuration (so called because it is responsible for *rigor mortis*) and the muscle quickly contracts until a molecule of ATP is attached.

- **Projection**. A molecule of ATP links to the notch behind the layer (i.e. on the furthest side from the actin filament) and immediately causes a slight change in the configuration of the domains that comprise the actin binding site. This reduces the affinity of the layer for *the actin* and allows the actin to move along the filament.

- **Power-stroke**. The notch closes tightly around the adenosinetriphosphate (ATP) molecule. This leads to a considerable change in the layer, which displaces roughly five nanometres along the filament. The ATP is hydrolysed only with the adenosinediphosphate (ADP) and the inorganic phosphate.

- **Force-generation**. A slight attachment of the myosin layer launches the actin of the inorganic phosphate produced by hydrolysis of the ATP to another site of the filament and the layer attaches to the actin. This launch causes the force-generation of the energy, during which the layer recovers its original conformation. During the launch, movement is activated, the layer loses its ADP and a new cycle is begun.

- **Union**. At the end of the cycle the myosin layer again binds firmly to the actin filament in a rigour configuration. Note that the layer moves to a new position with respect to the actin filament.

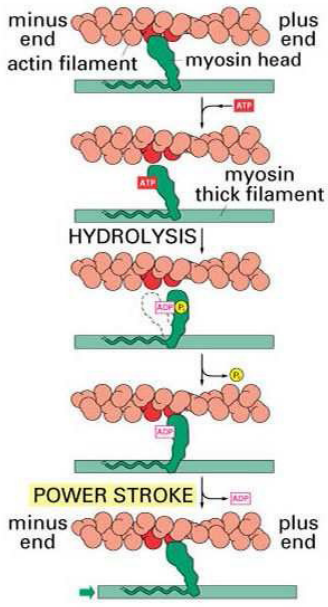

Figure 1.5: Cycle of sliding filaments by muscular fibre

The change in the ATP concentration of a muscle cell, and therefore the contraction of the muscle, leads spontaneously to the contraction of adjacent cells. This means that not all muscle cells need to be connected by nerves.

This sliding filament mechanism is common to all three muscle types (skeletal, smooth and cardiac) since it corresponds to the contractible unit, i.e. the sarcomere. The difference between the activities of the various types of muscle depends on the distribution of the sarcomeres and the intensity of the activation potential.

1.3.3 Physical Properties of Muscles

Here we focus on the physical properties that are common to all types of muscles or that are specific to skeletal muscles. We should bear in mind that while some physical properties are macroscopic and others are microscopic, all are explained on a microscopic level.

Contractibility

Three types of muscular contractions are reported:

Isometric. The muscle develops strength but does not undergo changes in length.

Isotopic. The muscle develops constant strength over time.

Auxotonic. The muscle develops variable strength and this one changes simultaneously with his length.

Keeping the contraction active always requires changes in the concentration of calcium ATP. This concentration increases the intensity of the contraction.

In the case of skeletal muscles in general and those of the inguinal region in particular, it is generally agreed that contraction is auxotonic.

Isovolumetry

It is widely agreed that, despite experiencing changes in shape and position, muscles retain their overall volume throughout contraction.

Viscoelasticity

During the relaxation process after contraction, muscles can autonomously recover their initial position. This property, called viscoelasticity, is different both from elasticity, in which a strained material does not recover its initial position autonomously, and from viscosity, which is the measure of a strained material's resistance to flow.

Unlike purely elastic substances, a viscoelastic substance has an elastic component and a viscous component. The viscosity of a viscoelastic substance gives the substance a strain rate dependent on time. Purely elastic materials do not dissipate energy (heat) when a load is applied, then removed. However, a viscoelastic substance loses energy when a load is applied, then removed. Hysteresis is observed in the stress-strain curve, with the area of the loop being equal to the energy lost during the loading cycle. A system with hysteresis can be summarised as a system that may be in any number of states, independent of the inputs to the system.

Since viscosity is the resistance to thermally activated plastic deformation, a viscous material will lose energy through a loading cycle. Plastic deformation results in lost energy, which is uncharacteristic of a purely elastic material's reaction to a loading cycle

Force vs Length

Starling's Law states that, electrical stimulation being equal, greater stretching of the muscular fibre produces a greater response by the strength developed. As is expected, however, stretching of the muscular fibre is limited, i.e. though a muscle receives an electrical impulse, its tension may not increase. This phenomenon can be explained through the microscope: while the force developed by a muscle depends on the number of actin-myosin bridges in the sarcomere, an over-stretched sarcomere does not have an effective response. The figure 1.6, shows the function determined experimentally and plots the length of the sarcomere against the percentage of tension compared to its maximum. Here we can see the role played by the force developed at the moment of activation.

Anisotropy

Anisotropy is the opposite of isotropy and means that a material's physical behaviour depends on the direction studied. Sarcomeres, and therefore muscle fibres, have two essentially different behaviours. One is in the direction in which the sarcomeres are arranged along the microfibres, which exert the contraction. On the other hand, the direction that is orthogonal to the fibres is

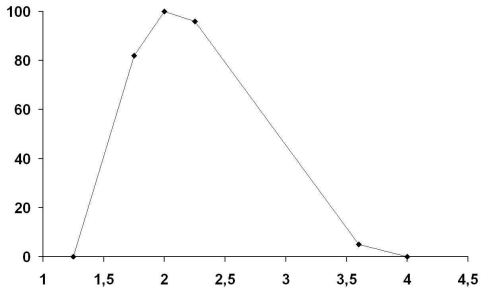

Figure 1.6: Stress versus length. In the horizontal axis, we have values of sarcomera's lenght in μm. In vertical axis, we have the percentage over maximal stress.

usually considered connective tissue and, therefore, passive to dynamic effects. For this reason muscles are considered anisotropic.

1.4 The Lower Abdominal Wall

The abdomen is located between the thorax and the pelvis. In mammals the abdomen contains the abdominal cavity, which is separated from the thorax by the diaphragm. Almost all the viscera in the cavity belong to the digestive system, though there are also other organs such as the kidneys and the suprarenal glands. Two thirds of the pressure exerted by these organs is supported by the front of the abdomen. The other third is supported by the back of the abdomen, which is made up of the lumbar vertebrae, the sacrum, the iliac bones and the back muscles. The abdominal cavity is lined with a dynamically passive membrane called the peritoneum that separates the organs.

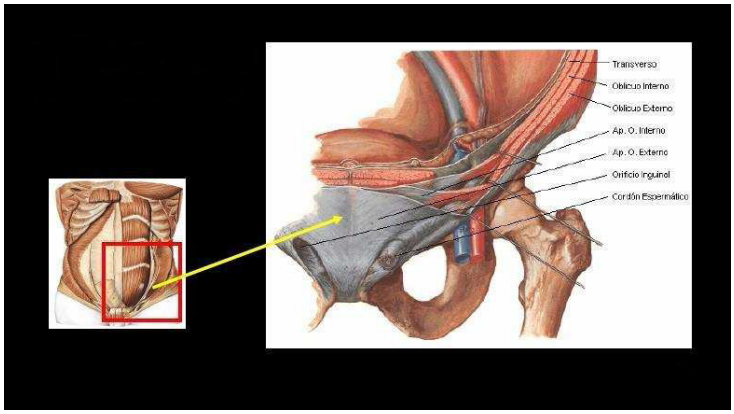

Figure 1.7: Picture of abdominal area

The ventral abdominal muscles lead to the lateral and medial walls of the abdominal cavity

and contain the last intercostal nerves and first lumbar nerves (ventral branches). These muscles are important because they reach until the abdominal cavity. There are four muscles in this region: the external oblique muscle, the internal oblique muscle, the transverse abdominal muscle, and the straight abdominal muscle. Each of these muscles is superimposed on the other. They originate in the dorsal region and are inserted ventrally via aponeurosis. The oblique muscles and the transverse muscle finish at the alba line, the fibrous tissue that runs from the sternum to the pubis and that reaches the abdominal cavity.

- **The rectus abdominal muscle** is surrounded by aponeurosis of the other three muscles (the oblique muscles and the transverse muscle). It originates in the lateral faces of the first few ribs and is inserted into the pubis. It is surrounded by aponeurosis of the cabal muscles. The fibres of the muscle run in the cranial-caudal direction.
- **The external oblique muscle** originates in the lateral faces of the ribs and is inserted into the linea alba. Its fibres run in the caudal-ventral direction.
- **The internal oblique muscle** originates at the thoracolumbar fascia, in the coxal tuberosity of the ilium and the transverse apophysis of the lumbar vertebrae. It is inserted into the linea alba. Its fibres run in the cranial-caudal direction.
- **The transverse abdominal muscle**, originates at the thoracolumbar fascia and the transverse apophysis of the lumbar vertebrae and is inserted into the alba line. Its fibres run in the dorsal-ventral direction.

The main dynamic functions of the abdominal muscles involve:

- Support for the abdominal viscera

- Miction.

- Defecation.

1.5 The Inguinal Hernias

Generally we can say that a hernia is a protrusion of an organ or tissue outside its usual body cavity. Hernias usually develop in the abdomen when a weakness in the abdominal wall creates an opening (normally in the myopectineal orifice) through which the protrusion appears. The inguinal region is the lower ventral part of the abdomen, where the abdomen is in contact with the pelvis. The groin is a naturally weak area of the abdominal wall and the most common

location for a hernia. Inguinal hernias affect both sexes and all ages but they are more likely to affect men (prevalence of 19:1). Estimated frequency is 3%, which means that they are an economic problem as well as a medical one.

Figure 1.8: Image of an inguinal direct hernia

1.5.1 Anatomy of the Myopectineal Orifice

The myopectineal orifice is approximately 3.75 cm long (figure 1.9). It is an oblique opening in the abdominal wall between the internal and external inguinal rings and is slightly higher and parallel to the femoral arch. The anterior part is made up of aponeurosis of the external oblique muscle and is reinforced towards the outside in front of the internal ring by insertion of the internal oblique muscle. Its roof comprises the arched fibres of the internal oblique and transverse muscles. Entering the canal between these two muscles is the small abdominogenital nerve. The conjoined tendon makes up the main part of the posterior wall of the canal behind the external inguinal ring. In front of the tendon is the portion reflects of the crural arch and behind it is the fascia transversalis, which makes up the rest of the posterior wall. The fascia transversalis provides the lower limit of the orifice by joining the femoral arch but some of the internal portion of the lower part is made up of the pectineal portion of the femoral arch, or inguinal ligament. Passing through the canal are: the spermatic cord or round uterus ligament, which tangle around themselves and run from the abdominal wall; the internal spermatic fascia or fibrous tunic, which originate in the internal ring of the fascia transversalis; the fascia cremasterica or muscular tunic, which derives from the conjoined tendon, and the external spermatic fascia, or cellulose tunic, which originates from the aponeurosis of the external oblique muscle at the external ring. In the fascia cremasterica, on the spermatic cord between the internal oblique and the spine of the pubis, are the fascicles of the cremaster. These receive their innervation from the genital branch of the genitocrural nerve.

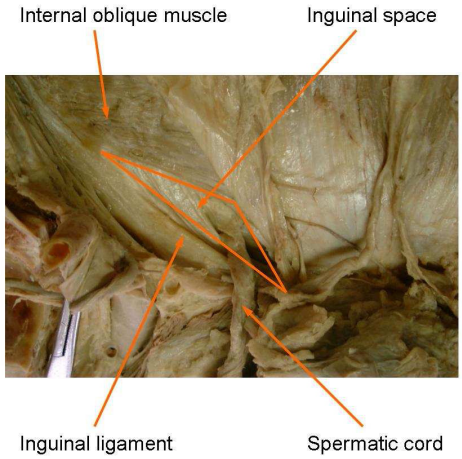

Figure 1.9: Miopectineus orifice and Hessert's triangle (in orange)

1.5.2 The Herniation

An inguinal hernia carries parietal peritoneum to the inguinal canal and protrudes through the external inguinal ring. The superficial tumefaction is therefore invariably covered in skin, both layers of the superficial aponeurosis, and the spermatic fascia. The tumefaction can reach until the scrotum. Inguinal hernias are defined according to the site of protrusion from the abdominal cavity. An oblique inguinal hernia enters the internal inguinal ring in the external inguinal fascia outside the epigastric artery and follows the length of the inguinal canal in front of the spermatic cord, with which it shares aponeurosis. A direct inguinal hernia enters the canal behind the spermatic cord and enters the epigastric artery through the medial or internal inguinal fossa, i.e. from outside or inside the fibrous cord of the obliterated umbilical artery. Oblique hernias are lined with aponeurosis from the fascia transversalis and are independent of the internal spermatic fascia that surrounds the cord. Being outside the conjoined tendon, the envelopes, which are tightly bound to the external spermatic fascia, are independent of those of the spermatic cord.

1.5.3 Anatomy of the Inguinal Hernia

The sac of an indirect hernia is actually a dilated persistent vaginal process. It passes through the deep ring and is located inside the spermatic cord, continuing along the indirect path of the cord as far as the scrotum. In the deep ring the sac occupies the antero-external side of the cord. It is often accompanied by preperitoneal fat and is known as lipoma of the cord, though the fat is not a tumor. Lipomas of the spermatic cord can look like the actual cord.

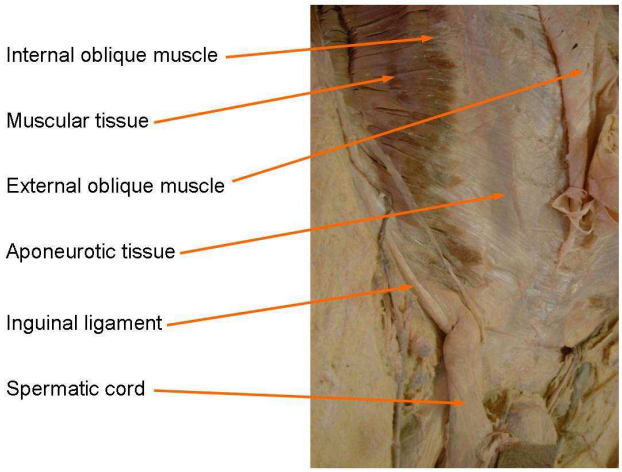

Figure 1.10: Elements more distinguished from the inguinal region

The sac of an indirect hernia is filled if it descends as far as the testicles and fills the side of the scrotum and is unfilled otherwise. If the vaginal process remains completely open, the testicle is located within the sac. Such cases, known as congenital hernias or communicating hydroceles, are common in infants but rare in adults.

Retroperitoneal organs such as the sigmoid colon, the caecum and the urethras can slide inside an indirect sac and become part of its wall. These organs are prone to damage during a hernioplasty. Hernias caused by sliding are often large but partially irreducible.

The sacs of a direct inguinal hernia originate from the inferior part of the inguinal canal, i.e. the Hessert triangle. They protrude directly and are repressed by aponeurosis of the external oblique muscle. They rarely grow large enough to force a path through the superficial ring and descend to the scrotum. Direct hernias are usually diffuse and cover the whole of the inferior part of the inguinal canal. Discrete hernias, which are less frequent, have small orifices and diverticular sacs. Direct inguinal hernias also originate laterally to the lower epigastric arteries and appear either through the deep ring or interstitially by sliding in zones of musculoadipose atrophy of the muscles that seal the deep ring. This type of direct inguinal hernia is rare and such hernias are generally wrongly classified as indirect extrafunicular hernias or indirect interstitial hernias. They do not follow the spermatic cord and grow interparietally. The lower gastric arteries are not an anatomical limit but they always represent the difference between a direct and an indirect hernia. The bladder is often a component because of the sliding of a direct hernia sac.

Inguinal hernias may be congenital or they may be acquired. In either case there is usually a familial antecedent. Most of these hernias, therefore, are transmitted genetically. All indirect inguinal hernias are congenital and result from the persistence of the vaginal process at birth.

80% of newborns and 50% of one-year-old infants suffer from a persistent vaginal process. Closure continues until the child is two years old. In adults the frequency of this condition is 20%.

The fact that a hernia is possible, however, does not mean that it will necessarily occur. There must be other factors causing incapacity of the transversal fascia to retain the visceral sac in the myopectineal orifice. An erection can lead to herniation through stretching and exposure of the groin. When a hernia occurs, gravity may cause the intestines to fall onto the hernial sac. Muscular deficiency also contributes to herniation. Congenital or acquired insufficiency of the internal oblique abdominal muscles in the groin exposes the deep ring and the lower part of the inguinal canal to problems due to intraabdominal pressure. Destruction of the conjunctive tissue caused by the physical force of such pressure, smoking, age, disorders of the conjunctive tissue as well as systemic problems reduce the strength of aponeurosis and the fascia transversalis. Fractured elastic fibres and alterations in the structure, quantity and metabolism of collagen have also been demonstrated in the structures of conjunctive tissue in hernia patients.

Several factors are sometimes important. Abdominal distension and a constant increase in intraabdominal pressure due to ascitis and peritoneal dialysis can damage the myopectineal orifice and lead to dilatation of a persistent vaginal process. Inguinal hernias of all types occur equally in sedentary and physically active males. Energetic physical activity is not the cause of inguinal hernias, though an intense effort can be a predisposing and precipitating factor.

1.5.4 Dynamic Mechanisms of the Inguinal Area

Two dynamic mechanisms of the inguinal region are generally accepted as influencing the onset of inguinal hernias: the shutter mechanism and the sphincter mechanism of the deep inguinal ring.

The *shutter mechanism* was first reported by A. Keith in 1923 [40] and described in further detail by W.J. Lytle [45] in 1945. It is based on the fact that the contraction of the internal oblique and transverse abdominal muscles enables their edges to approach the inguinal ligament and iliopubic tract(Keith and Skandalakis [71] in 1989; Nyhus et al.[55] in 1991; Abdallal and Mittelstaedt [1] in 2001), thus reinforcing the posterior wall of the inguinal canal. Abdallal and Mittelstaedt [71] observed that the high insertion of the internal oblique and transverse abdominal muscles in the sheath of the straight abdominal muscles leads to a broad inguinal triangle (top areas to 8,97 cm^2) in patients with inguinal hernias. They supported this observation by considering that in the case of broad triangles, the approximation of the lower fibres of the internal oblique and transverse abdominal muscles to the inguinal ligament, i.e. Keith's shutter mechanism, would not be sufficient to completely close the triangle, and inguinal hernias would therefore be more easily generated.

The *sphincter mechanism of the deep inguinal ring* is based on the fact that the crura of the deep inguinal ring are attached to the transverse abdominal muscle (Lytle [45] in 1945; Skandalakis [71] et al. in 1989; Nyhus et al. [55] in 1992; Menck and Lierse [50] in 1991; Pans et al. [59] in 1997). Contraction of this muscle therefore generates two actions: firstly, the crura get closer together, thus reducing the diameter of the deep inguinal ring; secondly, sliding occurs upwards and outwards from the orifice. MacGregor (1929) reported that this mechanism fails when preperitoneal cellulose-adipose tissue is introduced into the deep inguinal ring.

Other structures said to be involved in protection mechanisms for the inguinal region are the internal crus of the deep inguinal ring, which partly delimits the Hessert triangle, and the spermatic cord (or round ligament in women), which has a covering effect on the deep inguinal ring.

While the dynamic mechanisms have been documented and are generally accepted, they have not yet been confirmed. One aim of such studies should therefore be to confirm these mechanisms.

1.6 Conclusions

So far we have discussed the main physical properties of muscles, which are mainly responsible for the dynamics of the human body. Determining their properties and dynamics at the intracellular level should help to establish a model that reflects reality.

In this Chapter we have also described the nature, components and functions of the region we intend to simulate. Many elements play different active and passive roles in the origin of hernias. Each of these elements should be treated according to its particular properties and characteristics.

Chapter 2

Muscular Simulation

In this Chapter we present the bases for the numerical modelling of skeletal muscle, including Huxley's sliding filament model, the actin-myosin mechanism of muscular contraction modelled by Hill, and Zahalak's method of moments. We will also present several characteristics of J. Bestel's dynamic model of contractile elements.

2.1 Muscular Activity Models

Several studies of muscular simulation have been conducted. However, most of these have not been specific enough to meet their objectives. One of the most relevant approaches is the widely used Zajac's model [85] which treats the muscle as a single unit (figure 2.1 (a)). Another is Van de Linde's model [79] which uses a coarse discretization of the muscle. Another very common model is the mass-spring model, though this does not reproduce many of the muscle's physical properties. The most accurate model of muscular activity is surely **Huxley's sliding filaments theory**, which has been further developed and is now widely accepted for muscular simulations.

2.1.1 Huxley's Sliding Filaments Theory

A. F. Huxley's sliding filament theory was originally presented in [39]. Huxley considered a mid-sarcomere and named A as the binding site of actin and M as the head of myosin (figure 2.2), due to temperature, M oscillates from one band to another from the equilibrium position O, due to temperature. We denote by $\tilde{x}$ the distance from O to the closer position A. Huxley assumes that $\tilde{x}$ is strictly positive and lower to the maxim elongation h, therefore $\tilde{x} \in [0, h]$. Huxley proposed two functions of $\tilde{x}$, the f function that indicates the number of actin-myosin bridges that are

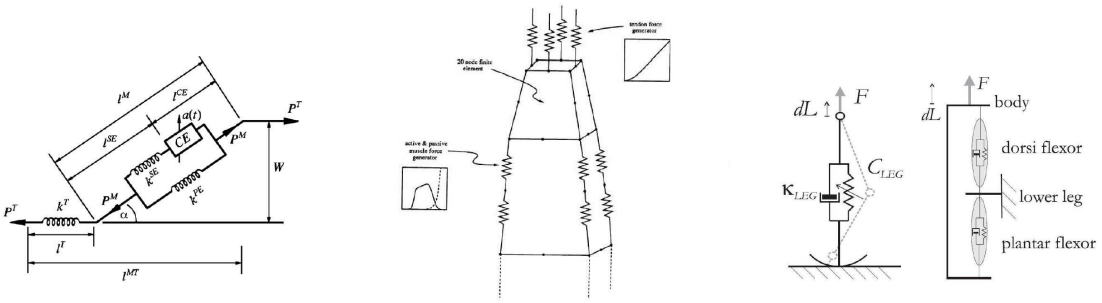

(a) Zajac's model (b) Chen's model (c) Van del Linde's model

Figure 2.1: Different muscle-tendon models

created per second and the g function that indicates the number of actin-myosin bridges that are destroyed per second (in figure 2.3 we can see an outline plot of these functions). We assume that the OM unions are elastic, so when a AM bridge is created the OM's force is produced in A. He also denotes by s the length of the sarcomere and $v = \dot{s}$ is the sliding velocity for the filaments. Huxley obtains a mathematical formula for the number of activated actin-myosin bridges as a function of n, to give the number of AM bridges that are activated, where now x, is the average of all $\tilde{x}$ what have been defined:

$$\frac{dn(x,t)}{dt} = \frac{\partial n}{\partial t} + \frac{\partial n}{\partial x}\frac{\partial x}{\partial t} = f(x) \cdot [N - n(x,t)] - g(x) \cdot n(x,t)$$

where $\dfrac{\partial x}{\partial t} = v = \dot{s}$ is the sliding velocity and n is the number of bridges between 0 and the maximum number of possible of bridges N.

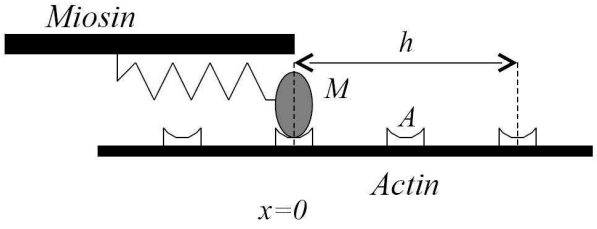

Figure 2.2: Scheme of sliding Huxley filaments

The functions f and g reflect the changes in the number of points. In fact, bridges are created and destroyed as the length increases. We can therefore assume that, as the bridges are renewed, the muscle will not achieve a state of *rigor*.

We can normalise the previous expression with $\xi = \frac{x}{h}$ and $\eta = \frac{s_0}{h}$, by considering s_0 to

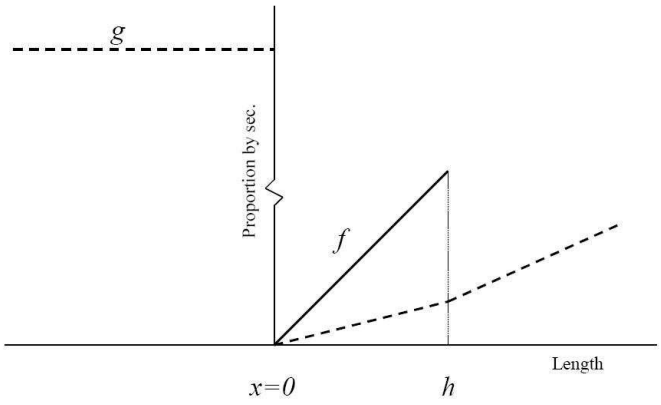

Figure 2.3: Functions f and g, it drives the number of bridges created and destroyed

be the length of the sarcomere of any reference state. Moreover, if we consider the strain of sarcomere ε_c we get $s = s_0\,(1+\varepsilon_c)$. Therefore, at time $t+\delta t$ the velocity will be $s_0\dot{\varepsilon}_c$ and we assume that there is a supplementary strain δx (if the filaments are rigid) which, in the second order, is approximated by $s_0\dot{\varepsilon}_c\delta t$. After normalising by h, interval $[\xi, \xi+\delta\xi]$ therefore becomes $\left[\xi+\eta\dot{\varepsilon}_c\delta t, \xi+\delta\xi+\eta\dot{\varepsilon}_c\delta t\right]$. Now, we are going to consider n as the proportion of bridges, a value between 0 and 1, so we can rewrite:

$$\dot{n} = \lim_{\delta t\to 0}\frac{1}{\delta t}\left(n\left(\xi+\eta\dot{\varepsilon}_c\delta t, t+\delta t\right) - n\left(\xi,t\right)\right) = \frac{\partial n}{\partial t} + \eta\dot{\varepsilon}_c\frac{\partial n}{\partial \xi}$$

and thus we can formulate the following Cauchy's problem:

$$\begin{cases} \dfrac{\partial n}{\partial t} + \eta\dot{\varepsilon}_c\dfrac{\partial n}{\partial \xi} = f(\xi,t)\left[1-n(\xi,t)\right] - g(\xi,t)n(\xi,t) \\ n(\xi,0) = n_0(\xi) \qquad\qquad \text{for all } \xi \end{cases}$$

where $\dot{\varepsilon}_c$ is a function of time and f and g are functions of two variables.

This is a first-order linear hyperbolic equation which, in a particular domain, provides the solution:

$$\forall t \geq 0 \qquad y(\xi,t) = \xi + \int_0^t \eta\dot{\varepsilon}_c(\tau)d\tau = \xi + \eta\left(\varepsilon_c(t) - \varepsilon_c(0)\right)$$

Now we can rewrite $N(\xi,t) = n(y(\xi,t),t)$ and we we obtain the following partial differential equation:

$$\begin{cases} \dot{N}(\xi,t) + [f(y(\xi,t),t) + g(y(\xi,t),t)]\, N(\xi,t) = f(y(\xi,t),t) \\ N(\xi,0) = n_0(\xi) \qquad\qquad\qquad\qquad \text{for all } \xi \end{cases}$$

2.2 Muscular Rehologic Model

For the full muscular model, we consider the binding of sarcomeres in a contractile element (EC) as in [12] since we assumed that the sarcomeres are arranged in series along the muscular fibre.

To obtain isometric strains we put another serial element (ES) mounted in series with EC (Hill model with two elements, figure 2.4): ES models a degree of internal freedom due to the strain of the fibre, which stretches when the EC contracts so the fibre remains at constant length.

We can also introduce a third element parallel to the EC (Voigt model) in parallel to the EC-ES (Maxwell model) which we shall call parallel element (EP) to this new resort. This new spring provides a force after a certain muscle length but does not respond to an external stimulus (figure 2.4). The latter two models are derived from of the Hill model.

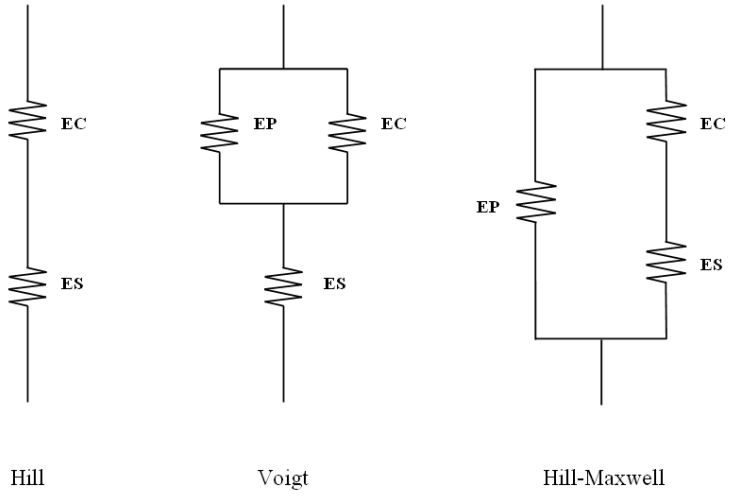

Figure 2.4: Muscular simulation models

Let us denote by l_c, l_s and l the lengths of the contractile element, series element and the complete fiber respectively, and consider l_{c_0}, l_{s_0} and l_0 the respective lengths for a rest reference state for the element contractile EC. We are going to define by ε_c, ε_s and ε the associated strains, therefore we have $l_c = l_{c_0}(1+\varepsilon_c)$, $l_s = l_{s_0}(1+\varepsilon_s)$ and $l = l_0(1+\varepsilon)$. In an analogous way let σ_c, σ_s, σ_p and σ be the stresses, the series element and the entire fiber respectively and let also be

k_c, k_s, k_p and k the rigidity for the same elements: contractible, the two series and the entire fiber respectively. I.Mirsky and W.W.Parmley in [51] studied and modeled the passive elements of the muscle. These premises were studied and accepted in [12].

Experimentally they found that the tension-strain properties of the passive elements were not linear and that the proposed models were of the type:

$$\frac{d\sigma}{d\varepsilon} = K_1\sigma + K_2$$

where K_1 and K_2 are two constants.

Besides the strain of EC, it is necessary to know the value of the chemical activation intensity and the rate of strain. As a consequence of the parallel assembly, the Hill-Maxwell model must satisfy the condition for the stress of the elements EC and EO, $\sigma_s = \sigma_c$ and the condition for the whole model $\sigma = \sigma_c + \sigma_p$.

Since the Hill-Voigt model requires the initial condition $\sigma_c = 0$, the flexibility of the model is limited. It is largely accepted [39] that the Hill-Maxwell model is simpler and more flexible since the isometry of the model means that we can use only the EP elements. In other fields (such as material mechanics) the Hill-Maxwell model is used because of its viscoelastic properties. We have also chosen the Hill-Maxwell model, since viscoelasticity is also a property we require for our model.

2.2.1 Mechanic Behavior for Actin-Miosin Bridges

Actin-myosin bridges play a leading role in the possible configurations of the sarcomeres (figure 2.5) and it is widely accepted that, as proposed in [39], their rigidity is linear.

With this premise, as well as a macroscopic view of the sarcomere and a statistic interpretation of Huxley's model, in [83] and [84], Zahalak calculated rigidity, strength and energy with moments of order 0, 1 and 2 for a sarcomere with:

$$M_p(t) = \int_{-\infty}^{+\infty} \xi^p n(\xi, t) d\xi \qquad \text{where} \qquad p = 0, 1, 2.$$

In the same study, Zahalak proposed the system of differential equations to verify the moments:

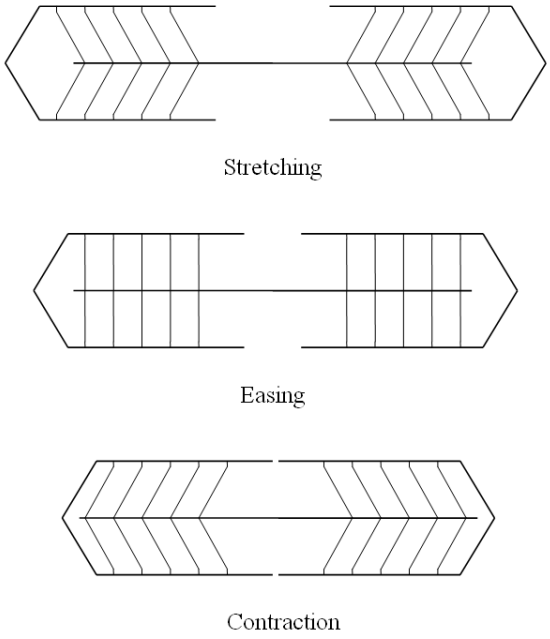

Figure 2.5: Scheme with the three positions that we are considering in the sarcomeres.

$$\begin{cases} \dfrac{dM_0}{dt} = b_0 - F_0 \\ \dfrac{dM_1}{dt} = b_1 - F_1 - v(t)M_0 \\ \dfrac{dM_2}{dt} = b_2 - F_2 - 2v(t)M_1 \end{cases} \tag{2.1}$$

where we have $p \in \{0, 1, 2\}$, $b_p = h^{p+1} \int_{-\infty}^{+\infty} \xi^p f(\xi) d\xi$ i $F_p = h^{p+1} \int_{-\infty}^{+\infty} \xi^p \left[f(\xi) + g(\xi) \right] n(\xi, t) d\xi$. This author proposed a Gaussian density in ξ and the F_p are therefore written as explicit functions in M_p. Therefore, given the initial conditions for M_p, rigidity, strength and energy for a distribution of bridges can be written as:

$$n(\xi, t) = \frac{M_0(t)}{\sigma(t)\sqrt{2\pi}} \exp\left(-\frac{\left[\xi - \mu_n(t)\right]^2}{2\sigma_n^2(t)} \right)$$

on $\mu_n = \frac{M_1(t)}{M_0(t)}$ i $\sigma_n(t) = \sqrt{\frac{M_2(t)}{M_0(t)} - \left(\frac{M_1(t)}{M_0(t)}\right)^2}$.

Zahalak noted that the approximation to a Gaussian density is rather coarse compared with the n exact solution of Huxley's model. However, this approximation can provide the evolution of force over time, a constant velocity of strain, and the relation between force and velocity.

2.3 The Bestel's Model

In [10] Bestel proposed a microscopic model for the muscular fibre of skeletal muscle. This development of Huxley's model, which incorporates Zahalak's contribution, defined the **activation potential** function, which relates the concentration of calcium with the number of bridges. As this model can be interpreted macroscopically, it can be used to perform numerical simulations.

2.3.1 Activation Potential

Bestel proposed two functions, f and g which were positive and dependent on strain ξ, —like in Huxley's model—but which had the properties proposed by Zahalak. So, from equation:

$$\frac{dn}{dt} = f(1-n) - gn$$

she proposed two new functions (f for binding and g for unbinding) which depend on t and ξ. Those new functions are defined from the constants k_{ATP} and k_{RS}.

The k_{ATP} constant is given by the adenosin trifosfat, that constant ride the muscular stress. The k_{RS} constant determinate the absorbtion capacity of calcium by the reticulum sarcoplasmic, it have an important role in the muscular viscoelastic properties.

- Union frequency: like Huxley's model $f = 0$ if $\xi \notin [0,1]$ and $f = k_{ATP}$ if $\xi \in [0,1]$ a constant which depends of ATP level.
- Disunion frequency: by the g function, where is $g = \left|\dot{\varepsilon}_c(t)\right|$ if $\xi \in [0,1]$ and $g = \left|\dot{\varepsilon}_c(t)\right| + k_{ATP}$ if $\xi \notin [0,1]$

However, the number of bridges depends on the concentration of calcium $C_a(t)$ in each cell. As the change in the activity of the cell takes place when the concentration surpasses a certain concentration $\overline{C}$, Bestel suggested that the definitions of functions f and g may depend on the concentration of calciom:

- If $C_a(t) \geq \overline{C} > 0$

$$\text{If} \qquad \xi \in [0,1] \qquad \begin{cases} f(\xi,t) = k_{ATP} \\ g(\xi,t) = \left|\dot{\varepsilon}_c(t)\right| \end{cases}$$

$$\text{If} \quad \xi \notin [0,1] \qquad \begin{cases} f(\xi,t) = 0 \\ g(\xi,t) = k_{ATP} + \left|\dot{\varepsilon}_c(t)\right| \end{cases}$$

- On the other hand, if $\overline{C} > C_a(t) > 0$

$$\forall \xi \qquad \begin{cases} f(\xi,t) = 0 \\ g(\xi,t) = k_{RS} + \left|\dot{\varepsilon}_c(t)\right| \end{cases}$$

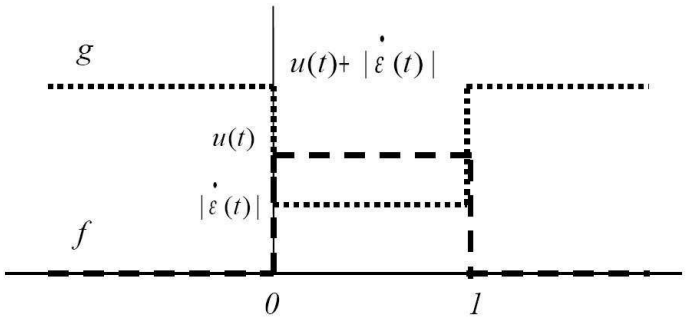

Figure 2.6: Functions f and g proposed by J.Bestel

She also assumed that if the cell is not stimulated, the concentration of calcium is null and, therefore, that functions f and g are also null. Into this environment we introduced a function $u(t)$, which we call activation potential and which combines the information from functions (eq. 2.2) and we can group in a unique expression the information f and g.

$$u(t) = |u(t)|_+ - |u(t)|_- \quad on \quad \begin{cases} |u(t)|_+ = k_{ATP} \cdot \chi_{\{C_a(t) > \overline{C}\}} \\ |u(t)|_- = k_{RS} \cdot \chi_{\{\overline{C} > C_a(t) > 0\}} \end{cases} \tag{2.2}$$

Figure 2.7 shows the correspondence between the concentration of calcium and function $u(t)$.

Functions f and g can now be rewritten in function of the activation potential $u(t)$ with:

$$f(\xi,t) = \begin{cases} |u(t)|_+ & \xi \in [0,1] \\ 0 & \xi \notin [0,1] \end{cases}$$

$$g(\xi,t) = |u(t)| + \left|\dot{\varepsilon}_c(t)\right| - f(\xi,t)$$

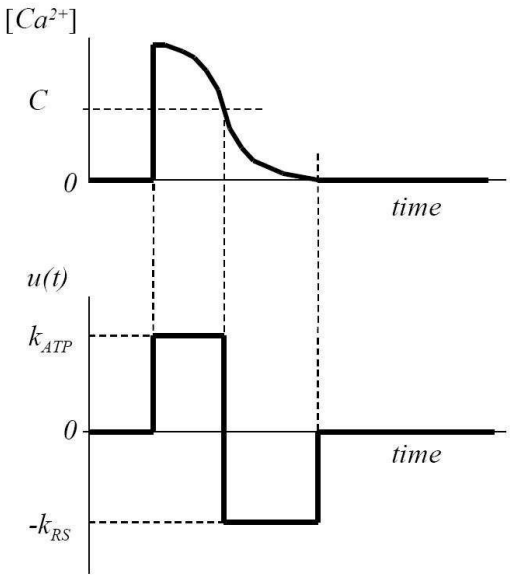

Figure 2.7: Relation between the calcium concentration and activation function.

2.3.2 Macroscopic Bestel's Model

Using these definitions of functions f, g and u, and reproducing the calculations of Zahalak, we can obtain the rigidity and tension by calculating the moments.

- The resulting rigidity (moment of order 0) is calculated from all the elemental rigidities assembled in parallel and with constant $\overline{k}$, which is the maximum rigidity in a sarcomere:

$$K(t) = \overline{k} \int_{-\infty}^{+\infty} n(\xi, t) d\xi = \overline{k} M_0(t)$$

- The stress (momentum of order one) can be calculated it the same way, with the maximum stress $\overline{\sigma}$:

$$\sigma_c(t) = \overline{\sigma} \int_{-\infty}^{+\infty} \xi n(\xi, t) d\xi = \overline{\sigma} M_1(t)$$

Now, if we reproduce Zahalak's calculations we saw in 2.1 for finding the differential equations that verify the moments, with the new functions f and g we can rewrite the differential equation to verify rigidity and tension as:

$$\dot{K} = -\left(|u| + \left|\dot{\varepsilon_c}\right|\right) K + \overline{k} \, |u|_+$$

$$\dot{\sigma_c} = -\left(|u| + \left|\dot{\varepsilon_c}\right|\right)\sigma_c + \dot{\varepsilon_c}K\eta + \frac{1}{2}\overline{\sigma}\,|u|_+$$

Now we assume that the groups of sarcomeres are made up of identical sarcomeres separated by Z lines. The macroscopic contractile element is then the result of grouping N sarcomeres of length s, $l_c = Ns$ where l_c is the length of the macroscopic contractile element.

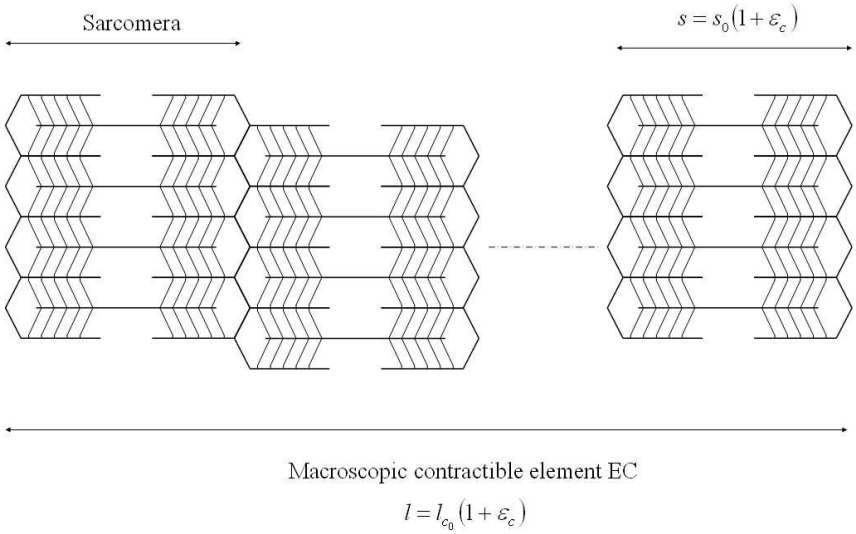

Figure 2.8: Distribution of sarcomeres along the muscle.

If we consider that the strain of this macroscopic element ε_c, which we assume to be uniform, is defined by $l_c = l_{c_0}(1+\varepsilon_c)$, we then get $\varepsilon_c = \frac{l_c - l_{c_0}}{l_{c_0}} = \frac{s-s_0}{s_0}$. Using these definitions and normalising, we can rewrite the differential equation that follows the contractile element:

$$\dot{k_c} = -\left(|u| + \left|\dot{\varepsilon_c}\right|\right)k_c + k_0\,|u|_+$$

$$\dot{\sigma_c} = -\left(|u| + \left|\dot{\varepsilon_c}\right|\right)\sigma_c + \dot{\varepsilon_c}k_c + \sigma_0\,|u|_+$$

and where σ_0 and k_0 are maximum values of stress and rigidity for the macroscopic element.

2.3.3 Complete Model of Muscular Fibre

After producing the model of the contractile element EC, CE, Bestel completed the Hill-Maxwell rheological model by modelling the passive elements ES and EP.

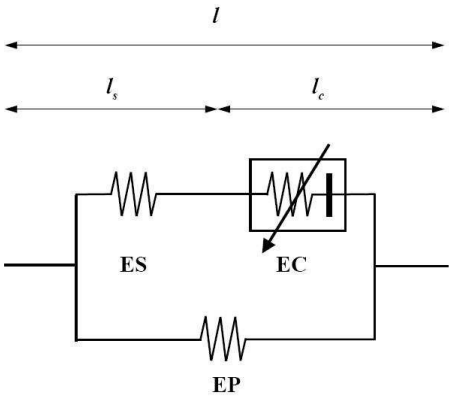

Figure 2.9: Rehological Hill-Maxwell's model.

As we have seen, it has been experimentally determined that the stress-strain ratio of a passive element satisfies equation $\frac{d\sigma}{d\varepsilon} = k\sigma + c$, however c is often rejected (see [19]). We will therefore assume that ES is a lineal resort with strain ε_s:

$$\sigma_s = k_s \varepsilon_s$$

Assembly in series imposes the relation between strains:

$$\varepsilon_s = \frac{l_0}{l_{s_0}}\varepsilon - \frac{l_{c_0}}{l_{s_0}}\varepsilon_c$$

and the relation between the rigidities of EC and ES:

$$\sigma_c = \sigma_s = k_s \frac{l_0}{l_{s_0}}\varepsilon - k_s \frac{l_{c_0}}{l_{s_0}}\varepsilon_c$$

The passive element EP will follow the same exponential model for the strain-stress relationship as that for ES:

$$\frac{d\sigma_p}{d\varepsilon} = k_{p_1}\sigma_p + k_{p_2}$$

provided the stress is null when the strain is null:

$$\sigma_p = \frac{k_{p_1}}{k_{p_2}} \left(e^{k_{p_1} \varepsilon_p} - 1 \right)$$

To simplify the calculations, however, a linearised expression is usually used (see [11]):

$$\sigma_p = k_p \varepsilon_p$$

Finally, to complete the one-dimensional model, we need only consider the Lagrange equation in partial derivatives, which determines the displacements of each node in cases of non-conservative force. We would need to assume that the longitudinal displacement $y(x,t)$ is a function of time t in a material point x, where $0 < x < 1$. This variation is related to the strain through $\varepsilon(x,t) = \frac{\partial y(x,t)}{\partial x}$, approaching v by y to time unit, using the Lagrange equation:

$$\rho \ddot{y} + c\dot{y} - \frac{d}{dx} \left(k_p \varepsilon + \sigma_c \right) = 0$$

where ρ is the density and c is the damping parameter.

Therefore we can now begin to simulate the one-dimensional model of muscular contraction. Let us assume that the elements in series are linear and that the initial strain is null. This leaves the system:

$$\begin{cases} \dot{k}_c = -\left(|u| + \left| \dot{\varepsilon}_c \right| \right) k_c + k_{c_{\max}} |u|_+ \\ \dot{\sigma}_c = -\left(|u| + \left| \dot{\varepsilon}_c \right| \right) \sigma_c + k_c \dot{\varepsilon}_c + \sigma_{c_{\max}} |u|_+ \\ \rho \ddot{y} + c\dot{y} - \frac{d}{dx} \left(k_p \varepsilon + \sigma_c \right) = 0 \\ \sigma_c = k_s \left(\varepsilon - \varepsilon_c \right) \end{cases} \tag{2.3}$$

where k_p and k_s are positive constants determined experimentally.

2.4 Geometric Model in 3D

Until now, we have been presented a one-dimensional geometric model (the rehological Hill-Maxwell's model)and now we want to built a three dimensional model for reproduce the movement of a muscle into the space. Assuming that the muscle have a main direction (the fibre direction) which produce the muscular force in our muscle. With the physic properties of a muscle, we assume that the the other two directions, orthogonal to the fibre, can't do stress

variations to the muscle. In this way, we are going to consider the orthogonal direction as a connective tissue, like a simple spring.

In this way, we propose an isoparametric unitary model in dimension 3 as an hexahedron (figure 2.10) having a special direction that behaves as the Bestel model (it's the vertical direction) and a plane that it have a behavior as connective tissue (the horizontal plane). This model can be used for the dynamic muscular simulation, so that we are going to meshing the muscle, in approximately orthogonal form (figure 2.11), where we are going to have an special direction, that it will be the direction of muscular fibre.

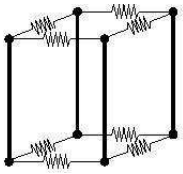

Figure 2.10: Unitary model for the 3D element

For the generation of these meshes, we are going to consider hexahedric elements adapted to the geometry of the anatomic data. Moreover, we must take care of the deformation in each mesh element in order to not affect the numerical solution for the system (equation 2.3).

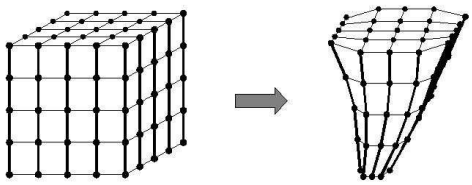

Figure 2.11: Muscular approximation by an orthogonal mesh

This model will verify the physic properties that we want to fulfill for the muscle behavior. One of the most important property required for the model the model is the incomprehensibility, i.e. that the volume is constant along the time, although the fiber direction can be shorter (figure 2.12). So that, we are going to impose the volume conservation of each hexahedron in our model, thus this does not generate unwanted strains.

To maintain the conservation of volume we have to emphasize two points, which have the repercussion to our solution method (see appendix A for details):

- **Stress tensor**. For each knot of the mesh we are going to apply the Hooke's law for the volume conservation, so that we are going to use the stress tensor. In the case of small

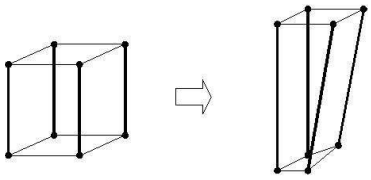

Figure 2.12: Incompressible model

deformations that tensor is the same of Piola-Kirchhof tensor, with the Poisson coefficient usual for the incomprehensibility of the materials $\nu \simeq 0,5$:

$$\underline{\underline{\sigma}} = \begin{bmatrix} \varepsilon & 0 & 0 \\ 0 & -\nu\varepsilon & 0 \\ 0 & 0 & -\nu\varepsilon \end{bmatrix}$$

where ε is the strain that it has been calculated in each knot.

- **Coordinates changes**. It is necessary for the simulation of the fibre direction has an appropriate orientation in the three dimensional space. So that, we need two coordinate systems, a local one for each one-dimensional element and another one, for the global coordinates.

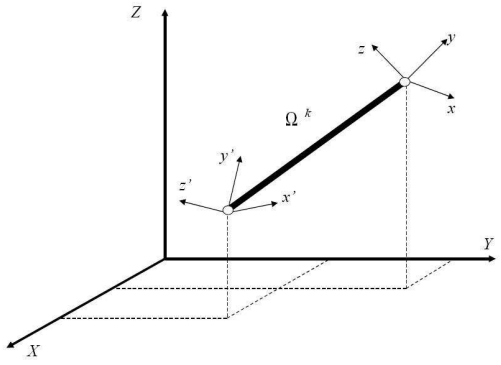

Figure 2.13: Local and global coordinate systems needed for orientation of the fibre.

2.5 Simulation of the Muscular Unit

After fixing the macroscopic muscular unit in the space, now following [11], we are going to describe the muscular movement using the formula for the dynamic of a continuous medium in

equilibrium. We apply the equations in three dimensions where $\underline{\underline{\varepsilon}}$ is the strain tensor, that have the same expression that the Green-Lagrange tensor, we obtain the strain tensor:

$$\underline{\underline{\varepsilon}} = \begin{pmatrix} \varepsilon_{11} & \varepsilon_{12} & \varepsilon_{13} \\ \varepsilon_{21} & \varepsilon_{22} & \varepsilon_{23} \\ \varepsilon_{31} & \varepsilon_{32} & \varepsilon_{33} \end{pmatrix} \tag{2.4}$$

$$\varepsilon_{ij} = \frac{1}{2}\left(\frac{\partial y_i}{\partial x_j} + \frac{\partial y_j}{\partial x_i} + \sum_k \frac{\partial y_k}{\partial x_i}\frac{\partial y_k}{\partial x_j}\right) \tag{2.5}$$

Then we must use the second strain tensor of Green-Lagrange denoted by $\underline{\underline{\sigma}}$. Because we want to use the rehologic Hill-Maxwell model, the total stress is the sum of stress in the two sides. In the side of the contractible element, the stress is just in the direction fibre, activated into the direction of tangent vector $\underline{n}$. So, we have:

$$\underline{\underline{\sigma}} = \underline{\underline{\sigma}}_p + \sigma_{1D} \cdot \underline{n} \otimes \underline{n} \tag{2.6}$$

where σ_{1D} is the number indicating the stress in the side in series of the contractible element and $\otimes$ is the tensorial product over one dimensional tensor $\underline{n}$. The kinematic of the sarcomeras distribution in dimension one of the contraction implies the corresponding stress of Green-Lagrange tensor:

$$\tau_{1D} = \sum_{i,j} \tau_{ij} n_i n_j$$

and verify:

$$1 + \tau_{1D} = (1 + \tau_c)(1 + \tau_s)$$

where τ_c is the stress for the contractible element and τ_s is the stress for the series element. On the other hand, as a result of the second stress tensor of Piola-Kirchhof ($\underline{\underline{\sigma}}$) we have:

$$\sigma_{1D} = \frac{\sigma_s}{(1 + \tau_c)} = \frac{\sigma_c}{(1 + \tau_s)}$$

A consequence of the parallel distribution is the stress relation: $\underline{\underline{\tau}} = \underline{\underline{\tau}}_p$

We can use the last equations and the properties for the elastic elements to rewrite σ_s and $\underline{\underline{\sigma}}_p$ as functions of τ_s and $\underline{\underline{\tau}}_p$, ($\sigma_s = \sigma_s(\tau_s)$, $\underline{\underline{\sigma}}_p = \underline{\underline{\sigma}}_p(\underline{\underline{\tau}}_p)$)

Now, with the equations of stress and strain for the Bestel model, the behavior in the three dimensions is defined and we can write the dynamic equation for the model:

$$div(\underline{\underline{F}} \cdot \underline{\underline{\sigma}}) - \rho \ddot{y} = \underline{0}$$

where y is the displacement vector, $\underline{\underline{F}}$ is the strain gradient and ρ is the material density.

In this way, we can start the simulation in the space from the 1D model for the muscular contraction and use it to simulate the 3-dimesional case. With the corresponding modification for the equation 2.3 we rewrite it as:

$$\begin{cases} \dot{k_c} = -\left(|u| + \left|\dot{\varepsilon_c}\right|\right) k_c + k_{c_{\max}} |u|_+ \\ \dot{\sigma_c} = -\left(|u| + \left|\dot{\varepsilon_c}\right|\right) \sigma_c + k_c \dot{\varepsilon_c} + \sigma_{c_{\max}} |u|_+ \\ \rho \ddot{y} + c\dot{y} - div(\underline{\underline{F}} \cdot \underline{\underline{\sigma}}) = \underline{0} \\ \sigma_c = k_s \left(\varepsilon - \varepsilon_c\right) \end{cases} \tag{2.7}$$

which is the system that we need to solve for the muscular simulation, and for each muscle that we want to simulate. Now, y, $\dot{y}$, $\ddot{y}$, σ_c, $\dot{\sigma_c}$, k_c, $\dot{k_c}$, ε, ε_c and $\dot{\varepsilon_c}$ are vectorial variables.

2.6 Data and Meshes

The data for building the geometrical model have been obtained from the work of M. Lopez-Cano et al.[44] where they extract the original data from The National Library of Medicine's (Visual Human Project[1]). They work with snake algorithms to get the data of all important elements of the inguinal region. They captured the data from the images (figure 2.14) and they generate some files where there are the limits of the elements of the abdominal wall (figure 2.6). We started to work with a single muscle, choosing the internal oblique muscle because it have the most important role in the dynamics of the area and it is proved for his active role in the genesis of inguinal hernia (figure 2.6). Now, we have a set of points in the boundary of the internal oblique muscle and we want to obtain a mesh for all the muscle with a reticular structure in hexahedric units. The mesh needs to fulfill some properties so that the procedure to do the mesh must be very *regular* and *smooth* at the same time to approximate the original data. On the other hand we want to use a flexible procedure to work with different meshes, with several densities to try to simulate different alive tissues. In this way, our model is a real model

[1] Human-Computer Interaction Lab. Univ. of Maryland at College Park.

because our data have a real origin and so that our results will be near of the real phenomenon in the human body.

(a) Cross slice (b) Slice origin

Figure 2.14: Visual Human Project pictures

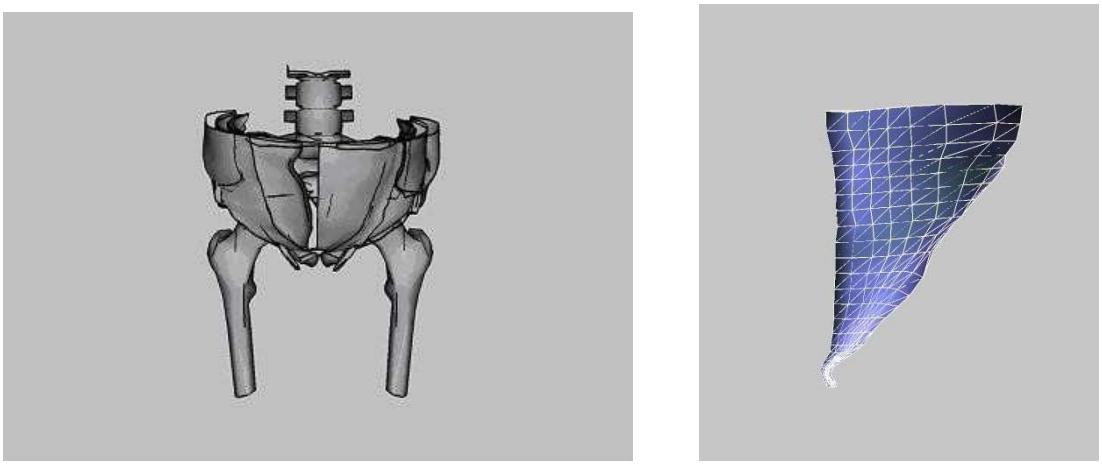

(a) Our real model (b) Oblique internal muscle

Figure 2.15: Our data extracted from Visual Human Project

The muscle have an elliptical section, so that we approximate the muscle boundary with two surfaces, then we generate a grid in each surface and finally we make the mesh with the union of the opposite knots (figure 2.17).

From the literature ([30],[65] and [22]) we have 4 options to generate these surfaces on the muscles boundary:

- **Coons surfaces**: This kind of surfaces have been used in many lighting questions, because has a big capacity of adaptation to many figures. The surface can be approximated by a collection of small surfaces, each one of these surfaces are quadrilateral which generate a

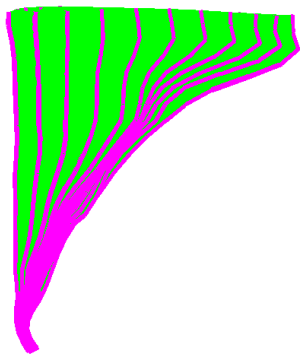

Figure 2.16: The fibre model along the muscle

partition of the original surface. The edges of these quadrilateral are select by cubic splines normalized. The result surface of class C^1 although it is very clumsy to do calculations, because although we have several techniques for the calculation, the generated surfaces are inflexible and we need a big number of data for their calculation.

- **Bézier surfaces**: In this case we have some control points or checkpoints where we can easily direct the surface, we have much more flexibility and much more softness because we can generate surfaces of class C^n in a mesh of $(n+1) \times (n+1)$ knots. Although, as the degree of these surfaces depend directly of the number of control dots this fact put several complications in the use of these surfaces, they are very unstable to small modifications of the control points, so that their parameterizations have few control, they are difficult to control and uniform meshes difficult to create.

- **B-Spline surfaces**: The surfaces Basis Spline resolved the majority of the limitations that we have in the previous cases. Now we can generate surfaces of class C^{n-1} for meshes with $(n+1) \times (n+1)$ nodes. The final surfaces can interpolate the collection of initial points, the surfaces are robust by changes of control points and we can do uniform equipartitions in to the surfaces. Also, with the **Cox-De Boor** formulation, we can parameterize the surface so easy as we will need, and we can evaluate this expression easily.

- **Non uniform rational B-Spline surfaces, NURBS**: The NURBS have the same properties of the B-Spline surfaces and they solve the unique limitation of these surfaces, the representation of planes and quadrics. On the other hand, we have an handicap when we have the same number of control (**De Boor** points) and the number of dots of the original mesh, then we have the **Runge** phenomena, in the unwanted undulation of the surface.

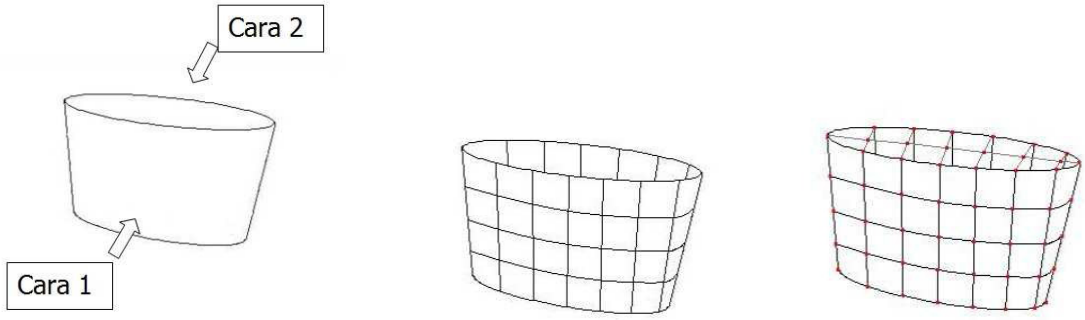

(a) Original element (b) Grid for the surfaces (c) Mesh for the element

Figure 2.17: Mesh generation

2.6.1 The Mesh Computation

Finally we generate a mesh from two NURBS surfaces, for each one of the muscles that we want to simulate. We will have a set of $r \times s$ nodes ordered in a rectangular sense and we are going to interpolate with a surface $x(u, v)$. We will determine a set of control points $\{B\}_{(i,j)=(1,1)}^{(n+1,m+1)}$, with $(n+1) \times (m+1)$ nodes where $n+1 \leq r$ and $m+1 \leq s$. These control points are chosen in the same way as the surfaces are realized with B-Splines and we will use the distances between neighbor points to obtain a parametrization that allows us a uniform partition of the nodes from the parameter uniform distribution. In addition, we have 2 integer numbers, k and l, that they satisfy $2 \leq k \leq n+1$ and $2 \leq l \leq m+1$, and two vectors $X = (x_1, ...x_{n+k+1})$ and $Y = (y_1, ...y_{m+l+1})$ known as vectors of knots, where $x_i \leq x_{i+1}$ and $y_i \leq y_{i+1}$ with parameters $(u, v) \in [x_k, x_{n+2}] \times [y_l, y_{m+1}]$. The vectors X and Y are in charge of the interpolation of the points of the initial data. In addition we have the set of weights $H = \{h_{i,j}\}_{(i,j)=(1,1)}^{(n+1,m+1)}$ with $h_{i,j} \geq 0$ that we are going to determinate later. With the usual formulas to generate the B-Spline functions of order g and h, we can parameterize our surface as:

$$x(u, v) = \sum_{i=1}^{n+1} \sum_{j=1}^{m+1} B_{i,j} S_{i,j}(u, v) \tag{2.8}$$

where,

$$S_{i,j}(u, v) = \frac{h_{i,j} N_{i,k}(u) M_{j,l}(v)}{\sum_{a=1}^{n+1} \sum_{b=1}^{m+1} h_{a,b} N_{a,k}(u) M_{b,l}(v)}$$

And the **Cox-De Boor** formulas for the B-Spline functions with the assumption $0/0 = 0$.

$$
\begin{aligned}
N_{i,1}(u) &= \begin{cases} 1 & \text{if } x_i \leq u < x_{i+1} \\ 0 & \text{in other case} \end{cases} \\
N_{i,g}(u) &= \frac{(u - x_i)\, N_{i,g-1}(u)}{x_{i+g-1} - x_i} + \frac{(x_{i+g} - u)\, N_{i+1,g-1}(u)}{x_{i+g} - x_{i+1}} \quad \text{with} \quad k \geq g > 1
\end{aligned}
$$

$$
\begin{aligned}
M_{j,1}(v) &= \begin{cases} 1 & \text{if } y_j \leq v < y_{j+1} \\ 0 & \text{in other case} \end{cases} \\
M_{j,h}(v) &= \frac{(v - y_j)\, M_{j,h-1}(v)}{y_{j+h-1} - y_j} + \frac{(y_{j+h} - v)\, M_{j+1,h-1}(v)}{y_{j+h} - y_{j+1}} \quad \text{with} \quad l \geq h > 1
\end{aligned}
$$

With the previous work in 2.8 we have already parameterized each of the surfaces that interpolate our point set that determines the exterior face of our muscles. Now only it is necessary to do a *distribution* of the surface to build a mesh on top. Once the distribution has been done in both surfaces, we will join the points using linear interpolation and, if it is necessary, will do another distribution

The thickness of the mesh will be decided from the physical properties of the muscles, so that we are going to choose the thickness that has an ideal behavior and the possibility to reproduce the properties expected for the muscles.

2.7 Conclusions

Most muscular simulations are still conducted by considering the muscle as a single macroscopic unit and their geometry and the various directions of the muscular fibre are omitted. Huxley's sliding filament model is the first one to provide a mathematical expression to muscular dynamics at the microscopic level. Now, thanks to the contributions by Zahalak and Bestel, a more detailed model of muscular dynamics can be constructed that will enable a detailed study of certain zones, such as the inguinal region, to be conducted.

Several authors have attempted to determine the activation function and we now have several models to choose from. However, the role of this function does not appear to depend on which model is chosen. All of the models are governed by the concentration of calcium and each of them provides a different response at each level.

Chapter 3

One Dimensional Simulation

3.1 One-dimensional Integration

In this chapter we consider the simulation of a muscle fiber, despite that it is a one-dimensional object, the simulation will be performed in the space, using the Bestel's model, following the system of equations 2.7 with the computational algorithm explained in Appendix A. Once the mesh has been built in the space, we fix a main direction, the fiber direction. The fiber direction has been determined by a succession of one dimensional contractile elements, built in the space. We grouped them suitably in the mesh and they form one longitudinal fiber that goes from the upper bound to the low end of the mesh. Hereby the integration of the PDE in 2.7 has been realized separately for each of the longitudinal fibers, as one-dimensional elements and carrying out the posterior coordinate change in the space. The motivation for this strategy is to reduce the size of the equation systems involved, avoiding the technical problems that appear if your systems are huge.

3.1.1 Methodology

We consider every longitudinal one-dimensional fiber in the space, so that we have a collection of consecutive segments and it is a procedure to perform the desired simulation. The methodology for the simulation has been explained previously in section 2.5, but there we do not introduce two fundamental steps for building our model. In Appendix A, there has a description of the numerical integration of an one-dimensional element of an isolated one-dimensional element is described in detail, here we consider the assembly of several contiguous elements. On the other hand, these one-dimensional elements are placed in the space so that it is needed to establish

the coordinates change for every node.

The Assembling

To reach the assembling of a structure with several nodes, we need to describe in an unique system the relative influence of the different components. The same procedure will be applied to the matrices $\left[K^k\right]$, $\left[M^k\right]$ and $\left[C^k\right]$ that we have to use to integrate the PDE. In Appendix A, we have defined the stiffness matrix for an one-dimensional element:

$$\left[K^k\right] = \begin{pmatrix} k_{11}^k & k_{12}^k \\ k_{21}^k & k_{22}^k \end{pmatrix}$$

Thus, as an example, if we have three aligned elements in dimension one (figure 3.1):

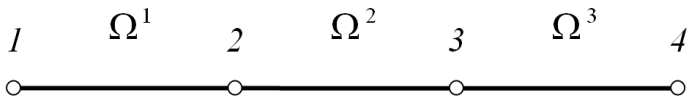

Figure 3.1: Succession of elements in dimension one

we can assemble them imposing the forces equilibrium equation in every in every node i:

$$\sum_k F_i^k = F^{ext}$$

We can write the following equations for every node:

$$\begin{gathered} k_{11}^1 u_1 + k_{12}^1 u_2 = -F \\ k_{21}^1 u_1 + \left(k_{22}^1 + k_{11}^2\right) u_2 + k_{12}^2 u_3 = 0 \\ k_{21}^2 u_2 + \left(k_{22}^2 + k_{11}^3\right) u_3 + k_{12}^3 u_4 = 0 \\ k_{21}^3 u_3 + k_{22}^3 u_4 = F \end{gathered}$$

where u_1, u_2, u_3 and u_4 are the nodal displacements and and the system matrix (the stiffness matrix) can be written as

$$\begin{pmatrix} k_{11}^1 & k_{12}^1 & 0 & 0 \\ k_{21}^1 & k_{22}^1 + k_{11}^2 & k_{12}^2 & 0 \\ 0 & k_{21}^2 & k_{22}^2 + k_{11}^3 & k_{12}^3 \\ 0 & 0 & k_{21}^3 & k_{22}^3 \end{pmatrix}$$

When more elements are considered, an analogous procedure is used to build the associated tridiagonal system and solve the problem.

3.1.2 The Coordinate Changes

Since our PDE is solved in dimension one, it is necessary to determine an univocal coordinate change from dimension three to dimension one. This change is completely determined for every one-dimensional element due to the position of every element and both angles delimited with the origin of coordinates, which locally determines an orthogonal base with the direction of the element, the normal direction to the element contained in the plane determined by the element and the origin, and the normal vector to this plane.

We want to emphasize that the nodes placed in the end of the longitudinal fiber, will have an unique change of coordinates (figure 3.2 (a)), whereas the ones placed between two elements of dimension one they can have two different changes (figure 3.2 (b)).

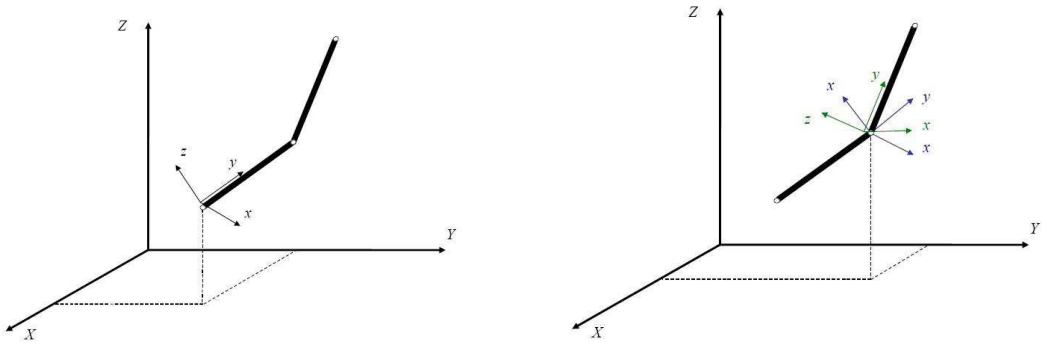

(a) Coordinates of an extreme node (b) Coordinates of an intermediate node

Figure 3.2: Possible coordinate changes

In every instant of time it is necessary to make these coordinate changes to calculate the new position of every node.

3.1.3 Integration Test

A validation test has been carrying out for our code to state its correctness. Thus, a cubic mesh has been generated with 64 three dimensional elements and the contractile fibers are arranged in the longitudinal direction. Every longitudinal fiber is composed by 4 one-dimensional elements projected in the space, we use the Finite Element Method (FEM as in the Appendix A) for one-dimensional problems. In each element, the matrices that we use are constant, so that we don't have to do a dynamical integration for every element.

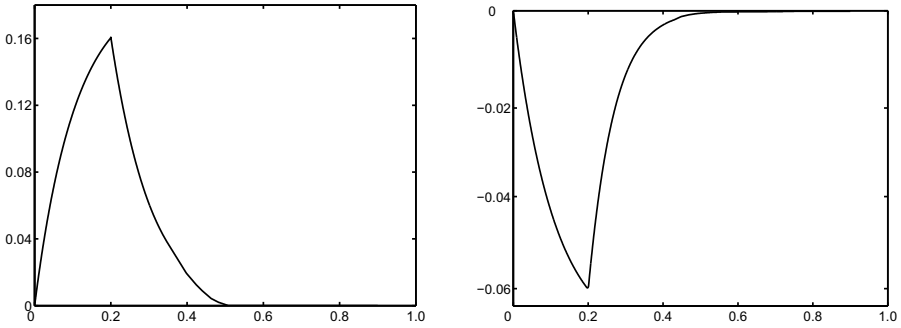

(a) Stress (b) Strain

Figure 3.3: Graph of stress and strain in our test

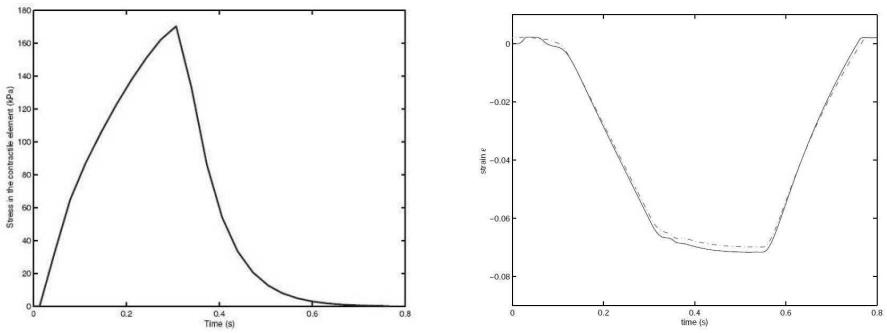

(a) Stress (b) Strain

Figure 3.4: Graph of stress and strain in Bestel work

The muscular contraction has been applied in the longitudinal fibers and there have been obtained the values of stress and strain similar to the obtained ones previously and coherent with those of the model in dimension three, considering that now we have interaction between the elements. It is possible to observe that there have been obtained values of stress and strain equivalent to the test realized with only one element (figure 3.3 and 3.4).

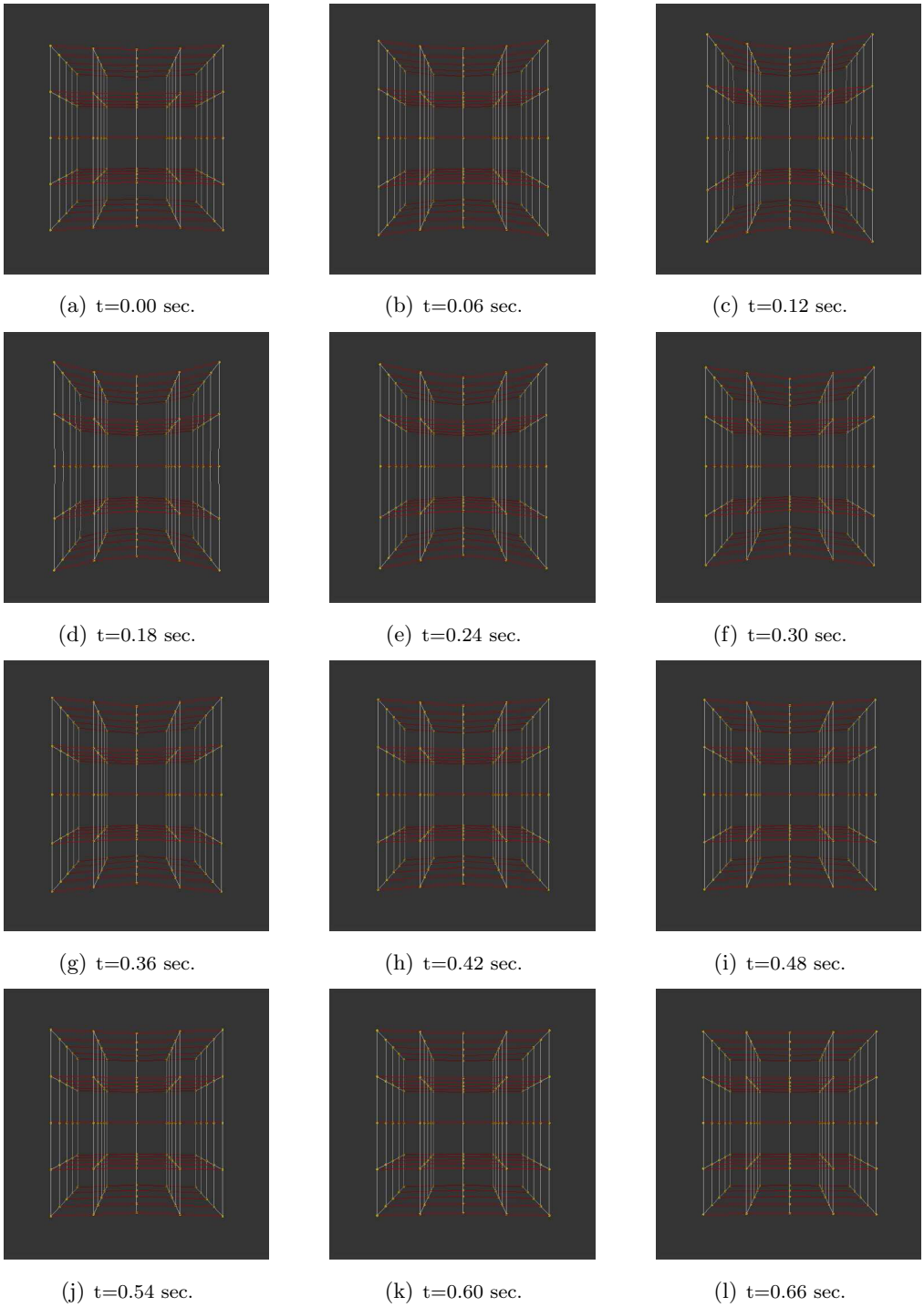

(a) t=0.00 sec. (b) t=0.06 sec. (c) t=0.12 sec.

(d) t=0.18 sec. (e) t=0.24 sec. (f) t=0.30 sec.

(g) t=0.36 sec. (h) t=0.42 sec. (i) t=0.48 sec.

(j) t=0.54 sec. (k) t=0.60 sec. (l) t=0.66 sec.

Figure 3.5: Sequence of significant images throughout 0.7 seconds in the integration test for the muscular contraction

The sequence of images of 3.5 illustrates the movement of the cubic mesh in 0.7 seconds. It is possible to observe (in figure 3.5 (d)) the effect of the stress and the maximum strain on the

configuration of the mesh.

3.2 Muscle Simulation: the Intern Oblique

After doing the first tests and confirming the validity of the results, we begin to simulate the movement of the oblique internal muscle. This muscle, together with the the inguinal ligament, it has a very significant role in the determination of the Hessert's triangle (this can be seen in [54]) and a variation of his parameters can give us a measure of the risk of suffering a hernia. In this way, the mesh has been generated following the instructions of the paragraph 2.6. The generated mesh has altogether 756 nodes and 480 three dimensional elements. The mesh has been subjected to the muscular contraction for a second and the results have been evaluated.

It is necessary to emphasize that the connective tissue has been assumed dynamically passive, therefore the position of the nodes only depends of the contraction of the longitudinal fiber and of the conservation of the volume.

3.2.1 Initial Values

The values of the different parameters involved have been extracted from the works of Semersant [68] and Bestel [10]. Using equivalents parameters we hope to obtain equivalents results or qualitatively equivalents.

Values for the Model and Material

ρ	Material density: $1.05e^{-5}\ MPa/mm^2$.
m	Young modulus: 0.076 MPa.
ν	Poisson's coefficient: 0.5
t	Time for the simulation: 1 seg.

Values for the Activation Potential Function: $u(t)$

T	0.4 seg. Time where the function $u(t)$ is activated (non zero)
φ_+	0.15 seg. Time where the function $u(t)$ is positive
φ_-	0.25 seg. Time where the function $u(t)$ is negative
K_{ATP}	10 seg^{-1} Constant for adenosinetriphosphate increment
K_{RS}	-10 seg^{-1} Constant for calcium reduction

Values for the Partial Differential Equation

c	Damping parameter for the PDE 7.10^{-5}.
u^0	Initial value for displacement in each node: 0.
$\dot{u}^0$	Initial value for the displacement velocity in each node: 0.

Values for the Differential Equation

$k_{c_{\max}}$	Maximum stiffness for the contractible element: 1.0 MPa.
k_p	Stiffness for the passive element: 2. MPa.
k_s	Stiffness for the series element: 100. MPa.
$\sigma_{c_{\max}}$	Maximum stress for the contractible element: 0.18 MPa.
$\dot{\varepsilon}_c(0)$	Initial velocity of strain: 0. MPa.
$\sigma_c(0)$	Initial stress: 0. MPa.
$k_c(0)$	Initial stiffness: 0. MPa.

3.2.2 Effects of the variation in parameters

With these values, the simulation has been done and the obtained values of stress and strain are shown in figure 3.6. We can see that our results are very similar to the ones obtained by Sermersant and Bestel, their behavior is essentially the same as their models.

We have measured the whole volume of the muscle throughout the time, for each of the three dimensional elements, and it has been verified that the variation of volume is always lower than 3 per cent of the initial volume (3.7).

There is also verified, that the angle determined by the aponeurotic tissue and the muscular tissue maximizes in the moment that produces the maximum strain (and also the maximum stress), so that also increase the probability to have an hernia.

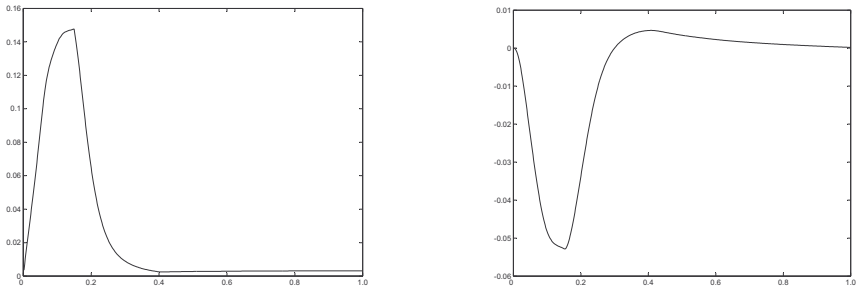

(a) Stress in MPa. (b) Strain

Figure 3.6: Plots of stress and strain over time

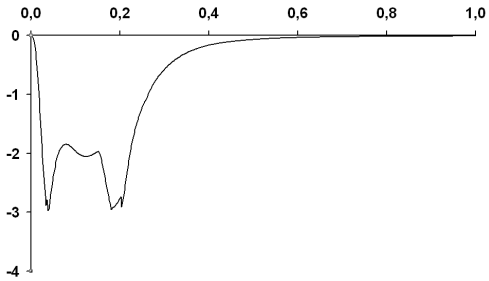

Figure 3.7: Percentage of volume variation for a second

3.2.3 Effects of the Variation of the Damping Parameter

The determination of the damping parameter is a very complex problem to solve in the integration of PDE equation, in many occasions an experimental procedure is needed for determined it. Here we use the initial value for the damping parameter proposed by Sermesant in his work. A series of viable values for the model have been crossed and their effect on the maxim variation of the angle have been verified. It is necessary to emphasize that concerning the initial proposed values, no significant significant differences between the values of stress and strain have been observed. Although, it has been observed an inverse dependence between the increase of the parameter and the maximum variation of the studied angle, as can be observed in figure 3.8.

3.2.4 Effects of Calcium Variation

The variation of calcium concentration have different effects. First, we observe a qualitatively equivalent behavior for the values of stress and strain. We have used different values for the velocity variation of calcium concentration $K_{ATP} = 5$, $K_{ATP} = 10$, $K_{ATP} = 15$ and $K_{ATP} = 20$, we can see the result of the test is in figure 3.9.

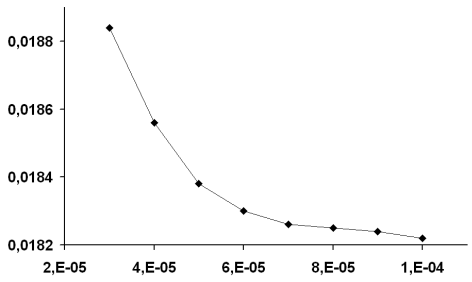

Figure 3.8: In vertical axis maximum angular variation in radians, in the other one we have values for the damping parameter.

With these values, one can state that the maximum variation of the angle increases with the highest calcium values, hereby we can establish that an increase of the concentration of calcium generates a bigger overture of the angle of Hessert's Triangle. We can look the results in the following table.

Due to the fact that an increase of the concentration of calcium represents a muscular increase of the stress and strain, we can establish that the concentration of calcium has a direct influence in the genesis of the inguinal hernias.

K_{ATP}	Maximum angular variation
5	0.01166 rad.
10	0.01826 rad.
15	0.02025 rad.
20	0.02114 rad.

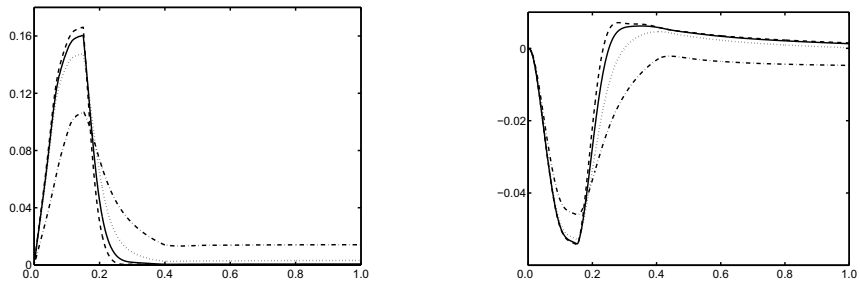

(a) Stress in MPa. (b) Strain

Figure 3.9: Strain and Stress plots for several values of K_{ATP}: $K_{ATP} = 5$ in line-dot line, $K_{ATP} = 10$ in dotted line, $K_{ATP} = 15$ in continue line and $K_{ATP} = 20$ in dashed line. The bigger the calcium concentration, the bigger the obtained stress and strain.

3.2.5 Effects of Intra-abdominal Pressure Variation

The differences of intra-abdominal pressure are added to our model as external forces acting on the muscle. In order to imitate the anatomy of the inguinal region, we are going to apply more pressure in the *central* part of the muscle has been considered. Therefore, an internal point of the abdomen has been considered, from which the force will be apply, and the following function will be applied to every node considering a constant force F and the coordinates centered at this point:

$$f(x, y, z) = \frac{F}{x^2 + y^2 + z^2 + 1}.$$

During the simulation we have submitted the oblique internal muscle to a constant intra-abdominal pressure. An increase of the maximum variation of the studied angle can be observed, which recover the initial position. So that, we can establish the pressure as a factor which increases the risk in the genesis of inguinal hernias. In the following table we can see the maximum variation of the angle subject to different values of the parameter F in the formula.

F	Maximum angular variation
0.1	0.01903 rad.
0.01	0.01828 rad.
0.001	0.01826 rad.
0.0	0.01826 rad.

3.2.6 Effects of Angular Variation

There have chosen three nodes that delimit the ends of Hessert's triangle and the variation of the major angle of Hessert's triangle has been measured (figure 4.1). Thus, we can observe a direct dependence between the increase of the area and the increase on the angle. So that, we can explain the enclosure of Hessert's triangle with the angular variation.

3.2.7 Effects of Repeated Effort

To study the repetition of the muscular effort, 10 contractions have been applied during a period of 10 seconds (figure 3.11). At every time instant, the variation of the angle has been measured up and we can establish that the minimum variation of the angle increases with the number of

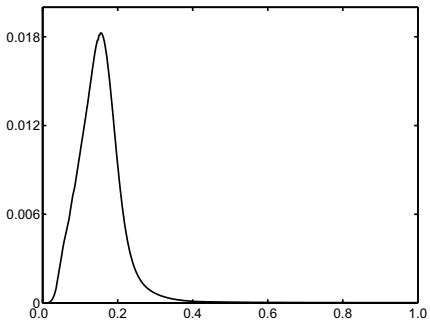

Figure 3.10: Angular variation measured in radians

impulses. This is due to that recovering time, or the time in which the activation function is null, is not sufficient in order that the muscle recovers its initial position in every impulse. In figure 3.11, we can see a certain number of impulses, the angle have an important increase in the variation of the rise in this angle. Therefore, we can conclude that a continued effort increases the risk of herniation, because of the rise in this angle. With this result we can establish a possible relationship between the repetition effort and the genesis of hernias.

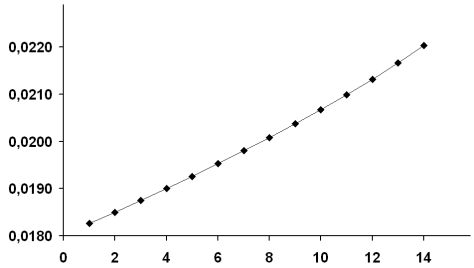

Figure 3.11: In vertical axis maximum angular variation in radians, in the horizontal one we have the contractions number.

3.3 Conclusions

The behabior of the inguinal region is mainly determined by the muscular dynamics, so that we need to have a good three dimensional model for the muscular simulation. In this way we propose a hexahedron as action unit in dimension three, to preserve the anisotropic property for the muscle. On the other hand, the hexahedron have some specific property, it can be stackable in a very easy way. This fact are going to facilitate the mesh generation in the space and we are going to identify the real muscular fibres as the sequence of contractible elements that we are using.

In this chapter, we have introduced the particular tools that we need to build a model for a muscle in the space. We use tools coming from different areas like surface modeling, numerical methods for PDE, mechanics of materials, etc., this is inherent to the applications of simulation to medicine or real live in general. We want to emphasize that we use original data, so that our model have an extra value because we have an approximate model of the reality.

Chapter 4

Three-dimensional Integration

In this Chapter, we are going to do the three-dimensional volumetric muscular simulation, using the Bestel's model and the equations system 2.7 the calculation algorithm (Appendix A) that we previously described. As in the previous chapter, we are going to consider the direction fibre as a special direction, that we can determinate by union of several contractible elements the **longitudinal fibre** along the muscle. In the previous chapter we integrate the longitudinal fibre contraction and translate this values to the mesh and we impose volume conservation for each element. Now, the integration is made using the whole mesh with the 3-dimensional elements.

The reader can see the importance of this change because the number of equations that we need to solve in each steep now is $3n$ where n is the number of nodes in our model, while in the previous chapter we need to solve n equations, and translate the values to the particular mesh.

In the biological tissue simulations, it is commonly used the constitutive equations for hyperelastic materials the Helmholtz free-energy function [32]. We can look several examples of constitutive equations in [33]. In the Chapter 5 we present the hyperelasticity with several details.

4.1 Introduction

The connective tissue is the responsible for the passive part of the muscle, in our case we assume it surrounds the contractible fibre. Here we are going to formulate it in the three dimensional space, with the finite element method (FEM) using an isoparametric eight-node continuum as finite element.

The nonlinear viscoelastic and poroelastic nature of muscular tissue have been introduced in other models using FEM or similar procedures, here, in order of getting a first approximation, we have omitted these properties. We treat the connective tissue of the muscle as volumetric, quasi-incompressible and elastic material, governed by a lineal stress-strain relationship in the constitutive equations.

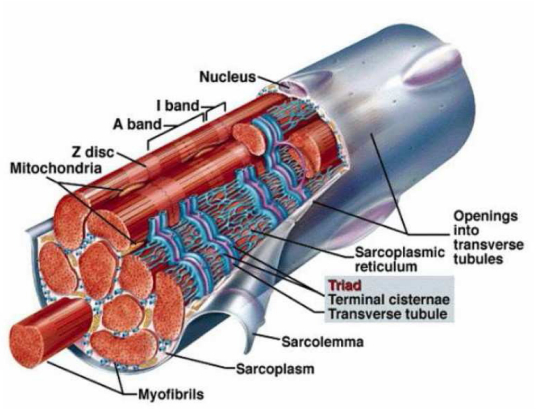

Figure 4.1: A muscular cell with fibres (myofibrils)

4.1.1 Linear Elasticity

The elastic materials can be considered that they have an initial shape to which they will return if the applied forces disappear. Since the changes of shape are very small, there is no difference between the reference configuration and current configuration. The linear elasticity theory gives an excellent model for the behavior of this sort of materials. We can obtain the stress with the partial derivatives Helmholtz free-energy function.

$$\sigma_{ij} = \frac{\partial W}{\partial \varepsilon_{ij}} = D_{ijkl}\varepsilon_{kl} \tag{4.1}$$

Where $D_{ijkl} = D_{klij} = D_{jikl} = D_{ijlk}$ is the elasticity tensor that relates the strains (ε_{kl}) and the stresses (σ_{ij}), considering small strains.

4.1.2 Elastic and Linear Approach

We can observe (figure 4.2) schematically a summary for the typical stress-stretch behavior of any muscle, when it is stretched along the fibre axis and across-fibre axis. In this case, the Omens work [56] is for the properties of the miocardium (in rat case), but it is well known

that properties of the miocardium are very similar, in a qualitative way, for all mammals and for all muscles. It has been observed the anysotropy and the non-linear properties, with the different values obtained for the same stretches, the non-linear behavior is more important for large strains than for small strains.

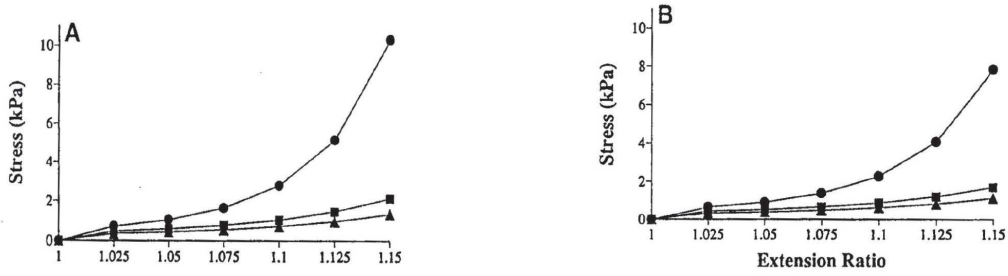

(a) In fibre direction

(b) In cross-fibre direction

Figure 4.2: Stress-extension relationship computed for equibiaxial loading. Triangles and boxes computed using two different methods, circles experimental values.

In figure 4.3, we can see the equibiaxial stretch data exercised in a thin rectangular slab of non-contracting muscle. It can be observed, the non-linear stress-stretch response over finite strains. Certain hysteresis in the behavior of the fiber direction and the cross-fibre direction.

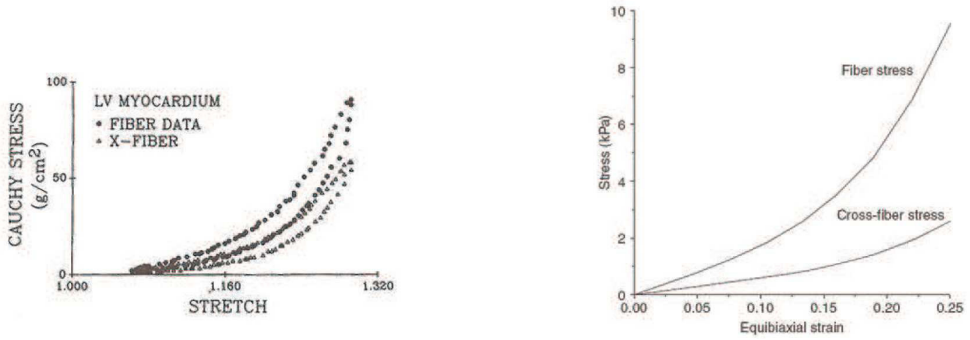

(a) Equibiaxial stretching data

(b) Equibiaxial strain data

Figure 4.3: Relationship computed for equibiaxial loading

In the work presented in this thesis, the fibre properties are modeled as a one-dimensional element and, in this chapter, we determine the properties of the passive part of the muscle to model it as a volumetric three dimensional finite element. In the figure 4.3(b) we can see that the fibre strain-stress curve which is due to the active part of the muscle and the Cross fibre stress-strain curve due to the passive part of the muscle.

If the connective tissue that surrounds the fibre is well joined to the fibres, we can make the hypothesis that the strains of the fibres are similar in order of magnitude than the strains of the

connective tissue in the same direction. Consequently and taking into account the information of the previous chapter, in which the values of the fibre strain $\varepsilon_f < 0.01$, we can consider that is a good first approximation. Some hysteresis in the stress-strain relationship are not been either taken into account. In chapter five, we are going to considerer the most realistic model (as a hyperelastic material) to describe the behavior of the passive part of the muscle due to the connective tissue.

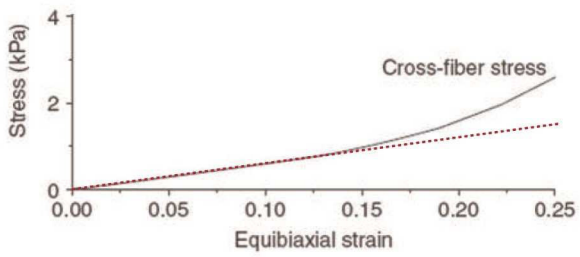

Figure 4.4: Considering linear elasticity for $\varepsilon_f < 0.1$

The numeric resolution in this case is very similar to the previous chapter. The main difference in this methodology is the calculus of the rigidity matrix $[K^k]$, the mass matrix $[M^k]$ and the force vector $[F^k]$. With this change of strategy, the results in each steep of the partial differential equation are the nodal displacements in every one direction of the space. In the Appendix B we can see the details this formulation based on the finite element method using isoparametric hexahedrical elements.

4.2 Linear Elastic Simulation

Once we have build our model, we can simulate the dynamics of the Inguinal region. First we do not consider any pathology in order to obtain a normalized dynamic behavior. After that, we will study the influence of the different parameters involved in the simulation. These results will provide a better understanding of the hernia genesis.

4.2.1 Initial Values

We have make the simulation for the normal behavior with the values obtained of the previous works of J.Bestel and of M.Sermesant. Moreover, we have incorporated the values of reference more usual for the magnitudes not included in these works.

Values for the Model and Material

ρ	Density of the material: $1.05e^{-5}\ MPa/mm^2$.
m_1	Young modulus for muscular tissue: 0.076 MPa.
m_2	Young modulus for tendinous tissue: 50 MPa.
ν	Poisson's coefficient: 0.49
t	Time for the simulation: 1 seg.

Values for the Activation Potential Function: $u(t)$

T	Time where the function $u(t)$ is activated (non zero): 0.45 seg.
φ_+	Time where the function $u(t)$ is positive: 0.2 seg.
φ_-	Time where the function $u(t)$ is negative: 0.25 seg.
K_{ATP}	Constant for adenosinetriphosphate increment: 10 seg^{-1}
K_{RS}	Constant for calcium reduction: $-10\ seg^{-1}$

Values for the Partial Differential Equation

u^0	Initial value for displacement in each node: 0 mm.
$\dot{u}^0$	Initial value for the displacement velocity in each node: 0 mm.

Values for the Differential Equation

$k_{c_{\max}}$	Maximum stiffness for the contractible element: 1 MPa.
k_p	Stiffness for the passive element: 2 MPa.
k_s	Stiffness for the series element: 100 MPa.
$\sigma_{c_{\max}}$	Maximum stress for the contractible element: 0.18 MPa.
$\dot{\varepsilon}_c(0)$	Initial velocity of strain: 0 MPa.
$\sigma_c(0)$	Initial stress: 0 MPa.
$k_c(0)$	Initial stiffness: 0 MPa.

4.3 Dynamic Mechanisms Description

We can state that the obtained results are qualitative and quantitatively equivalent to the works realized by M. Sermesant and J. Bestel in what it recounts to tension deformation and nodal

displacement. In spite of it, we can observe that now it exists a minor variation of volume of the muscle along the contraction (less than 1.e-4 per cent), so that here is assumed that the model reproduces with major reliability the real model.

In the next section, we will emphasize that the dynamic mechanisms proposed by A.Keith happen in the same form that he postulated, both the shutter mechanism and the closing of the inguinal deep ring. In any case, we can affirm that it exist a defence mechanism for healthy individuals, considering that we have also observed pathological cases in which the shutter mechanism not only is not a defence mechanism, but in addition it could facilitate the appearance of hernias.

Finally, we show how is the dynamic in the internal oblique muscle with the image sequences (figure 4.10). We can appreciate the special behavior in the area of the Hessert's triangle.

4.3.1 The Shutter Mechanism

The first dynamic mechanism for the inguinal region is the one described by A.Keith: the shutter mechanism. This mechanism was presented in 1923 and was described as a defence mechanisms, and also it have to support the intra-abdominal pressures in the inguinal orifice. There has been stated how it works the closing mechanism for Hessert's triangle. We can see a scheme of the close up of the triangle in the figure 4.5. The area of the above mentioned triangle has been measured in every instant of time and there has been stated that from an initial value of 8,97 cm (according to [54]) his area has got down until 8,2 in the moment of maximum contraction, and to recover finally his original area.

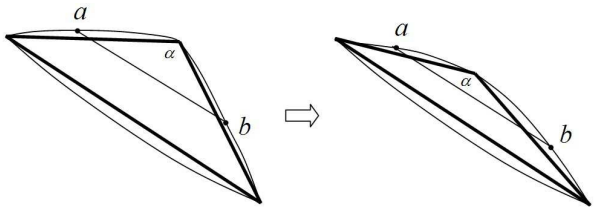

Figure 4.5: Scheme of the variation of Hessert's triangle in a contraction, the distance between the points a and b increases when the angle increases

In turn we have also measured the angular variation of the angle included between the oblique internal muscle and the aponeurotic tissue of the transverse muscle of the abdomen. We have verified that this angle opens up during the contraction of the muscle and closes up again during the relaxation and recovers his initial position (figure 4.6).

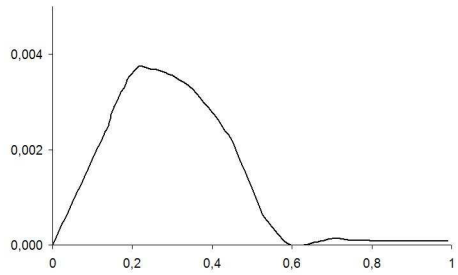

Figure 4.6: Graph of values in radians the variation of the angle of Hessert's triangle

4.3.2 Enclosure of the Internal Ring

The second dynamic mechanism described by A.Keith is the closing of the inguinal deep ring. This mechanism was presented in 1923 and was described as a defense mechanism, that supports the intra-abdominal pressures on the inguinal orifice. The closing of the inguinal deep ring consists on the fact that the props of the inguinal ring (composed by tendinous tissue) approach the muscular tissue of the oblique internal muscle. In the figure 4.7 one can see a scheme of the closing of the inguinal deep ring, which takes place during the phase of muscular contraction. To simulate the inguinal deep ring we have used the fact that this one is composed of tendinous tissue, the composition of the tendinous tissue is sufficiently documented ([33], [70], [20]). To determine his position and form, we have used photographic documentation, and the help of Dr. Manuel Lopez Cano, who has guided us all the time.

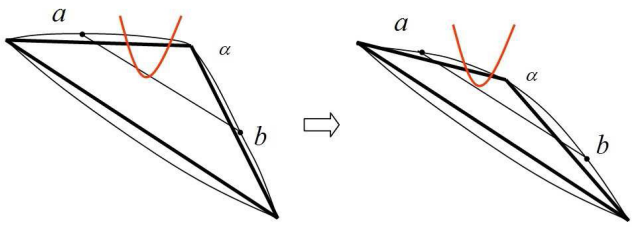

Figure 4.7: The inguinal deep ring (in red) is closed when the muscular contraction takes place

In this case, at each instant we have taken the measure of the area included between the props of the inguinal ring and the muscular tissue of the oblique internal muscle. We have stated that the area included by the inguinal ring decreases up to the moment of maximum contraction to recover finally its initial position (figure 4.8).

As a consequence of the obtained results in our simulations, we can conclude that the de-

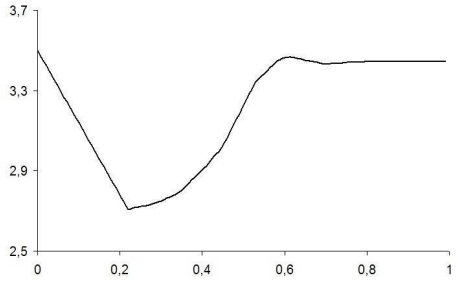

Figure 4.8: Variation of the area included by the internal ring, in the vertical axis we have the measure of the area in cm^2 and in the horizontal one we have the time in seconds.

scription of the defense mechanisms introduced by A. Keith behave as he predicts.

4.3.3 Stress on the Fascia

Finally, we are going to observe the results obtained during the simulation of the weakest element of the inguinal region, the fascia. This membrane represents the only structural element preventing the internal organs from crossing the inguinal orifice. It is necessary to emphasize, that this membrane in spite of having high breaking resistance, is the weakest element of the region, so that it seems natural that this is the one yields when an extreme effort takes place. It is also important to emphasize the weakness of the facia because it has no more than 0.3 mm of thickness.

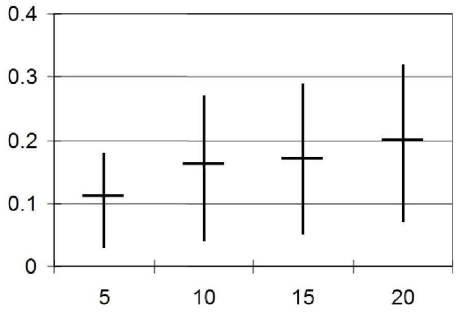

Figure 4.9: Range of values of the force supported by a segment ab of Hessert' triangle in parallel to the inguinal ligament, with his median in the horizontal line, in the horizontal axis K_{ATP}'s different values and in the vertical axis the force obtained in N.

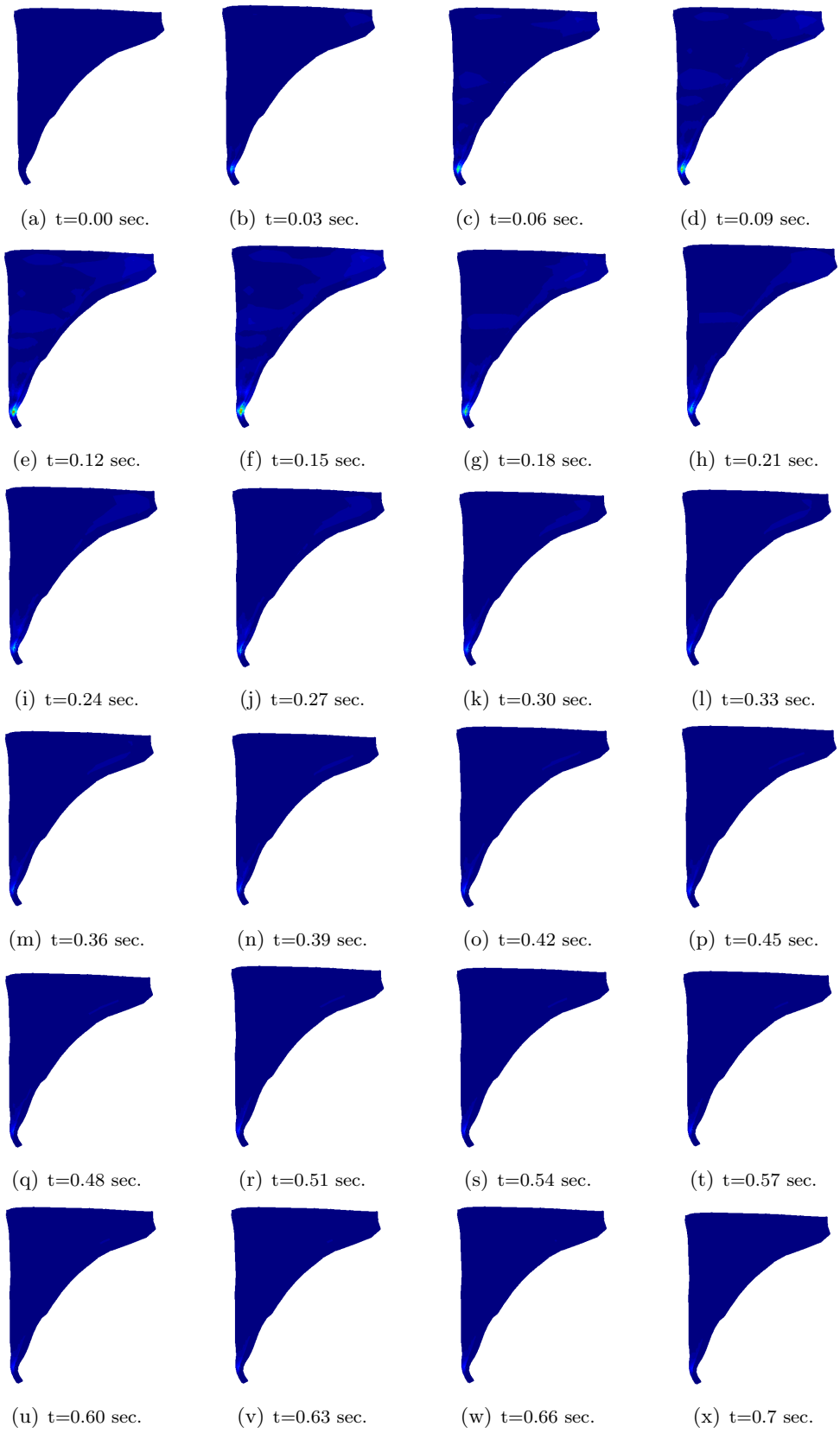

(a) t=0.00 sec. (b) t=0.03 sec. (c) t=0.06 sec. (d) t=0.09 sec.

(e) t=0.12 sec. (f) t=0.15 sec. (g) t=0.18 sec. (h) t=0.21 sec.

(i) t=0.24 sec. (j) t=0.27 sec. (k) t=0.30 sec. (l) t=0.33 sec.

(m) t=0.36 sec. (n) t=0.39 sec. (o) t=0.42 sec. (p) t=0.45 sec.

(q) t=0.48 sec. (r) t=0.51 sec. (s) t=0.54 sec. (t) t=0.57 sec.

(u) t=0.60 sec. (v) t=0.63 sec. (w) t=0.66 sec. (x) t=0.7 sec.

Figure 4.10: Sequence of stress variation in the internal oblique muscle in 0.7 sec. We can observe the maximum stress in red at instant 0.15 in the area of Hessert's triangle.

4.4 Study of the System Under the Variation of Parameters

In the next sections we will study the influence on the inguinal region dynamics when we change the different parameters involved in the simulation. Moreover, the natural variability of these parameters forces us to study how the system behaves under their slight variations. Variations in these parameters are associated with several pathologies in the region [64] that eventually lead to failure of the natural hernia-protection mechanisms.

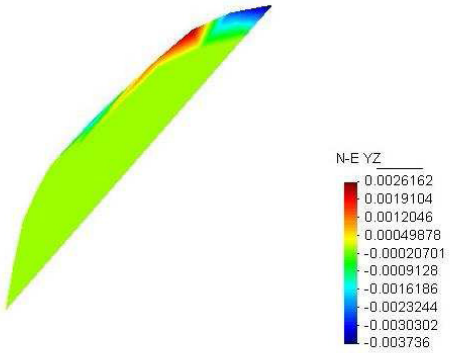

Figure 4.11: Diagram of strains of the fascia placed in Hessert's triangle in the moment of contraction. The zone in red fits with the region of the fascia in touch with the muscular tissue.

More specifically, we focus on the effects on the fascia transversalis since it is widely accepted that this tissue plays an important role in the origin of inguinal hernias. Figure 4.11 shows the strain on the fascia transversalis. Assuming that the tissue is uniform, these areas in red are the ones with the highest risk of fracturing due to the strain exerted. These maximum strain values will be the main focus of our attention. Since for the reference simulation, maximum strain in the fascia is 0.00023 any values above this figure will indicate greater strain and therefore a greater risk of fracture. Values below this figure will indicate lesser strain and therefore a lower risk of fracture.

We have also observed the variation in dynamics of the internal oblique muscle (see figure 4.12). Strain and stress were measured for the whole period of simulation. However, unlike what happened with the fascia, we did not observe any significant values that would explain the muscle disfunction. This does not happened when a hernia occurs.

Since there are only few real measurements of the properties of the fascia, we can use numerical simulation to achieve a first approximation to the real situation. Variation in the physical parameters, using measurements of the region from previous studies [59], [66] and [54], is used to represent the variability we would find in a random sample of individuals.

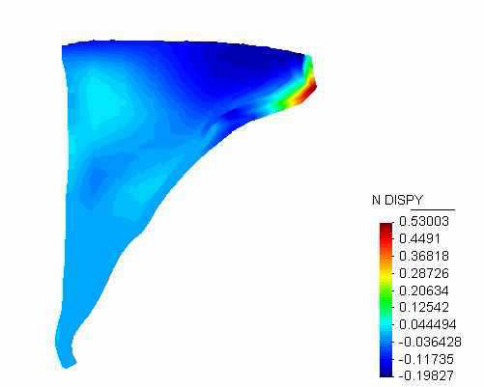

Figure 4.12: Graph of nodal displacements of the internal oblique muscle in the moment of maximum contraction.

For the simulations performed in the next Sections, we only modify the physical and chemical properties of the internal oblique muscle or of activation mechanisms that are not involved in the muscle's macroscopic behaviour. For the properties of the fascia we took normal values of healthy individuals (non-pathological cases) in order to determine how these parameters affect a normal model and explain actual movement.

Our study is based on parameters that are relevant to the origin of hernias, though their real effect has not yet been proof. Our aim is to evaluate the real effect of these parameters on the properties of the fascia and, more specifically, on the strain supported by this tissue. The relationship between strain and these parameters will indicate possible elements of risk or protection in the origin of hernias. At the same time, we hope to confirm or reject several current theories.

4.5 Study of Chemical Parameters

In this section we will study the effect of the velocity calcium variation (K_{ATP}), the inflexibility elements in Hill-Maxwell model (Ks and Kc_{max} in figure 2.9) and the variation on period of contraction affects in the maximum strain values on the fascia transversalis.

4.5.1 Effect of Variation in K_{ATP}

The constant K_{ATP} regulates the velocity with which calcium crosses the walls of the sarcomeres. It is therefore largely responsible both for the amount of calcium in the sarcomere and the strain generated by the sarcomere, since this is regulated by the calcium concentration. Figure 2.7

shows the relationship between calcium concentration and K_{ATP}, the constant of the model used.

As we have seen in our study of muscular contraction, muscular tissue activity is a consequence of the activity of the sarcomeres. The actin-myosin bridges must be created, so the calcium concentration must change if muscular activity is to be registered. The velocity with which the calcium enters the sarcomeres is related to the muscular contraction since the activation of the muscle and the force exerted by it are direct consequences of this value K_{ATP}. It is natural to suppose that the change in these increases in concentration must alter the muscular force developed and the results of our simulation confirm this supposition. Using similar values to those of J.Bestel [10] we observed (figure 4.13) a direct dependence between the increase in this parameter (K_{ATP}) and the stress developed by the muscle.

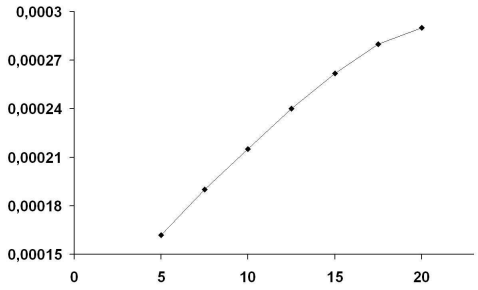

Figure 4.13: Graph of the maximum strain in the fascia in vertical axis. In the horizontal axis, we have various values for K_{ATP}, in sec^{-1}.

4.5.2 Variation in Ks and Kc_{max}

We performed several simulations with variations in parameters Ks and Kc_{max}. Parameter Ks is associated with the maximum inflexibility of the element in series (figure 2.9) of the Maxwell model. Parameter Kc_{max} is the maximum inflexibility of the contractile element of that model.

For parameter Ks, we started from the reference value of 100 MPa and the values taken for the various simulations ranged from 75 MPa to 125 MPa. After the contraction and recuperation processes had been completed, several differences were observed until the initial position was regained. However, these differences were not significant during the contraction process either in the fascia or in the internal oblique muscle, so we rejected the possibility of any link to the cause of hernias.

For parameter Kc_{max} we started from the reference value of $0.18MPa$ and the values taken for the various simulations ranged from $0.12MPa$ to $0.25MPa$. After contraction, no significant differences in the simulations were observed either in the contraction process or in the process

to regain initial position. However, we cannot disregard the importance of this parameter for our simulation because in cases with extreme values we did observe important differences in behaviour, though we were unable to find any correspondence between them and the real situation.

4.5.3 Variation in the Period of Contraction

We studied how the period of contraction affects the Hessert triangle by varying the time during which the muscle is in the contraction phase, i.e. the time during which the sarcomere contracts. As we have seen, this parameter is directly related to the curve of the calcium used in our model and to the calcium concentration.

The time during which the contraction process is active is expected to have a direct effect on movement in the region. We therefore varied the time during which the sarcomere is in contraction with increments of 0.01 seconds from the initial reference value of 0.15 seconds. As expected, we found that strain increases as the period of contraction increases (see figure 4.14).

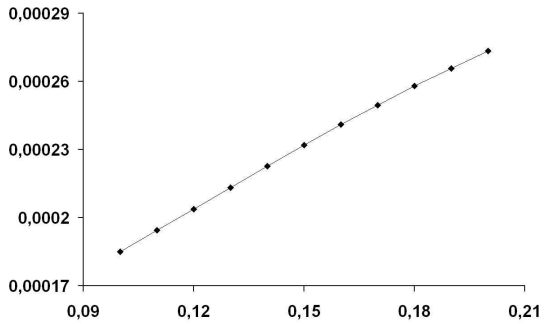

Figure 4.14: Graph of the maximum strain in the fascia in vertical axis. In the horizontal axis, we have various values for that last phase of contraction in s.

4.6 Study of Physical Parameters

In this section we will study the effect of the muscular stress, Young's modulus in the muscular tissue and tendinous tissue, the density variation, Poisson's ratio, intraabdominal pressure and gravity affects in the maximum strain values on the fascia transversalis on the muscular contraction.

4.6.1 Variation in Muscular Stress

As J.Bestel and other authors have shown, the maximum stress observed in healthy muscular tissue is approximately $0.18Mpa$ at the time of maximum contraction. For several reasons, however, changes to this value are common and observed values range between $0.10Mpa$ and $0.20Mpa$. Figure 4.15 shows the results of our simulations for several values of muscular strain.

When we measured maximum strain in the fascia transversalis (figure 4.11), we observed that the strain at the time of maximum contraction increases as muscular stress increases (figure 4.15). The stress borne by the fascia therefore also increases as the muscular stress increases.

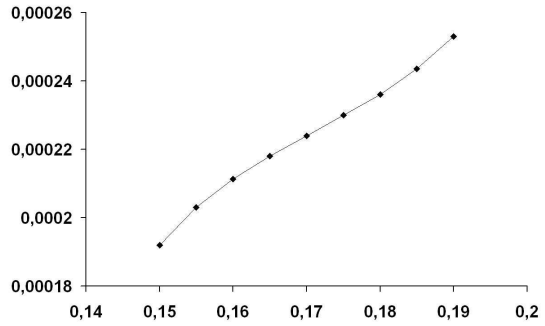

Figure 4.15: Graph of the maximum strain in the fascia in vertical axis. In the horizontal axis, we have various values of the muscular maximum stress in MPa.

4.6.2 Variation in Young's Modulus

Young's modulus, or the elasticity modulus, characterises the elastic behaviour of a material according to the direction in which a force is applied to it. For a linear isotropic material, Young's modulus has the same values for traction and compression since this constant is independent of the effort exerted on the material provided this does not exceed the maximum (called the elastic limit). These values are always greater than zero: if, for example, we exert traction on a rod of a certain material, the increase in length never decreases. This behaviour was first observed and analysed by English scientist Thomas Young in the nineteenth century.

Both Young's modulus and the elastic limit depend on the material. The elasticity modulus is an elastic constant and, like the elastic limit, it can be calculated empirically for a sample of material by subjecting it to traction.

The elastic limit is not important for our simulations of muscular contraction. In accordance with [82], the values of stress are much lower than the elastic limits of the materials (the muscular and tendinous tissues)

Effect of Variation in Young's Modulus on Muscular Tissue

We have subjected our model of muscular contraction to several simulations using the state of reference and several values of Young's modulus for muscular tissue obtained previously in T. Wolloscheck et al. [82].

It is generally agreed that the average value of Young's modulus for healthy muscular tissue is determined in [67]. Variations in this value depend on the individuals in the sample.

When we measured maximum strain on the fascia transversalis (figure 4.11), we observed that the strain to which the fascia is subjected at the time of maximum contraction diminshes as Young's modulus increases (figure 4.16). The stress borne of the fascia therefore also dimninishes as Young's modulus increases. This observation coincides with that of M.L. Ajmani and K.

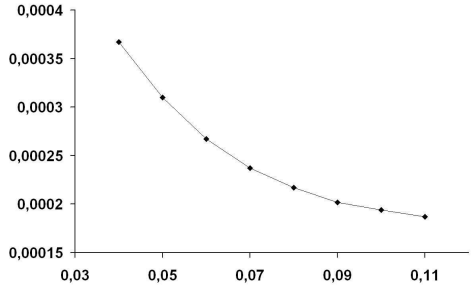

Figure 4.16: Graph of the maximum strain in the fascia in vertical axis. In the horizontal axis, we have values of Young's module in MPa. The maxim strain value for the reference simulation is 0.00023

Ajmani [4], who established a direct relationship between the origin of the muscular tissue and the appearance of hernias such that the higher Young's modulus in muscular tissue, the lower the risk of suffering a hernia.

Degradation of Tendinous Tissue

We subjected our model of muscular contraction to several simulations using the state of reference and several values of Young's modulus for tendinous tissue obtained previously by T. Wolloscheck et al.[82]. It is generally agreed that the average value of Young's modulus for healthy tendinous tissue can be found in [67] and fixed in 1.05 MPa/mm^2. However, values for tendinous tissue can depend both on the area from which the sample is extracted and on the concerned individual.

When we measured maximum strain in the fascia transversalis (figure 4.11), we observed that the strain to which the fascia is subjected at the time of maximum contraction increases as

Young's modulus increases (figure 4.17). The stress borne of the fascia therefore also increases as Young's modulus increases.

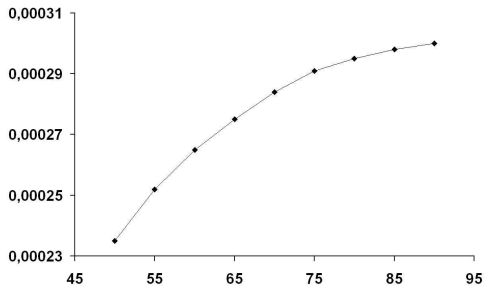

Figure 4.17: Graph of the maximum strain in the fascia in vertical axis. In the horizontal axis, we have values of Young's module in MPa/mm^2.

This observation coincides with that of Ajabnoor et al. [3] and by Condon [16], who established a predisposition for the development of hernias in individuals with flexible tendinous tissue that has lost some of its natural properties.

4.6.3 Effect of Variation in Density

Density is associated with the quality of muscular tissue. Above-normal density is associated with muscle rigidity, muscle ageing and hypertrophy, while below-normal density is associated with an abnormal increase in connective tissue probably due to an increase in the concentration of fatty tissue in the interior of the muscle. It is often caused by a sedentary lifestyle.

We subjected our model of muscular contraction to several simulations using the state of reference and several values of muscle tissue density obtained previously in [82].

It is generally agreed that the average density of live tissue is near of $1.05e^{-5}MPa/mm$[2 [67]. When we measured maximum strain in the fascia transversalis, we observed that the strain to which the fascia (figure 4.11) is subjected at the time of maximum contraction decreases as density increases. The stress borne of the fascia therefore also decreases as density increases.

4.6.4 Variation in the Coefficient of Incompressibility

The Poisson ratio ν is an elastic constant that measures the narrowing of a section of a prism of a linear isotropic elastic material when this stretches longitudinally and contracts in directions perpendicular to the stretching.

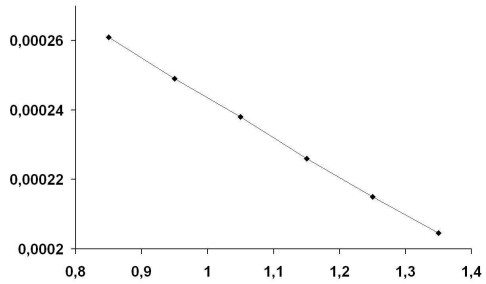

Figure 4.18: Graph of the maximum strain in the fascia in vertical axis. In the horizontal axis, we have values of the module of density in gr/mm^3.

It is generally agreed that muscular tissue is incompressible so, as several studies have shown, the Poisson ratio should be around 0.5. Specifically, as [68] indicates, the reference values are roughly these [10] for healthy muscular tissue. For several reasons, however, variations in this value are common and, in agreement with the bibliography, we used values between 0.42 and 0.49. Figure 4.19 shows the results of our simulations.

When we measured maximum strain in the fascia transversalis (figure 4.11), we observed that the strain at the time of maximum contraction increases as the Poisson ratio decreases (4.19). The maximum stress borne of the fascia therefore decreases as the Poisson ratio increases.

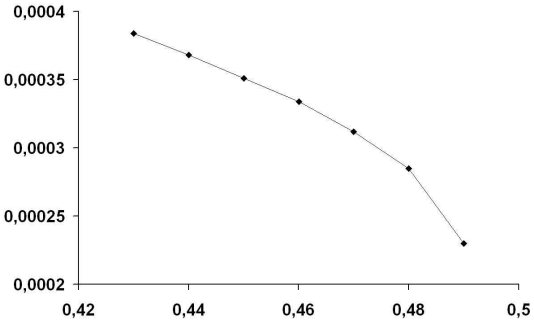

Figure 4.19: Graph of the maximum strain in the fascia in vertical axis. In the horizontal axis, we have various values for Poisson's coefficient.

4.6.5 Variation in Intraabdominal pressure

In normal conditions the pressure in the abdominal cavity (PIA) is equal to atmospheric pressure (i.e. 0) and may be even lower in newborns diagnosed with congenital diaphragmatic hernias, though transitory increases may occur physiologically due to respiratory movements, coughing, sneezing, defecation, etc. or progressively due to pregnancy, peritoneal dialysis treatment or the presence of ascitis. Intraabdominal hypertension is defined as an increase in pressure above 10

mmHg (approx. 0.00133 Mpa) inside the abdominal cavity in a state of rest.

Using the reference values obtained in [66], [31], [59] and the previously described pressure model, we conducted several simulations at several values of intraabdominal pressure. Pressure was highest in the centre of the muscle and tended to diminish towards the sides. Our results are

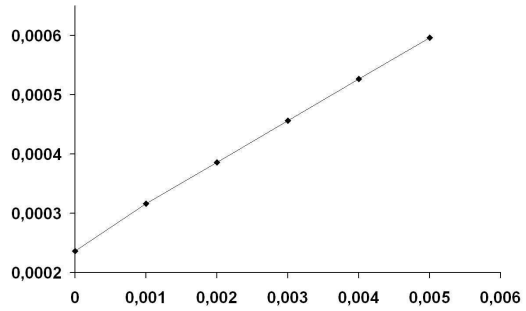

Figure 4.20: Graph of the maximum strain in the fascia in vertical axis. In the horizontal axis (in MPa.), we have various values for the intraabdominal pressure.

agree with those of [7] and [55], which established a direct relationship between intraabdominal pressure and the origin of hernias, since an increase in the strain borne by the fascia transversalis makes it more likely that the fascia will tear.

4.6.6 Effects of Gravity

So far in this study, we have conducted simulations of free objects in space without considering the effects of gravity. In this Section we have added the effects of the force of gravity described in subsection 3.2.5 to the reference simulation of the previous chapter.

We observed no qualitatively significant differences due to the effect of gravity. The maximum strain borne by the fascia $0,0002526$ is higher than when its weight is not considered $0,0002355$ but not by so much.

As including gravity does not lead to any major change, we will use the former result to continue our qualitative (not quantitative) study of the stresses and strains borne by the tissue in this region since it will enable us to compare with the previous results more easily.

(a) Scheme of fascia trasversalis without gravity (b) Scheme of fascia trasversalis with gravity

Figure 4.21: Plot of the strains for the fascia with gravity and without gravity

4.7 Study of Geometrical Parameters

In this section we will study the variation effect of the muscular position in the maximum strain values on the fascia transversalis.

4.7.1 Variation in Muscular Mass

It is generally agreed that a relationship exists between muscular mass and the force developed by this mass in the longitudinal direction in which the muscle fibres are arranged. We can say, therefore (though this is not an aim of the study), that in the model used the increase in mass leads to an increase in the force developed at the ends.

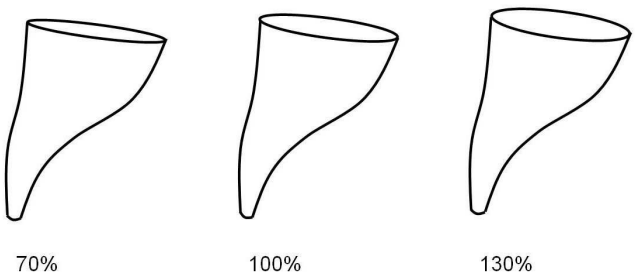

Figure 4.22: Scheme of variation in muscular mass for the internal oblique muscle.

In our study, however, we have varied the muscular mass in the direction orthogonal to the fibre (in figure 4.22). In this way we have varied the volume but not the length. After subjecting

the resulting models to muscular contraction, we measured the maximum strain on the fascia transversalis at the time of maximum contraction. Figure 4.23 shows that strain is maximal when the muscular mass is lowest.

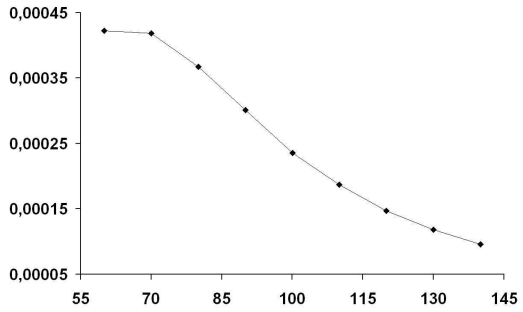

Figure 4.23: Graph of the strain of the fascia. In the horizontal axis they find diverse values of the muscular mass in %, in the vertical one we have the values of strain.

This observation coincides with those of A. Keith [41] and C. Ogilvie [57], who demonstrated that individuals whose abdominal fibromuscular wall in the inguinal region is weaker have a greater propensity to develop inguinal hernias.

4.7.2 Variation in the Extension of the Muscular Tissue

Each muscle contains one part with muscle tissue (dynamically active) and one part with tendinous tissue (dynamically passive). How these parts are distributed depends on both the muscle and the individual in question. In this section we study how different proportions of tendinous tissue affect the internal oblique muscle and the area of the Hessert triangle covered by the fascia transversalis.

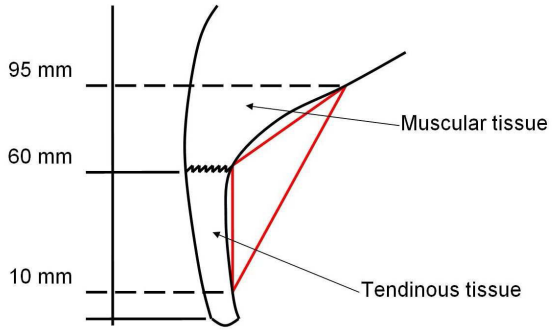

Figure 4.24: Scheme of the insertion of muscular tissue in the tendinous tissue. Usually, we find this insertion around 60 mm. from the muscle origin. The Hessert's triangle in red.

The study by Munhequete [54] showed that the average length of the origin of the lower fibres of the internal oblique muscle from the pubic tubercle is about 60 mm. In some cases the tendon can reach 90 mm and cover the whole triangle. In other cases it can be just 10 mm long.

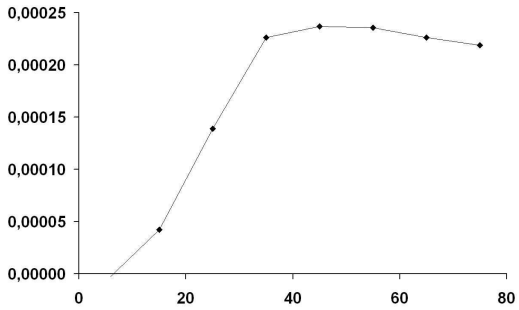

Figure 4.25: Graph of the maximum strain in the fascia in vertical axis. In the horizontal axis (in *mm.*), we have various values for the length of the tendinous tissue.

Experimental data in this area are inconclusive but it seems to be a direct relationship between the extension of the tendinous tissue and the origin of hernias. The study by Munhequete suggested a possible relationship between the length of tendinous tissue and the propensity to suffer hernias. The study by M.L. Ajmani and K. Ajmani [4] established a direct relationship between the origin of hernias and the distance from the origin of muscle fibres in the internal oblique muscle. Our results therefore coincide with the results of these studies.

4.7.3 Variation in the Area of the Hessert Triangle

The area of the Hessert triangle has been studied in detail in [54], which showed that the size of the triangle depends on each individual.

Several studies ([1], [29]) have directly related the size of the Hessert triangle with the risk of suffering a hernia. [29], for example, showed that there is a great risk of hernia when the triangle is over 150 mm long.

In our model, however, we found no significant differences due solely to variations in the size of this area. We did find significant differences that can be attributed to conditions related to movement in the Hessert triangle (e.g. changes in the length of tendinous and muscle tissues), but we cannot state that these are due exclusively to the size of the triangle.

4.7.4 Variation in the Position of the Muscle in Space

Given such diversity in individuals, we now consider variation in the relative positions of the elements of the lower abdomen by performing two different movements in the internal oblique muscle. In accordance with human anatomy, we consider that the interior of this muscle is fixed because this is where the pubic tubercle is located. We then perform two turns with their centres located in the pubic tubercle 4.26. The first of these turns is from the front to the back and the second is from left to right.

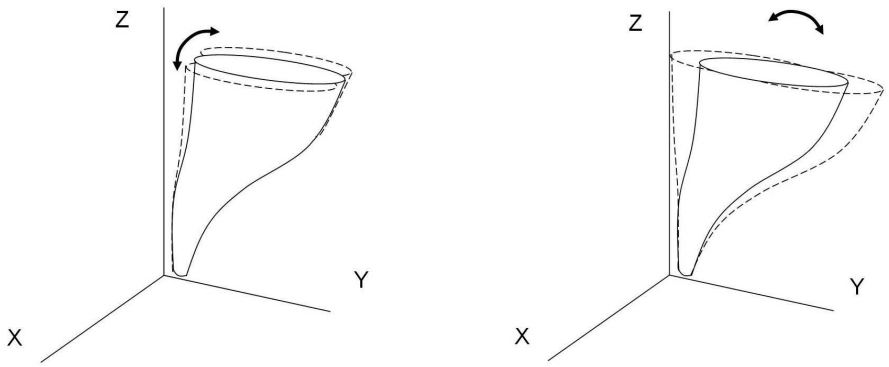

(a) Turn in longitudinal angle (b) Turn in transversal angle

Figure 4.26: Two angular variations for the muscular position.

To analyse these variations we will consider the same model as in the previous cases except that now we will also consider gravity.

Variation in the Longitudinal Angle

With the centre in the pubic tubercle and with the turning axis parallel to the Y axis, we performed several simulations with turning angles ranging from -10 to $+10$ degrees. At the time of maximum contraction, we measured the greatest strain in the fascia transversalis.

The negative angle indicates a more vertical position of the muscle, while the positive angle indicates a more horizontal position. We observed that the most horizontal position produced the greatest strain on the fascia.

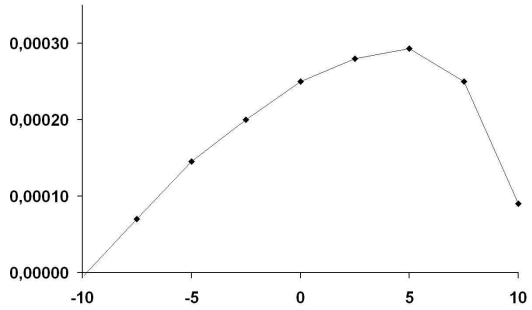

Figure 4.27: Graph of the maximum strain in the fascia in vertical axis. In the horizontal axis (in mm.), we have various values for the length of the tendinous tissue.

Variation in the Transversal Angle

With the centre in the pubic tubercle and with the turning axis parallel to the X axis, we performed several simulations with turning angles ranging from -10 to $+10$ degrees. At the time of maximum contraction, we measured the greatest strain in the fascia transversalis.

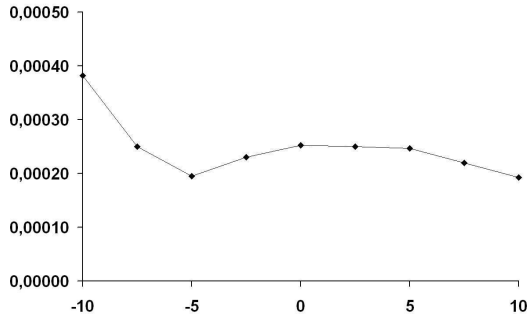

Figure 4.28: Graph of the maximum strain in the fascia in vertical axis. In the horizontal axis (in mm.), we have various values for the length of the tendinous tissue.

The negative angle indicates a turn to the left (see figure 4.26), while the positive angle indicates a turn to the right. We observed that in this case changing the angle produced no significant differences in the values of maximum strain borne of the fascia.

4.7.5 Variation in the Angle of Insertion

The convergence in the pubic tubercle of the medial insertion of the lower fibres of the internal oblique muscle and the inguinal ligament forms an angle usually of around 22 degrees. This angle is called the angle of insertion between the internal oblique muscle and the inguinal ligament. It

reflects a greater or lesser extension of the area of inguinal space for the same length of inguinal ligament.

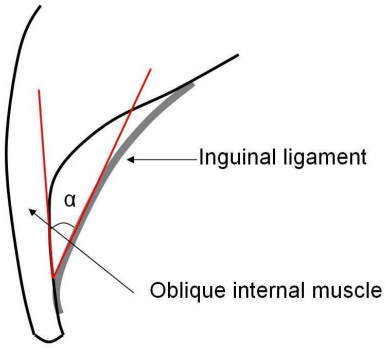

Figure 4.29: Plot of alpha angle (in red) between the internal muscle and the inguinal ligament.

In agreement with [54], though variations in this angle do not produce statistically significant differences between races or sexes, we found this angle to be greater in individuals with hernias.

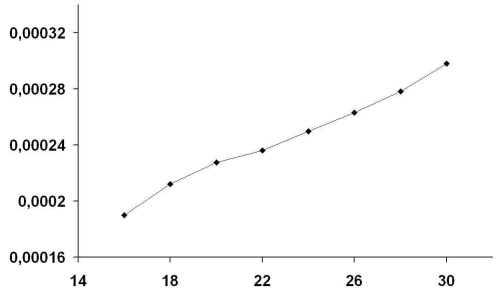

Figure 4.30: Graph of the maximum strain in the fascia in vertical axis. In the horizontal axis, we have various values for the angle.

We also found that this angle had a direct effect on the risk of hernias since the greatest values of strain on the fascia transversalis were recorded in simulations with the largest angle.

4.8 Conclusions

In this chapter, it has been studied the mechanical behavior of the inguinal region. The first aim has been proof of the certainty of the dynamic elements described by A.Keith. For the usual conditions for the simulation of the muscular contraction, we can corroborate the certainty of the shutter mechanism and of the closing of the inguinal deep ring. These two mechanisms have been accepted commonly by the medical community, as mechanisms of defense for the genesis

of inguinal hernias. In spite of this, the obtained results seem to show that these mechanisms are of defense in case of healthy tissue, but it not clear for the case that some pathologies that could appear.

In this Chapter, we have also studied the various parameters that plays a role physically or chemically in our model in order to better understand the dynamic behaviour of the region and, more specifically, that of the fascia transversalis.

We observed that several parameters, such as density and Young's modulus, have an important role in the dynamics of the region. We also verified that the period of muscular contraction has a direct effect on the strain borne by the fascia transversalis. This result has been confirmed empirically in cases of individuals with hernias.

We found that our model was consistent with these studies and we confirmed our hypotheses, thus validating our model as a tool for indirectly measuring the real dynamics of the region, especially regarding intraabdominal pressure and the distribution of tendinous tissue in the internal oblique muscle. For a more specific study of the region's mechanical characteristics, however, greater knowledge of the properties of the materials in the region and a more concrete model are needed.

Unfortunately few studies have analysed sufficient physical and chemical properties with real patients. Although a certain risk has been detected in the origin of hernias, with real increases in stress and strain in the weakest element of the region, we are unable to conduct a more detailed study. Despite the lack of data both on healthy individuals and on the physicochemical properties of individuals who develop hernias, however, we have established a direct relationship between our results and reality. This enables us to suggest possible risk factors in the origin of hernias.

Chapter 5

Non Linear Problem

All the previous considerations are in the range of small deformations, in this case we can assume lineal relations for all deformations in the body. In this chapter we are going to assume big deformations in the process. We need to distinguish between the reference configuration, where we fixe the initial position for the body and the deformed configuration, the configuration for each instant. Therefore, to study the relation describing the behavior for the solid deformations, we are going to use the reference configuration and also the deformed configuration.

Now, these stresses result from the deformation of the material, and it is necessary to express them in terms of some measure of this deformation such us, for instance the strain. These relationships, known as constitutive equations, obviously depend on the type of material under consideration and may be dependent or independent of time.

In this chapter the constitutive equations will be established in the context of a hyperelastic material, whereby stresses are derived from a stored elastic energy function. Although there are number of alternative material descriptions that could be introduced , hyperelasticity is a particularly convenient constitutive equation. In the Appendix C, we can see the usual notation for the non linear problem in biological tissues following the indications of [32]

5.1 Hyperelasticity

Materials for which the constitutive behavior is only a function of the current state of deformation are generally known as elastic. Here, $X \in \mathbb{R}^3$ designates the position of a particle in the reference configuration Ω. All tensor quantities are written in Cartesian systems throughout this chapter. Whenever indicial notation is employed, lower-case letters refer to the deformed configuration

and upper case to the reference configuration. The deformed and reference configurations are related by:

$$\varphi(\mathbf{X}) = \mathbf{X} + u(\mathbf{X})$$

Under such conditions, any stress measure at a particle $\mathbf{X}$ is a function of the current deformation gradient $\mathbf{F}$ associated with a particle and u is the displacement.

$$\mathbf{F} := \frac{\partial \varphi}{\partial \mathbf{X}}$$

Further, let

$$J := det\mathbf{F} = \frac{\rho_0}{\rho}$$

be the jacobian of the deformation, ρ_0 is the density in the reference state and ρ is the density in the actuality. For a volume-preserving deformation, $J = 1$. The right and left Cauchy-Green deformation tensors are, respectively,

$$\mathbf{C} := \mathbf{F}^T\mathbf{F} \quad and \quad \mathbf{B} := \mathbf{F}\mathbf{F}^T$$

The deformation gradient $\mathbf{F}$, together with the conjugate first Piola-Kirchhoff stress measure tensor $\mathbf{P}$, will be retained in order to define the basic material relationships. Consequently, elasticity can be expressed as,

$$\mathbf{P} = \mathbf{P}(\mathbf{F}(\mathbf{X}), \mathbf{X})$$

where the direct dependency upon $\mathbf{X}$ allows for the possible inhomogeneity of the material.

In the special case when the work done by the stresses during a deformation process only on the initial state at time t_0 and the final configuration at time t, the behavior of the material is said to be path-independent and the material is termed hyperelastic. As a consequence of the path-independent behavior and recalling from (Principle of virtual work) that $\mathbf{P}$ is work conjugate with the rate deformation gradient $\dot{\mathbf{F}}$, a stored strain energy function or elastic potential Ψ per unit undeformed volume can be established as the work done by the stresses from the initial to the current position as,

$$\Psi(\mathbf{F}(\mathbf{X}),\mathbf{X}) = \int_{t_0}^{t} \mathbf{P}(\mathbf{F}(\mathbf{X}),\mathbf{X}) : \dot{\mathbf{F}} dt; \qquad \dot{\Psi} = \mathbf{P} : \dot{\mathbf{F}} \tag{5.1}$$

Presuming that from physical experiments it is possible to construct the function $\Psi(\mathbf{F},\mathbf{X})$, which defines a given material, then the rate of change of the potential can be alternatively expressed as,

$$\dot{\Psi} = \sum_{i,j=1}^{3} \frac{\partial \Psi}{\partial \mathbf{F}_{i,j}} \dot{\mathbf{F}}_{ij}$$

Comparing this with equation 5.1 reveals that the components of the two-point tensor P are,

$$P_{i,j} = \frac{\partial \Psi}{\partial \mathbf{F}_{i,j}}$$

For notational convenience this expression is rewritten in a more compact form as,

$$\mathbf{P}(\mathbf{F}(\mathbf{X}),\mathbf{X}) = \frac{\partial \Psi(\mathbf{F}(\mathbf{X}),\mathbf{X})}{\partial \mathbf{F}} \tag{5.2}$$

Equation 5.2 followed by equation 5.1 is often used as a definition of a hyperelastic material ([32],[81] and [74]). The general constitutive equation 5.2 can be further developed by recalling the restrictions imposed by objectivity as discussed in [32].

To this end,Ψ a must remain invariant when the current configuration undergoes a rigid body rotation. This implies that Ψ a depends on $\mathbf{F}$ only via the stretch component $\mathbf{U}$ and is independent of the rotation component $\mathbf{R}$. For convenience, however,Ψ a is often expressed as a function of $\mathbf{C} = \mathbf{U}^2 = \mathbf{F}^T\mathbf{F}$ as,

$$\Psi(\mathbf{F}(\mathbf{X}),\mathbf{X}) = \Psi(\mathbf{C}(\mathbf{X}),\mathbf{X})$$

Observing that $\frac{1}{2}\dot{\mathbf{C}} = \dot{\mathbf{E}}$ is work conjugate to the second Piola.Kirchhoff stress $\mathbf{S}$, enables a totally Lagrangian constitutive equation to be constructed in the same manner as equation 5.2 to give,

$$\dot{\Psi} = \frac{\partial \Psi}{\partial \mathbf{C}} : \dot{\mathbf{C}} = \frac{1}{2}\mathbf{S} : \dot{\mathbf{C}}; \qquad \mathbf{S}(\mathbf{C}(\mathbf{X}),\mathbf{X}) = 2\frac{\partial \Psi}{\partial \mathbf{C}} = \frac{\partial \Psi}{\partial \mathbf{E}} \tag{5.3}$$

5.1.1 The Lagrangian Elasticity Tensor

The relationship between $\mathbf{S}$ and $\mathbf{C}$ or $\mathbf{E} = \frac{1}{2}(\mathbf{C} - \mathbf{I})$, given by equation 5.3 will invariably be nonlinear. Within the framework of a solution process, this relationship will need to be linearized with respect to an increment u in the current configuration. Using the chain rule, a linear relationship between the directional derivative of $\mathbf{S}$ and the linearized strain $D\mathbf{E}[\mathbf{u}]$ can be obtained, initially in a component form as,

$$DS_{IJ}[u] = \frac{d}{d\epsilon}|_{\epsilon=0} S_{IJ}(E_{KL}[\phi + \epsilon\mathbf{u}]) =$$

$$= \sum_{K,L=1}^{3} \frac{\partial S_{IJ}}{\partial E_{KL}} \frac{d}{d\epsilon}|_{\epsilon=0} E_{KL}[\phi + \epsilon\mathbf{u}]$$

$$\sum_{K,L=1}^{3} \frac{\partial S_{IJ}}{\partial E_{KL}} DE_{KL}[\mathbf{u}]$$

This relationship between the directional derivatives of $\mathbf{S}$ and $\mathbf{E}$ is more concisely expressed as,

$$D\mathbf{S}[\mathbf{u}] = \mathcal{C} : D\mathbf{E}[\mathbf{u}] \tag{5.4}$$

where the symmetric fourth-order tensor $\mathcal{C}$, known as the Lagrangian or material elasticity tensor, is defined by the partial derivatives as,

$$\mathcal{C} = \sum_{I,J,K,L=1}^{3} \mathcal{C}_{IJKL} \mathbf{E}_I \otimes \mathbf{E}_J \otimes \mathbf{E}_K \otimes \mathbf{E}_L$$

$$\mathcal{C}_{IJKL} = \frac{\partial S_{IJ}}{\partial E_{KL}} = \frac{4\partial^2 \Psi}{\partial C_{IJ} \partial C_{KL}} = \mathcal{C}_{KLIJ}$$

For convenience these expressions are often abbreviated as,

$$\mathcal{C} = \frac{\partial \mathbf{S}}{\partial \mathbf{E}} = 2\frac{\partial \mathbf{S}}{\partial \mathbf{C}} = \frac{4\partial \Psi}{\partial \mathbf{C} \partial \mathbf{C}}$$

5.1.2 The Eulerian Elasticity Tensor

It would now be pertinent to attempt to find a spatial equivalent to equation 5.4, and it would be tempting to suppose that this would involve a relationship between the linearized Cauchy stress and the linearized Almansi strain. Although, in principle, this can be achieved, the resulting expression is intractable. An easier route is to interpret equation 5.4 in a rate form and apply the push forward operation to the resulting equation. This is achieved by linearizing $\mathbf{S}$ and $\mathbf{E}$ in the direction of $\mathbf{v}$, rather than $\mathbf{u}$.

Recalling that $D\mathbf{S}[\mathbf{v}] = \dot{\mathbf{S}}$ and $D\mathbf{E}[\mathbf{v}] = \dot{\mathbf{E}}$ gives,

$$\dot{\mathbf{S}} = \mathcal{C} : \dot{\mathbf{E}} \tag{5.5}$$

Because the push forward of $\dot{\mathbf{S}}$ as well known to be the Truesdell rate of the Kirchhoff stress $\tau^0 = J\sigma^0$ and the push forward of $\dot{\mathbf{E}}$ is d, namely, it is now possible to obtain the spatial equivalent of the material linearized constitutive equation 5.5 as,

$$\sigma^0 = \mathfrak{c} : d \tag{5.6}$$

where $\mathfrak{c}$,the Eulerian or spatial elasticity tensor, is defined as the Piola push forward of $\mathcal{C}$ and after some careful indicial manipulations can be obtained as,

$$\mathfrak{c} = J^{-1}\phi_*[\mathcal{C}]; \qquad \mathfrak{c} = \sum_{i,j,k,l=1;I,J,K,L=1}^{3} J^{-1}F_{iI}F_{jJ}F_{kK}F_{lL}\mathcal{C}_{IJKL}e_i \otimes e_j \otimes e_k \otimes e_l$$

Often, equation 5.6 is used, together with convenient coefficients in $\mathfrak{c}$, as the fundamental constitutive equation that defines the material behavior. Use of such an approach will, in general, not guarantee hyperelastic behavior, and therefore the stresses cannot be obtained directly from an elastic potential. In such cases, the rate equation has to be integrated in time, and this can cause substantial difficulties in a finite element analysis because of problems associated with objectivity over a finite time increment.

5.2 Transverse Isotropy

There are two approaches to introducing the directional dependence on the deformation into the strain energy: restrict the way in which the strain energy can depend on the deformation, or

introduce a vector representing the material preferred direction explicitly into the strain energy. In the former approach, the strain energy can be expressed as a function of the Lagrange strain components in a coordinate system aligned with the fiber direction. Thus, all computations must be performed in this local coordinate system. In the presentation that follows, we choose the second approach.

We introduce a unit vector field $\mathbf{a}^0$ in the undeformed configuration that describes the local fiber direction, and require that the strain energy depend on this vector. In this case, the strain energy can be expressed as a function of the right Cauchy-Green deformation tensor and the vector field defining the preferred direction. Further, the strain energy now becomes an isotropic function in both arguments. Smith and Rivlin [72] developed a representation theorem for this case and Spencer [73] has presented relations for the strain energy at a material point in terms of five scalar quantities (invariants) derived from the tensor and vector fields. In the field of biomechanics, this type of representation has been used to model the material behavior with a fiber direction.

When the material undergoes deformation, the vector field $a^0(\mathbf{X})$ will deform with the body. After deformation the fibre direction may be described by a unit vector field $a(\varphi(\mathbf{X}))$. In general the fibers will also undergo length change. The fiber stretch, λ, can be determined in terms of the deformation gradient, $\mathbf{F}$ and the fiber direction in the undeformed direction,

$$\lambda \mathbf{a} = \mathbf{F}\mathbf{a}^0$$

Also, since $\mathbf{a}$ is a unit vector,

$$\lambda^2 \mathbf{a}\mathbf{a} = \mathbf{a}^0\mathbf{F}^0\mathbf{F}\mathbf{a}^0 = \mathbf{a}^0\mathbf{C}\mathbf{a}^0$$

This determines the fiber stretch in terms of the deformation gradient and the fiber direction in the undeformed configuration. A material with the above symmetry is called transversely isotropic. If it is hyperelastic as well, the form of $\tilde{\Psi}$ must be such that at a point X a function in terms of X, $\mathbf{C}$ and $\mathbf{a}^0$.

The dependence of the strain energy on $\mathbf{a}^0$ can be introduced explicitly into $\tilde{\Psi}$. This implies that the relationship between $\tilde{\Psi}$ and $C = F^T F$ can't be independent of the material axes chosen and, consequently, $\tilde{\Psi}$ is a function of the invariants of C and the fibre direction. Spencer has show that the following set of invariants can be used to fully define the relations,

$$\tilde{\Psi}(\mathbf{C}, X, \mathbf{a}^0) = \Psi(X, I_1(\mathbf{C}), I_2(\mathbf{C}), I_3(\mathbf{C}), I_4(\mathbf{C}, \mathbf{a}^0), I_5(\mathbf{C}, \mathbf{a}^0)) \tag{5.7}$$

where the invariants of C are defined here as,

$$I_1(\mathbf{C}) = tr\mathbf{C}; \qquad I_2(\mathbf{C}) = \frac{1}{2}[(tr\mathbf{C})^2 - tr\mathbf{C}^2]; \qquad I_3(\mathbf{C}) = det\mathbf{C} = J^2$$

$$I_4(\mathbf{C}, \mathbf{a}^0) = \mathbf{a}^0\mathbf{C}\mathbf{a}^0; \qquad I_5(\mathbf{C}, \mathbf{a}^0) = \mathbf{a}^0\mathbf{C}^2\mathbf{a}^0$$

Here, I_1, I_2 and I_3 are the standard invariants of the Cauchy-Green deformation tensor and the complete set of invariants associated with isotropic material behavior. The invariants I_4 and I_5 arise directly from the anisotropy introduced by reinforcing fiber family. These invariants represent contributions to the strain energy from the properties of the fibers and their interaction with other material constituents; I_4, for instance, is the square of the stretch along the fiber direction.

With the form 5.7 chosen for the strain energy, the satisfaction of material frame indifference and the material symmetry restrictions for transverse isotropy are assured. This relation is the starting point for deriving the stress and elasticity tensors and also provides the basis for the constitutive model.

5.2.1 Approach the Stress Tensor

Our interest is in developing a robust computational representation of transversely isotropic hyperelastic for an finite element code. The formulation is based upon a linearization about the current configuration, so we require expressions for both the Cauchy stress and spatial version of the 2nd elasticity tensor. This section provide explicit expressions for these tensor in a form suitable for numerical implementation of the corresponding constitutive behavior.

For a hyperelastic material, the 2nd Piola-Kirchhoff stress is derived from the strain energy as

$$\mathbf{S} = 2\frac{\partial \Psi}{\partial \mathbf{C}}$$

Using 5.7, we can express $\mathbf{S}$ as

$$\mathbf{S} = 2\left(\sum_{i=1}^{5} \frac{\partial \Psi}{\partial I_i}\frac{\partial I_i}{\partial \mathbf{C}}\right)$$

The terms $\partial I_i/\partial \mathbf{C}$ can be computed as,

$$\frac{\partial I_1}{\partial \mathbf{C}} = \mathbf{1}; \qquad \frac{\partial I_2}{\partial \mathbf{C}} = I_1\mathbf{1} - \mathbf{C}; \qquad \frac{\partial I_3}{\partial \mathbf{C}} = I_2\mathbf{1} - I_1\mathbf{C} + \mathbf{C}^2 = I_3\mathbf{C}^{-1}$$

$$\frac{\partial I_4}{\partial \mathbf{C}} = \mathbf{a}^0 \otimes \mathbf{a}^0; \qquad \frac{\partial I_5}{\partial \mathbf{C}} = \mathbf{a}^0 \otimes \mathbf{C}\cdot\mathbf{a}^0 + \mathbf{a}^0 \cdot \mathbf{C} \otimes \mathbf{a}^0;$$

where $\mathbf{1}$ represents the identity tensor.

If the material is incompressible, $I_3 = J^2 = 1$, Ψ is a function of only I_1, I_2, I_4 and I_5; however, an unknown pressure p enters the stress as reaction to the kinematic constraint on the deformation field. In this case, the 2nd Piola-Kirchhoff stress for an incompressible, transversely isotropic hyperelastic material can be written as

$$\mathbf{S} = 2\{(\Psi_1 + I_1\Psi_2)\mathbf{1} - \Psi_2\mathbf{C} + \Psi_4\mathbf{a}^0 \otimes \mathbf{a}^0 + \Psi_5(\mathbf{a}^0 \otimes \mathbf{C}\cdot\mathbf{a}^0 + \mathbf{a}^0 \cdot \mathbf{C} \otimes \mathbf{a}^0)\} + pJ\mathbf{C}^{-1}$$

The Cauchy stress is the push-forward of $\mathbf{S}$ by the deformation φ

$$\sigma = \frac{1}{J}\varphi_*(\mathbf{S}) \Leftrightarrow \sigma_{ij} = \frac{1}{J}\mathbf{F}_{iI}\mathbf{F}_{jJ}\mathbf{S}_{IJ}$$
$$= 2\{(\Psi_1 + I_1\Psi_2)\mathbf{B} - \Psi_2\mathbf{B}^2 + I_4\Psi_4\mathbf{a}^0 \otimes \mathbf{a}^0 + I_4\Psi_5(\mathbf{a}^0 \otimes \mathbf{B}\cdot\mathbf{a}^0 + \mathbf{a}^0 \cdot \mathbf{B} \otimes \mathbf{a}^0)\} + p\mathbf{1}$$

With, the notation $\Psi_a = \partial\Psi/\partial I_a$. Note that both $\mathbf{S}$ and σ are symmetric and the term in p is the hydrostatic pressure.

5.3 A particular Ψ for Muscular Tissue

Biological soft tissues are anisotropic, viscoelastic, inhomogeneous and undergo large deformations. However, the constitutive behavior of many tissues is relatively insensitive to strain over several decades of variation [25]. Also, these tissues reach a *preconditioned* state after repeated loadings; the loading and unloading cycles of the material are then repeatable and there is a minimal amount of hysteresis. There is also a minimal amount of the relaxation-creep and the peak stress during cyclic loading no longer decreases with time. These *pseudoelastic* tissues can then modeled using a hyperelastic approach. Hyperelasticity provides an ideal framework for numerical modeling of pseudoelastic soft tissue structures because it allows for large deformations and anisotropy. With a finite element approach, inhomogeneities can be modeled if data

are available. These models can be easily modified to extend their applicability to viscoelasticity and damage mechanichs.

Many soft tissues, as the muscles, are composed of fibers that run parallel to predominant axis of loading in vivo. These tissues also contain elastin, proteoglycans, glycolipids, water and fobroblasts (cells). All the tissue components together, are referred to as ground substance matrix. The water comprises between 60 and 70 % of the total weight of tissues such as ligaments and tendons, but it appears to be tightly bound to the matrix as it is difficult exude any significant amount compressive pressure. The microstructural organization of the constituents in these soft tissues yields mechanical characteristics that are crucial to physiological function. The overall response of the tissue to applied loads ans/or deformation is directly a result of the mechanical response of and interaction between its constituent materials.

5.3.1 The Energy

For the purposes of this model, the elastic response of the tissue will be assumed to arise from the resistance of the fiber family, the ground substance matrix, and their interaction. Further, it is assumed that the fibers are responsible for the transversely isotropic symmetry and that the ground substance, or matrix, is isotropic. Within the framework of incompressible, transversely isotropic hyperelasticity, the strain energy can be written as

$$\Psi = F_1(I_1, I_2) + F_2(I_4) + F_3(I_1, I_2, I_4) \tag{5.8}$$

where I_1, I_2 and I_4 are the invariants of the right Cauchy-Green deformation tensor. The function F_1 represents the material response of the isotropic ground substance matrix, F_2 represents the contribution from the fiber family, and F_3 is the interaction between the fibers and matrix.

The dependence of Ψ on I_4, can easily be replaced by an equivalent dependence on the stretch along the fiber direction, λ. This makes it somewhat easier to fit experimental data function. The dependence on I_3 has been omitted because of the incompressibility constraint ($J = \sqrt{I_3} = 1$). The dependence on I_5 has been omitted as well, as many of the effects governed by I_5 can be introduced into the function through the derivatives of the strain energy with respect to I_4.

The form 5.8 generalizes many constitutive equations that have been successfully used in the past to describe biological tissues ([15],[35],[36]). While this relation represents a large simplification when compared to the general case, it also embodies almost all the material behavior that one would expect from transversely isotropic, large-deformation matrix-fiber composites.

The Moonley-Rivlin material [53] offers an example of a form that can be used to describe the ground substance matrix:

$$F_1 = \frac{C_1}{2}(I_1 - 3) + \frac{C_2}{2}(I_2 - 3)$$

where the constants C_1 and C_2 are to be determined from experimental tests. If the constant C_2 is zero, then the resulting model is the neo-Hookean material. For many biological tissues, an exponential function may be appropriate for F_2 [26].

The function F_3 controls the interaction between the fiber family and the ground substance matrix. This can take several forms. Stretch along the fiber direction could cause stress to develop in the matrix, or vice versa. It is more likely that such an interaction would take the form of a shear coupling. Because shear testing is required to determine such effects, the experimental aspects are difficult. The applicability of 5.8 to the modeling of tissue has been determined by experiment.

A similar form to 5.8 is used to define the deviatoric strain energy, but instead of the strain energy being a function of the invariants, they are functions of their debiatoric counterparts, defined in terms of $\tilde{\mathbf{C}} = J^{3/2}\mathbf{C}$:

$$\tilde{I}_1 = tr\tilde{\mathbf{C}} = J^{-2/3}tr\mathbf{C}$$
$$\tilde{I}_2 = \frac{1}{2}((tr\tilde{\mathbf{C}})^2 - tr\tilde{\mathbf{C}}^2) = J^{-4/3}((tr\mathbf{C})^2 - tr\mathbf{C}^2)$$
$$\tilde{I}_4 = \mathbf{a}^0 \cdot \tilde{\mathbf{C}} \cdot \mathbf{a}^0 = J^{-2/3}\mathbf{a}^0 \cdot \mathbf{C} \cdot \mathbf{a}^0$$

Clearly, for an incompressible material, these invariants are equivalent to their counterparts defined. Now the strain energy is extended to the compressible range and is assumed to take an uncoupled from as defined by:

$$\Psi = \tilde{\Psi}(\tilde{\mathbf{C}}) = \tilde{F}_1(\tilde{I}_1, \tilde{I}_2) + \tilde{F}_2(\tilde{I}_4) + \tilde{F}_3(\tilde{I}_1, \tilde{I}_2, \tilde{I}_4)$$

With assumption, the stress can be written as,

$$\mathbf{S} = 2J^{-2/3}DEV\left[\frac{\partial\tilde{\Psi}}{\partial\tilde{\mathbf{C}}}\right]$$

The operator $DEV[\cdot]$ is the deviatoric projection operator for stress-like quantities in the reference configuration:

$$DEV[\cdot] = [\cdot] - \frac{1}{3}([\cdot] : \mathbf{1})\mathbf{1}$$

and

$$\frac{\partial \tilde{\Psi}}{\partial \tilde{\mathbf{C}}} = (\tilde{\Psi}_1 + \tilde{\Psi}_2 \tilde{I}_1)\mathbf{1} - \tilde{\Psi}_2 \tilde{\mathbf{C}} + \tilde{\Psi}_4 \mathbf{a}^0 \otimes \mathbf{a}^0$$

Now the 2nd Piola-Kirchhoff stress is given by:

$$\mathbf{S} = 2J^{2/3}\{(\tilde{\Psi}_1 + \tilde{I}_1\tilde{\Psi}_2)\mathbf{1} - \tilde{\Psi}_2\tilde{\mathbf{C}} + \tilde{\Psi}_4\mathbf{a}^0 \otimes \mathbf{a}^0 - \frac{1}{3}(\tilde{\Psi}_1\tilde{I}_1 + 2\tilde{\Psi}_2\tilde{I}_2 + \tilde{\Psi}_4\tilde{I}_4)\mathbf{1}\}$$

5.4 The Model

Finally, we are going to purpose a model with a nonlinear behavior. Thus, as the same way used in [69] we have the following 2nd Piola-Kirchhoff stress tensor:

$$S = S_s + S_h$$

where S_s is the part of the strain energy for an hyperelastic material and S_h is the linear stress of the J.Bestel model. S_h is well known for us, we have presented in the past chapters. S_s is defined by the strain energy and only have repercussion in non lineal terms. S is included following the indications in [86].

To define an accurate energy function to obtain S_s, we use the literature that exists in this sense [5] [32] [34] [60] [61], we need to define some functions F_1, F_2 and F_3 for our purpose. First, we are going to use a function F_1 as is defined for a Moonley-Rivlin material. Second, to ensure that the stress update and tangent stiffness were properly implemented into the existing code, numerical tests are performed. Finally, the extension of the Mooney-Rivlin model used for the our tests:

$$\tilde{\Psi}(\tilde{I}_1, \tilde{I}_2, \tilde{I}_4) = C_1(\tilde{I}_1 - 3) + C_2(\tilde{I}_2 - 3) + C_3(exp(\tilde{I}_4 - 1) - \tilde{I}_4)$$

This form has exponential behavior in the fiber direction, one of the characteristics seen in most soft tissues. For our reference simulation, we have taken usual values of parameter for alive tissue and more explicitly for the muscular tissue in the Mooney-Rivlin model([6], [74]). In this

sense, in the fiber direction we use the value $\lambda = 1.05$, and for the other constants we take the common values for alive tissue $C_1 = 1.5$, $C_2 = 0.$ and $C_3 = 0.2$.

5.5 Results

To do the simulation in our model we have used the same initial values that we have used in the previous chapters 7 and 8. We want to evaluate the difference between the elastic model and the hyperelastic model, so that we put the same initial conditions for the model and for the contour conditions. With this assumption, we will do a muscular contraction in our model and we have observed the same parameters that in the previous chapters.

The first observation is the same values for the strains and stresses in the elastic model and hyperelastic model (figure 5.1) for the extreme values. We can see a bit difference with the values in the recuperation phase, with the different curves of stresses. In any case, we have the same values for the maximal values, so that we can assume the same effect in the fascia transversalis in the moment of maximal contraction.

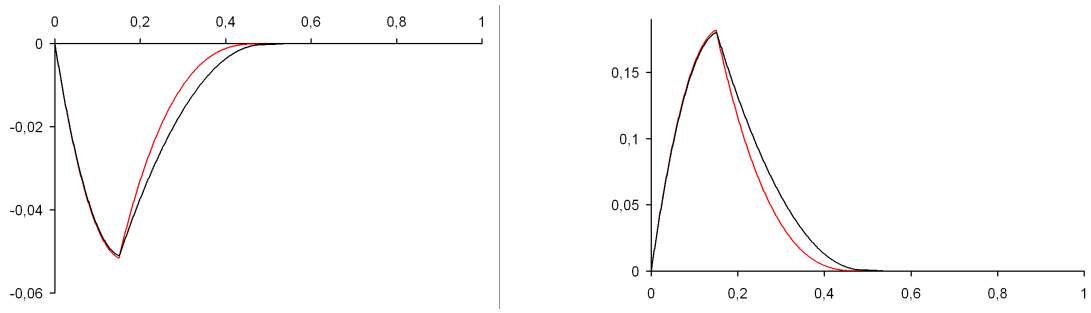

(a) Strain

(b) Stress in MPa.

Figure 5.1: Plots of strains and stresses for the elastic model (in black) and hyperelastic model (in red) for the same fibre.

In figures 5.3 and 5.4 we can observe some sequences of stresses with similar values of the elastic case, in figure 5.2 we can see the equivalent sequence than in the elastic case.

5.6 Conclusions

The obtained results show that the simulation in the non linear case is very similar to the linear case. This fact, allows to think that the conclusions (for the studied parameters) in the linear case will be the same in the non linear case, and for an initial study the linear case is sufficient.

In any case, the non linear model, allows to do a more accurate qualitative study and a first approximation to the quantitative study because we are using the most accepted model for alive tissue. In spite of this, we want to remark the non existence of accurate models for muscular tissue, so that the parameters used in our model are generic and we can't establish in absolute sense the real behavior of the area. In the future, we need to do some work to explore the parameters to the real values of the tissues in the area.

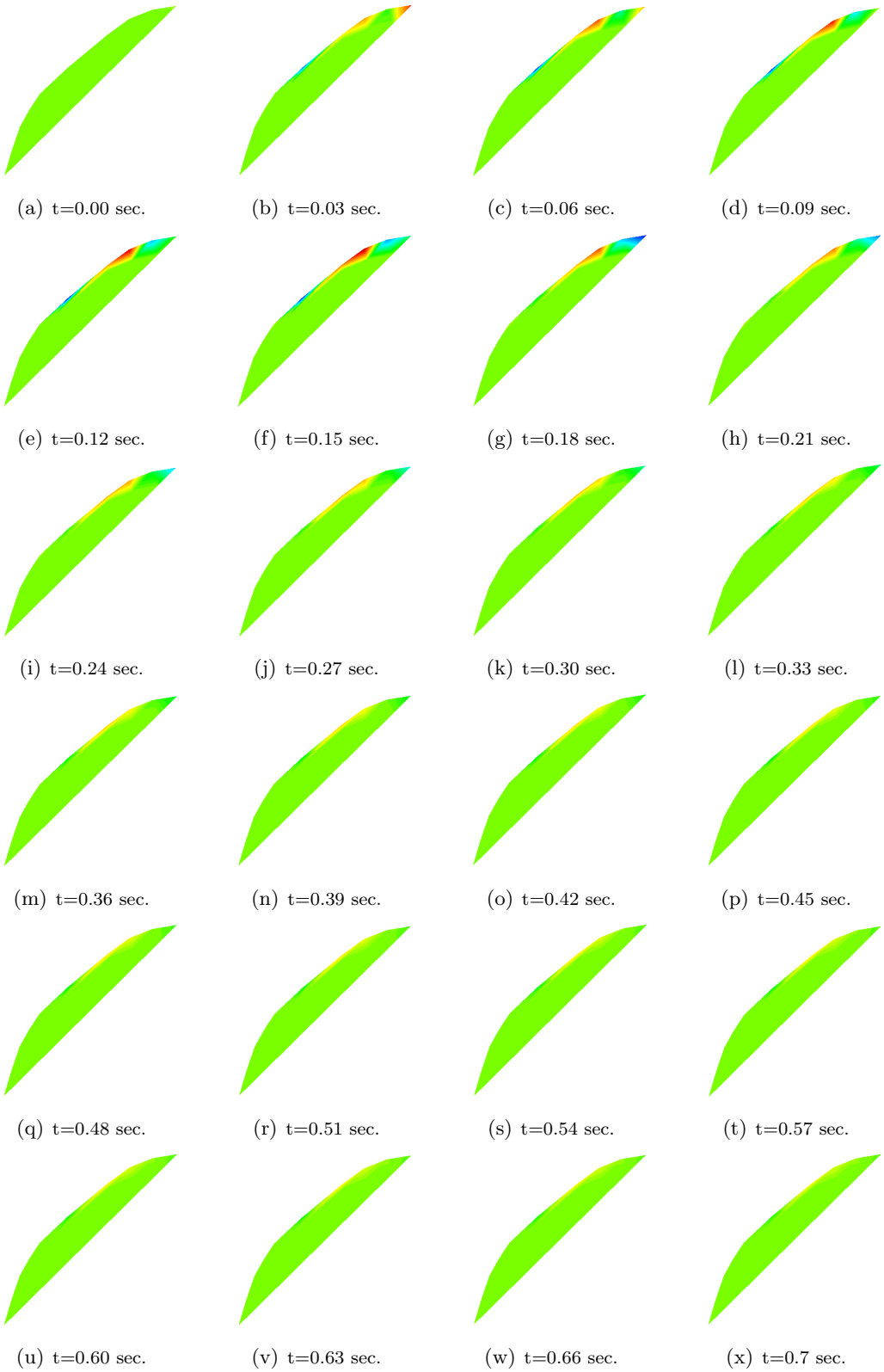

(a) t=0.00 sec. (b) t=0.03 sec. (c) t=0.06 sec. (d) t=0.09 sec.

(e) t=0.12 sec. (f) t=0.15 sec. (g) t=0.18 sec. (h) t=0.21 sec.

(i) t=0.24 sec. (j) t=0.27 sec. (k) t=0.30 sec. (l) t=0.33 sec.

(m) t=0.36 sec. (n) t=0.39 sec. (o) t=0.42 sec. (p) t=0.45 sec.

(q) t=0.48 sec. (r) t=0.51 sec. (s) t=0.54 sec. (t) t=0.57 sec.

(u) t=0.60 sec. (v) t=0.63 sec. (w) t=0.66 sec. (x) t=0.7 sec.

Figure 5.2: Sequence of strain variation in the fascia transversalis in 0.7 sec.

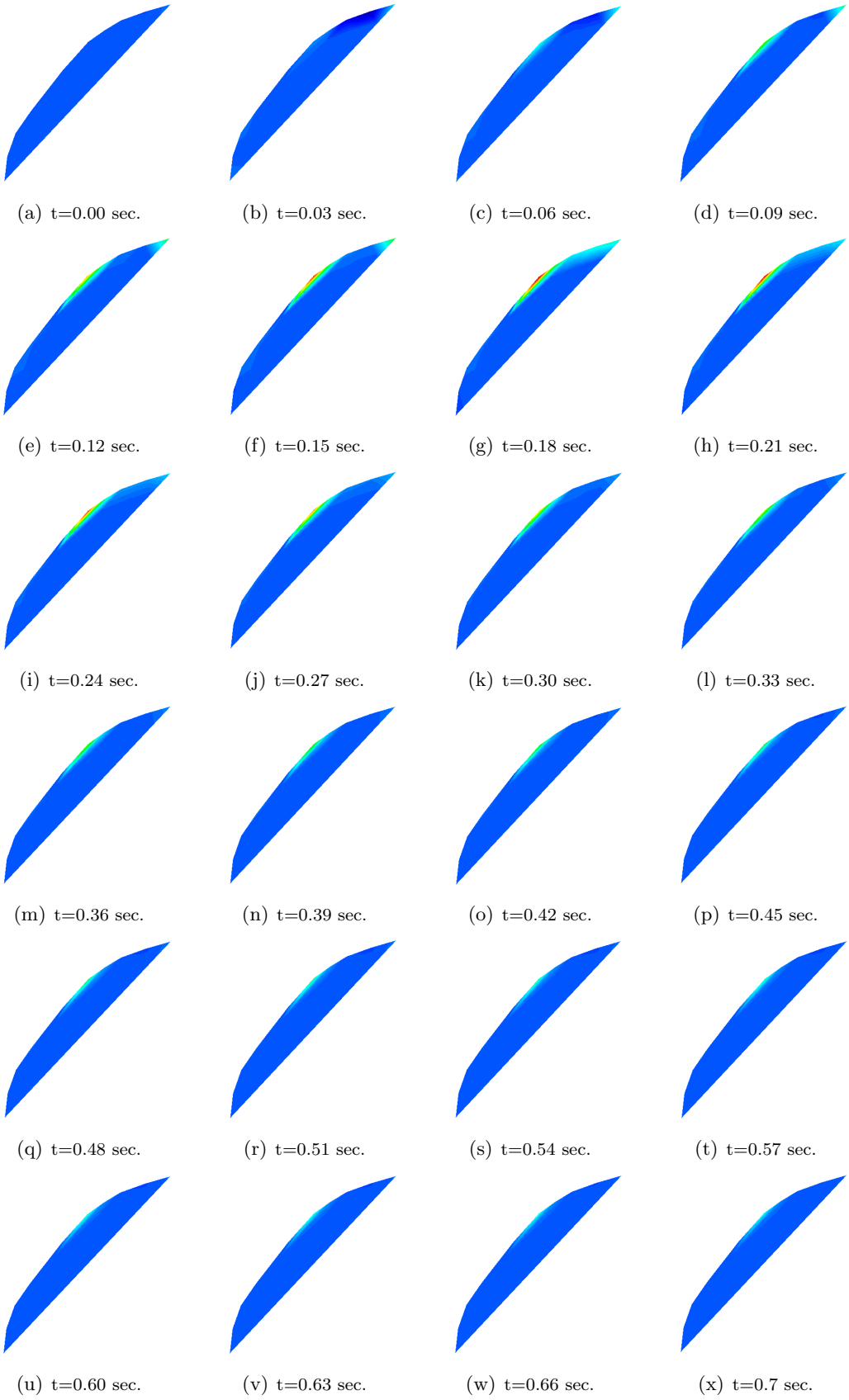

(a) t=0.00 sec. (b) t=0.03 sec. (c) t=0.06 sec. (d) t=0.09 sec.

(e) t=0.12 sec. (f) t=0.15 sec. (g) t=0.18 sec. (h) t=0.21 sec.

(i) t=0.24 sec. (j) t=0.27 sec. (k) t=0.30 sec. (l) t=0.33 sec.

(m) t=0.36 sec. (n) t=0.39 sec. (o) t=0.42 sec. (p) t=0.45 sec.

(q) t=0.48 sec. (r) t=0.51 sec. (s) t=0.54 sec. (t) t=0.57 sec.

(u) t=0.60 sec. (v) t=0.63 sec. (w) t=0.66 sec. (x) t=0.7 sec.

Figure 5.3: Sequence of stress variation in the fascia transversalis in 0.7 sec.

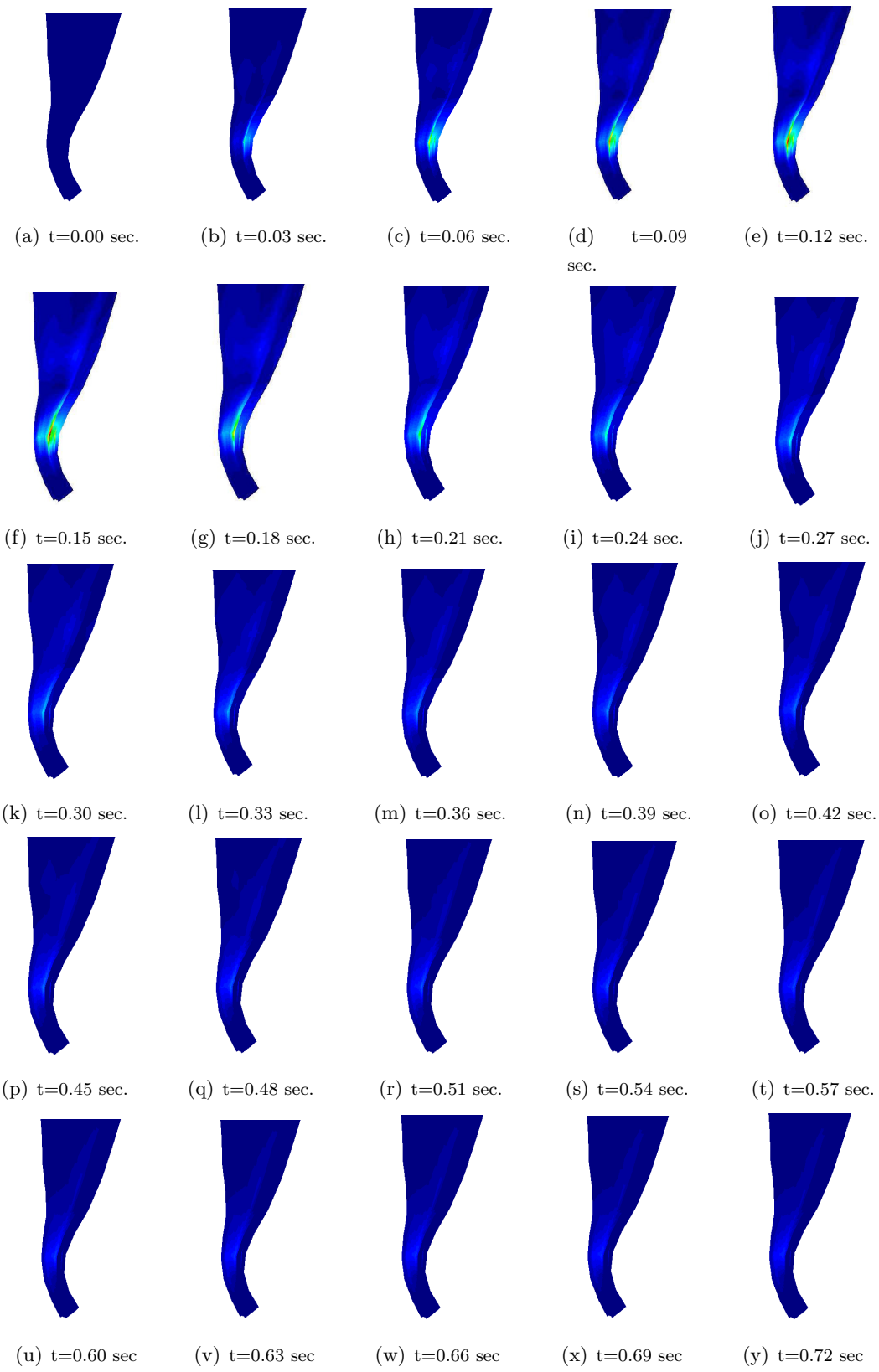

(a) t=0.00 sec. (b) t=0.03 sec. (c) t=0.06 sec. (d) t=0.09 sec. (e) t=0.12 sec.

(f) t=0.15 sec. (g) t=0.18 sec. (h) t=0.21 sec. (i) t=0.24 sec. (j) t=0.27 sec.

(k) t=0.30 sec. (l) t=0.33 sec. (m) t=0.36 sec. (n) t=0.39 sec. (o) t=0.42 sec.

(p) t=0.45 sec. (q) t=0.48 sec. (r) t=0.51 sec. (s) t=0.54 sec. (t) t=0.57 sec.

(u) t=0.60 sec (v) t=0.63 sec (w) t=0.66 sec (x) t=0.69 sec (y) t=0.72 sec

Figure 5.4: Sequence of stress variation in the internal oblique muscle in the area of the fascia transversalis in 0.7 sec.

Chapter 6

Conclusions and Future Works

6.1 Conclusions

We have analysed the genesis of inguinal hernias and completed a first approach for simulating the dynamics of the inguinal region. From the ample data recorded in these simulations, we can draw the following conclusions about the model, the simulations and the results.

6.1.1 Conclusions about the Model

It is important to have a correct and detailed model of the region in order to study its dynamics. Using our model we were able to reproduce the structure and composition of the region. To make further progress in this area we need to form a team of researchers that is large enough to complete this information (the anatomic model, the mechanic properties and the specific biological composition) and incorporate it into the model. Our results are valid partly thanks to the precision and conditions of the model. After validating the muscular contraction model, we need to complete the multitude of tissues that exist in the region. A model that is consistent with reality is fundamental to giving our results real meaning.

Thanks to the work of Manuel López Cano et al [44], we were able to construct a real and coherent model. All computational models must be able to reproduce real models in order to validate their result. The more realistic the model is, the better the results will reflect the real dynamics. Also essential is experimental knowledge of the region in order to establish the real properties of the tissues. The work by Munhequete [54] in establishing and defining the physical properties of the tissues has been fundamental.

6.1.2 Conclusions about the Simulations

The simulations are the fundamental part of our study. On one hand we had to create a three-dimensional unitary model for the simulations and on the other we had to propose an elastic or hyperelastic model. We aimed to make the model "natural", in agreement with existing models for the theoretical muscular contraction and the properties of the simulated materials. We then used this knowledge to move our simulations and our real model closer to the real dynamics of the region.

Conclusions about the Simulation Model

Hill-Maxwell's rheological model and the contribution by J. Bestel provided a rigorous model of muscular contraction. Then, by choosing the unitary hexahedric element we easily reproduced the structure of the muscle. Given the characteristics of the problem, the finite elements method is the most natural one to use for this problem. Unfortunately, due to the particularities of the model, i.e. the forces exercised were internal, we were unable to use the usual commercial software for this method (ABAQUS, ANSYS, etc.) and had to develop our own code in C++ language. To our knowledge, this is the first muscular contraction model that incorporates the properties of the muscles.

Conclusions about the Model and the Material

Essentially, we have simulated two types of materials (elastic and hyperelastic). In both cases we used the normal methodology and observed no qualitative differences between the two models. We did find quantitative differences but, because of their orders of magnitude, we are unable to confirm that these were substantially different, considering the integration step we used.

We should also stress the importance of correctly adjusting the values of the parameters in the two models (aided by the literature), since these simulations are highly sensitive to the conditions imposed.

6.1.3 Conclusions about the Results

Our results with these simulations are qualitatively coherent with those in the literature. The main physical properties of the region are verified and their dynamics are as we expected. We can say that this is the first real dynamic model of the human inguinal region.

Using this model we conducted an itemized study of various physical and chemical aspects, thus contributing to knowledge on the region and its diverse phenomena.

We constructed the dynamic model with the dynamics of the most correct one-dimensional model of muscular contraction, presented for heart contraction by J. Bestel and M. Sermesant. We used this in our study of the musculature of the abdominal wall. Our results are therefore the first for the actual dynamics of the region and muscular contraction in general.

Our main conclusions are:

- the shutter mechanism occurs as A. Keith stated in 1923 and occurs in the Hessert triangle;
- the sphincter mechanism of the inguinal ring occurs as predicted by W. J. Lytle in 1945;
- these are not just defence mechanisms: they can also cause hernias in individuals with unhealthy tissues;
- diverse geometric, physical or chemical alterations have several repercussions that have been predicted but until now have not been quantified.

6.2 Future works

We can say that this study, which is just the first approach towards our initial objective, has opened up more questions than it has solved. Muscle simulation has been the object of few scientific contributions, so a correct model of muscular contraction will provide greater knowledge about medical conditions caused by shortcomings in the muscular tissue or in tissues affected by the muscles.

There are several aspects in which further effort is needed. These include computation, modeling, and interaction with other elements.

6.2.1 About the Model

One of our future objectives is to model the whole abdominal wall, including all the active and passive elements, in order to conduct a combined study of their dynamics. We also intend to study how the various elements interact and how this affects the region.

Once we have modeled the whole abdominal wall, it will be relatively simple to study the appearance of hernias and other eventrations in different regions.

We also need to complete the current model with all the small structures (tissues, fat accumulations, bowels, etc.). Although these probably do not have a direct effect on the dynamics, a complete model will enable us to get closer to the real model.

It is also important for future research to incorporate dynamic models of the diffusion of calcium inside the muscular tissue. Calcium plays a fundamental role in muscular contraction, so a correct model of its distribution inside the muscle at each moment would enable us to better reproduce contraction.

We will need to incorporate into the code an automatic grid algorithm to provide structured grids simply and with good properties for conducting their simulation. We need to study the future incorporation of non-structured meshes and their generation algorithms (the Delaunay method or the Advancing Front method) because the irregular geometry of the muscles can lead to this type of non-structured meshes.

6.2.2 About the Simulations

To obtain an operative code we will need to parallelize the original code in order to substantially improve calculation time and approach real-time simulations. This would help to incorporate the code into a future surgical simulator.

We will also consider changing the unitary three-dimensional elements of the hexahedron with 8 nodes to a hexahedron with 16 nodes because the latter have quadratic precision for calculating the solution. A rigorous study of the previous code is needed because the calculation time will be greatly affected.

We also need to consider interacting this code with existing commercial software in order to obtain greater flexibility when modifying the simulations, especially for the dynamically passive elements. We will then be able to study the real effect of these elements on the real dynamics, and their variations, with greater precision.

6.2.3 About the Material

We also intend to develop a hyperelastic model of muscular tissue that reflects the wide range of pathologies found in individuals. This would enable us to evaluate the risk of a hernia more correctly since we would have a more correct model for each muscle. However, we need to establish contact with a laboratory that will allow us to read the various physical parameters of the muscles. Recording these values and their variability under different conditions would enable us to obtain the correct parameters for the various realities.

Also, we need to incorporate recent research on the extracellular matrix in live tissue (particularly muscular tissue) in order to reproduce microscopic properties of the tissue that are consistent with the actual properties.

6.2.4 About Future Applications

First we must ask several questions that remain unanswered in the field of biomechanics. We need to study interaction with passive external elements (e.g. surgical meshes), the behaviour of these elements and their mechanical requirements. We need to study current surgical techniques in order to determine how they work and what risk they present for future pathologies.

Nevertheless, we now have a dynamic model of muscular contraction. In the future, we will be able to evaluate the risk of several pathologies by measuring the properties of a certain muscular mass and use the model for treating certain patients.

We will be able to conduct biomechanical studies of static elements more accurately and determine which real elements of protection we need to incorporate (e.g. if we can determine the real function of the back muscles at moments of strong impact, we can know the protection mechanisms against fundamental injuries in accidents).

All these questions can be answered by applying the muscular contraction model described in this study and incorporating real information about the biomechanical properties of the muscles involved.

Part II

Appendices

Appendix A

One Dimensional Resolution

At this point, we have already defined the system of the equations that govern the dynamics of every muscle as one dimensional element, his resolution will give us variation of the position of several elements with the time. After fixing this system, we must notice that we have a system with two ordinary differential equations, on partial derivative equation and finally one linear equation. According to this, we must do some considerations before his resolution:

- **About the partial derivative equation**. The partial derivative equation is the Lagrange equation with the non-zero independent term, which corresponds to a no conservative field (usually used in classical mechanics). This equation computes the displacement that is modeled by the usual resolution of a hyperbolic partial derivative equation:

$$\left[K^k\right] u^k + \left[C^k\right] \dot{u}^k + \left[M^k\right] \ddot{u}^k = F^k \tag{A.1}$$

  Where u^k, $\dot{u}^k$ and $\ddot{u}^k$ are the position vectors, velocity and acceleration of the variation in the initial position for each element k. Thus we have for each instant time t the new position for each point with the equation $P(t) = P(0) + u(t)$. Moreover we consider the matrix $\left[K^k\right]$ as the stiffness matrix, the matrix $\left[M^k\right]$ as the mass matrix (mass lumping) and $\left[C^k\right]$ that is the dumping matrix. These matrices will be considered for each time instant t_s although they will not vary over time.

- **About the integration of ordinary differential equations**. To integrate the system of ordinary differential equations, we are going to use the four order Runge-Kutta classic method.

- **Determination of the size steep of integration**. To determine the integration size steep system, we are going to use the *Courant* criteria, this criteria fix a limit steep more sure for the integration of the differential equation system, on having considered the material rigidity. For a material with the muscular rigidity we obtain a integration steep near of $\Delta t < 10^{-5}$.

A.1 Numeric Resolution for the one dimensional PDE

For the one dimensional elements with a node in each extreme, the linear matrices that we need to calculate on solving the PDE are 2×2 matrices. There are a lot of literature about this theme [58][86], although we are going to do a brief scheme of this calculation.

A.1.1 Computation the $[K^k]$ Matrix and the $[F^k]$ Vector

To built the rigidity matrix for the three dimensional elements we need to use the Virtual Work Principle, but in the one dimensional case we can built the matrix with a more intuitive idea with the material resistance principle *the strain function in each point of the element is equal to the enlargement of the element*. Then:

$$\varepsilon = \frac{\Delta l_k}{l_k} = \frac{u^{k_2} - u^{k_1}}{l_k}$$

where u^{k_2} and u^{k_1} are the nodal displacements for the extreme elements for the element k, and l_k is the element. On the other hand, we have the relation between the stress σ and the strain ε with the Hooke low $\sigma = E\varepsilon$ where E is the Young's module (material elasticity module). Now, we can integrate by the section A, we compute the axle effort N which is translate to the adjacent elements. When we assume that our material is homogeneous and isotropic, we have $N = A\sigma$. Finally, we can establish the equilibrium between the axil forces that we have at the extremes R^{s_1} and R^{s_2} then:

$$R^{k_2} = -R^{k_1} = N = \left(\frac{EA}{l_k}\right)\left(u^{k_2} - u^{k_1}\right) = \frac{k}{l_k}\left(u^{k_2} - u^{k_1}\right)$$

thus we can write in matrix form as:

$$q^k = \begin{pmatrix} R^{k_1} \\ R^{k_2} \end{pmatrix} = \frac{k}{l_k}\begin{pmatrix} 1 & -1 \\ -1 & 1 \end{pmatrix}\begin{pmatrix} u^{k_1} \\ u^{k_2} \end{pmatrix} = K^k u^k$$

where K^k is the rigidity matrix for an element, u^k is the displacement vector and q^k is the vector of the forces in the knots. Now, we need to consider the elasticity and the section as uniform along the time, so that the matrix can't have variation over time.

When a force acts also evenly distributed per unit length and intensity, the previous equation transforms acting equally on every node as:

$$q^k = \begin{pmatrix} R^{k_1} \\ R^{k_2} \end{pmatrix} = \frac{k}{l_k}\begin{pmatrix} 1 & -1 \\ -1 & 1 \end{pmatrix}\begin{pmatrix} u^{k_1} \\ u^{k_2} \end{pmatrix} - \frac{f_k(t) l_k}{2}\begin{pmatrix} 1 \\ 1 \end{pmatrix} = K^k a^k - F^k$$

where $f_k(t)$ a function time for the force. In our case, the resolution of the governing equations of the fibre is done using the finite element method. So that, we are going to show how is transformed the one dimensional differential equation to a lineal system of equations. Starting from the rheological Hill-Maxwell's model,

$$-\frac{d}{dx}\left(k_p \frac{dy}{dx} + \sigma_c\right) = 0$$

and the boundary conditions are,

$$y(0) = 0; \qquad \left(k_p \frac{dy}{dx} + \sigma_c\right)_{x=L} = q^0$$

In order to obtain the weak form, we are going to consider the linear element $\Omega^k = [x_A, x_B]$ in dimension one, the weak form of the ponderable integration is

$$\int_{x_A} x_B \left(\frac{dw}{dx} \left(k_p \frac{dy}{dx} + \sigma_c \right) \right) - \left[w \left(k_p \frac{dy}{dx} + \sigma_c \right) \right]_{x_A}^{x_B} = 0$$

We assume that all elements are one dimensional linear elements, the primary variables are $y_A = y(x_A)$ and $y_B = y(x_B)$, and the secondary variables are Q_A and Q_B such as,

$$Q_A = -\left(k_p \frac{dy}{dx} + \sigma_c \right)_{x=x_A}; \qquad Q_B = \left(k_p \frac{dy}{dx} + \sigma_c \right)_{x=x_B}$$

In the weak form of the variational form appear the secondary variables but not the boundary conditions of the primary variables. These will be included in the approximation of the solution $u(x)$ in the element Ω^k by an interpolation in the nodes. Using Lagrange interpolating polynomial $\Psi_j^k(x)$ $j = 1, 2$.

$$U^k(x) = \sum_{j=1}^{2} u_j^k \Psi_j^k(x) = u_1^k \Psi_1^k(x) + u_2^k \Psi_2^k(x)$$

We are going to use the Rayleigh-Ritz method in which is applied the Galerkin variational method in the weak form to obtain a system of n equations in the element Ω^k. The approximation of the solution is a lineal combination of the interpolation functions $\Psi_j^k(x)$,

$$y(x) \simeq U^k(x) = \sum_{j=1}^{2} u_j^k \Psi_j^k(x)$$

The function $u(x)$ is substituted by the expression $U^k(x)$ in the weak form to obtain algebraic relations between the nodal values u_i^k and Q_i^k of the element Ω^k. The weight function w is substituted by each function Ψ in order to obtain as many equations as nodes has the element.

$$\sum_{j=1}^{2} \left[\int_{x_A}^{x_B} k_p \frac{d\Psi_i^k}{dx} \frac{d\Psi_j^k}{dx} dx \right] u_j^k + \int_{x_A}^{x_B} \frac{d\Psi_i^k}{dx} \sigma_c dx = 0$$

In a compact form, the equation's system can be written as $\left[K^k\right] u^k + \sigma_c^k = 0$. This is the equation's system of the element in which $\left[K^k\right]$ is the stiffness matrix and σ_c^k the stress vector. Introducing a change of coordinates to a normalized element $\Omega^R = [-1, 1]$ where $dx = \frac{h_k}{2} d\xi$ and $h_k = x_A - x_B$ is the element's length, the interpolation function are written as

$$\Psi_1^R(\xi) = \frac{1}{2}(1 - \xi); \qquad \Psi_2^R(\xi) = \frac{1}{2}(1 + \xi)$$

We are using this variables change,

$$K_{ij}^k = \int_{x_A}^{x_B} k_p \frac{d\Psi_i^k}{dx} \frac{d\Psi_j^k}{dx} dx = \int_{-1}^{1} k_p \frac{d\Psi_i^R}{d\xi} \frac{2}{h_k} \frac{d\Psi_j^R}{d\xi} \frac{2}{h_k} \frac{h_k}{2} d\xi$$

$$\sigma_{c,i} = \int_{-1}^{1} k_p \frac{d\Psi_i^R}{d\xi} \frac{2}{h_k} \sigma_c \frac{h_k}{2} d\xi$$

For any normalized element in the normalized coordinate system, the stiffness matrix and the stress vector can be written as,

$$\left[K^k\right] = \frac{k_p}{h_k} \begin{pmatrix} 1 & -1 \\ -1 & 1 \end{pmatrix}; \qquad \sigma_c^k = \sigma_c \begin{pmatrix} 1 \\ -1 \end{pmatrix}$$

A.1.2 Calculus of the $[M^k]$ Matrix

The mass matrix is defined as the matrix $[M]$ where their components $m_{i,j}$ are calculated with:

$$m_{i,j} = \int N_i \rho N_j d\Omega$$

where N_i is the interpolator Lagrange polynomial in the node i, Ω is the domain where we are writing the mass matrix and ρ is the material density that we are considering. Thus we have

$$\left[M^k\right] = \frac{\rho l_k}{6} \begin{pmatrix} 2 & 1 \\ 1 & 2 \end{pmatrix}$$

where l_k is the length for the element k.

A.2 Calculation Algorithm

We can assume known as all the values until the instant t_{s-1} then we want to compute the values of f in t_s following this methodology:

1. We evaluate the potential activation function 2.2 at time t_s. We obtain $|u(t_{s+1})|$ (the absolute value the potential activation function) and $|u(t_s)|_+$ the value of k_{ATP} if $C_a(t_s) \geq \overline{C}$.
2. We integrate to t_{s-1} until t_s with the Runge-Kutta method of fourth order the system with two differential equations, then we obtain $k_c(t_s)$ and $\sigma_c(t_s)$.
3. We integrate the PDE with the Newmark method since t_{s-1} until t_s, then we obtain u_s^k, $\dot{u}_s^k$ and $\ddot{u}_s^k$ and then we use u_s^k to compute the strain ε with:

   $$\varepsilon(t_s) = \frac{u_s^k}{l_k}$$

   where l_k is the element's length.
4. With the strain ε, and using that ES is a passive element and fact the rehologic model has a montage in parallel, we can compute $\varepsilon_c(t_s)$ with:

   $$\varepsilon_c(t_s) = \varepsilon(t_s) - \frac{\sigma_c(t_s)}{k_s}$$

   where k_s is a constant that we have been compute previously.
5. We approximate the first stress derivative $\dot{\varepsilon}_c(t_s)$ with the quotient:

   $$\dot{\varepsilon}_c(t_s) = \frac{(\varepsilon_c(t_s) - \varepsilon_c(t_{s-1}))}{\Delta t_s}$$

   and we return to the first steep until we arrive to the final time.

Appendix B

Problem Statement

We consider the equilibrium problem of a general three-dimensional body. The body is located in the fixed Cartesian coordinate system $\{x, y, z\}$. Considering the body surface area, the body is supported on the area S^u with described displacements $\mathbf{u}$ and is subject to the surface traction $\mathbf{f}^S$ on the surface area $\mathbf{S}^f$. In addition, the body is submited to externally applied body forces $\mathbf{f}^B$ and concentrated loads $\mathbf{r}^i$ in a point i of the body. In general, the externally applied forces have three components corresponding to the $\{x, y, z\}$ coordinate axis. The components of $\mathbf{f}^B$ and $\mathbf{f}^S$ vary as a function of $\{x, y, z\}$ and for $\mathbf{f}^B$ are considered the local coordinates of the surface $\mathbf{S}^f$.

$$\mathbf{f}^B = \begin{pmatrix} f_x^B \\ f_y^B \\ f_z^B \end{pmatrix}; \quad \mathbf{f}^S = \begin{pmatrix} f_x^S \\ f_y^S \\ f_z^S \end{pmatrix}; \quad \mathbf{r}^i = \begin{pmatrix} r_x^i \\ r_y^i \\ r_z^i \end{pmatrix};$$

In a three-dimensional solid, the movement of a point in the space is determined with the displacements of the body in the coordinate system $\{x, y, z\}$ and denoted by $u = u(x, y, z) = (u, v, w)^T$. Now, according to the classic theory of elasticity, the strains corresponding vector to u are,

$$\varepsilon = (\varepsilon_{xx}, \varepsilon_{yy}, \varepsilon_{zz}, \varepsilon_{xy}, \varepsilon_{xz}, \varepsilon_{yz})^T \tag{B.1}$$

and

$$\begin{array}{ccc} \varepsilon_{xx} = \frac{\partial u}{\partial x}; & \varepsilon_{yy} = \frac{\partial v}{\partial y}; & \varepsilon_{zz} = \frac{\partial w}{\partial z}; \\ \varepsilon_{xy} = \frac{\partial u}{\partial y} + \frac{\partial v}{\partial x}; & \varepsilon_{xz} = \frac{\partial w}{\partial x} + \frac{\partial u}{\partial z}; & \varepsilon_{yz} = \frac{\partial v}{\partial z} + \frac{\partial w}{\partial y}; \end{array} \tag{B.2}$$

where ε_{xx}, ε_{yy}, ε_{zz} are the normal strains and ε_{xy}, ε_{xz},ε_{yz} are the tangential strains.

On the other hand, the stresses corresponding to ε are:

$$\sigma = (\sigma_{xx}, \sigma_{yy}, \sigma_{zz}, \sigma_{xy}, \sigma_{xz}, \sigma_{yz})^T$$

where σ_{xx}, σ_{yy}, σ_{zz} are the normal stresses and σ_{xy},σ_{xz},σ_{yz} are the tangential stresses.

The relationship between stresses and strains, is governed by a 6×6 matrix, symmetric and with twenty-one independent coefficients. As the muscle is considered as an anisotropic material, that rela-

tionship can be expressed with nine parameters with:

$$\begin{aligned}\varepsilon_x &= \tfrac{1}{E_x}\sigma_x - \tfrac{\upsilon_{yx}}{E_y}\sigma_y - \tfrac{\upsilon_{zx}}{E_z}\sigma_z \\ \varepsilon_y &= \tfrac{1}{E_y}\sigma_y - \tfrac{\upsilon_{xy}}{E_x}\sigma_x - \tfrac{\upsilon_{zy}}{E_z}\sigma_z \\ \varepsilon_z &= \tfrac{1}{E_z}\sigma_z - \tfrac{\upsilon_{xz}}{E_x}\sigma_y - \tfrac{\upsilon_{yz}}{E_y}\sigma_y \\ \gamma_{xy} = \tfrac{\tau_{xy}}{G_{xy}};\quad \gamma_{xz} &= \tfrac{\tau_{xz}}{G_{xz}};\quad \gamma_{yz} = \tfrac{\tau_{yz}}{G_{yz}};\end{aligned}$$

where x, y, z are the isotropy directions, E_x, E_y, E_z are the rigidities in the isotropy directions and using the Maxwell-Betti theorem, we have the symmetric property so that we have:

$$E_x\nu_{yx} = E_y\nu_{xy};\quad E_y\nu_{zy} = E_z\nu_{yz};\quad E_z\nu_{xz} = E_x\nu_{zx};$$

and the constants G_{xy}, G_{xz}, G_{yz} are determinate with the cross coefficients:

$$G_{xy} = \tfrac{2(1+\nu_{xy})}{E_{xy}};\quad G_{xz} = \tfrac{2(1+\nu_{xz})}{E_{xz}};\quad G_{yz} = \tfrac{2(1+\nu_{yz})}{E_{yz}};$$

Finally, the relationship between stress and strains is defined by the stress-strain material matrix $\mathbf{D}$ which is taking into account the constitutive equation of the material and the initial stresses σ^0 and strains ε^0,

$$\sigma = \mathbf{D}(\varepsilon - \varepsilon^0) + \sigma^0 \tag{B.3}$$

The constitutive equation in isotropic elasticity can be written in local axis as a symmetric matrix such as

$$\mathbf{D} = \frac{E\,(1-\nu)}{(1+\nu)\,(1-2\nu)}\begin{pmatrix} 1 & \frac{\nu}{1-\nu} & \frac{\nu}{1-\nu} & 0 & 0 & 0 \\ \frac{\nu}{1-\nu} & 1 & \frac{\nu}{1-\nu} & 0 & 0 & 0 \\ \frac{\nu}{1-\nu} & \frac{\nu}{1-\nu} & 1 & 0 & 0 & 0 \\ 0 & 0 & 0 & \frac{(1-2\nu)}{2(1-\nu)} & 0 & 0 \\ 0 & 0 & 0 & 0 & \frac{(1-2\nu)}{2(1-\nu)} & 0 \\ 0 & 0 & 0 & 0 & 0 & \frac{(1-2\nu)}{2(1-\nu)} \end{pmatrix}$$

where E is elasticity modulus and ν is the Poisson coefficient.

B.1 The Virtual Displacements Principle

The basis of the displacement-based finite element solution is the principle of virtual displacements, this body state requires that for any small virtual compatible displacements imposed on the body in its of equilibrium state, the total internal virtual work is equal to the total external virtual work: "A structure is in equilibrium state under the action of a force system, if when we put some discretional displacements structurally possible, the performed work by the forces over the displacements is equal to the work performed by the stress over the deformations produced by the displacements"

This principle can be expressed analytically as:

$$\int_V \delta\varepsilon^T\sigma dV = \int_V \delta u^T\mathbf{f}^B dV + \int_{S^f} \delta u^T\mathbf{f}^S dS + \sum_i \delta u_i^T\mathbf{r}_i \tag{B.4}$$

where $\delta\mathbf{u}$ are the virtual displacements, $\delta\varepsilon$ are the corresponding virtual strains and V and S are the volume and the surface of the body where the forces $\mathbf{f}^B$, $\mathbf{f}^S$ and $\mathbf{r}_i$ are acting. The principle of virtual displacements is satisfied for all virtual displacement admissible with the stress σ obtained from a continuous displacement field u that satisfies the displacement boundary conditions on S.

B.2 Finite Element Equations

For to govern the finite element equations is considered the response of the general three-dimensional body which is approximated as an assemblage of discrete finite elements interconnected at nodal points on the element boundaries. The displacements measured in a convenient local coordinate system $\{x, y, z\}$ within each element are assumed to be a function of the displacements at the n finite element nodal points. Therefore, for any element Ω, the discretization of the displacement field inside the element is

$$\mathbf{u}^{(\Omega)} = \mathbf{N}^{(\Omega)}\mathbf{a}^{(\Omega)} \tag{B.5}$$

Where $\mathbf{N}^{(\Omega)}$ is the displacement interpolation matrix in the element Ω and $\mathbf{a}^{(\Omega)}$ is a vector of the three global displacements components u_i, v_i and w_i at all nodal points including those at the supports of the element assemblage

$$\mathbf{a}^{(\Omega)} = \begin{pmatrix} \mathbf{a}_1^{(\Omega)} \\ \mathbf{a}_2^{(\Omega)} \\ \vdots \\ \mathbf{a}_n^{(\Omega)} \end{pmatrix}; \qquad \mathbf{a}_i^{(\Omega)} = \begin{pmatrix} u_i \\ v_i \\ w_i \end{pmatrix} \tag{B.6}$$

Where $\mathbf{a}_i^{(\Omega)}$ may correspond to a displacement in any direction in the coordinate system $\{x, y, z\}$ or even in a direction not aligned with these coordinate axis but aligned with the axis of another local coordinate system. Since $\mathbf{a}^{(\Omega)}$ includes the displacements at the supports of the element assemblage and is needed to impose, at a later time, the known value of $\mathbf{a}^{(\Omega)}$ prior to solving for the nodal point displacements.

The choice of element and the construction of the corresponding entries in $\mathbf{N}^{(\Omega)}$, which depend on the element geometry, the number of element nodes/degree of freedom, and convergence requirements, constitute the basic steps of a finite element solution and this are discussed in the next section.

With the assumption on the displacements can now evaluate the corresponding element strains:

$$\varepsilon^{(\Omega)} = \mathbf{B}^{(\Omega)}\mathbf{a}^{(\Omega)} \tag{B.7}$$

where $\mathbf{B}^{(\Omega)}$ is the strain-displacements matrix; the rows of $\mathbf{B}^{(\Omega)}$ are obtained by the derivatives and combining the expressions of the equation B.2 in which u, v and w are in function of the interpolation functions. The use of B.5 and B.6 in the principle of virtual displacements will automatically lead to an effective assemblage process of all element matrices into the governing structure matrices.

The stresses in a finite element are related to the element strains, using the constitutive equation and the elasticity matrix $\mathbf{D}^{(\Omega)}$ for the element Ω are $\sigma^{(\Omega)} = \mathbf{D}^{(\Omega)}\varepsilon^{(\Omega)} = \mathbf{D}^{(\Omega)}\mathbf{B}^{(\Omega)}\mathbf{a}^{(\Omega)}$ Using the assumption on the displacements within each finite element, as expressed in B.5, the equilibrium equations that correspond to the nodal point displacements of the assemblage of finite elements can be derived. The equation B.4 is rewritten as a sum of integrations over the volume and areas of all finite elements.

$$\sum_{\Omega}\int_{V^{(\Omega)}} \delta\varepsilon^T\sigma dV = \sum_{\Omega}\int_{V^{(\Omega)}} \delta\mathbf{u}^T\mathbf{f}^B dV + \sum_{\Omega}\int_{\Sigma S^{(\Omega)}} \delta\mathbf{u}^T\mathbf{f}^S dS + \sum_i \delta\mathbf{u}_i^T\mathbf{r}_i \tag{B.8}$$

Where $\Sigma S^{(\Omega)}$ denotes the element surface that are part of the body surface S (the surface where $\mathbf{f}^S$ are applied). For elements totally surrounded by other elements no such surfaces exists and is assumed that

nodal points have been placed at the points where concentrated loads are applied, although a concentrated load can (of course) also be included in the surface force integrals.

Since the interaction are performed, over the element volumes and surfaces, for efficiency may be used a different and any convenient coordinate system for each element in the calculations. But, it is assumed that for each integral we need to have a unique coordinate system for all variables employed; $\delta\mathbf{u}$ is defined in the same coordinate system as $\mathbf{f}^B$.

Knowing that $\mathbf{a}$ are the displacements in the nodes and considering of $\mathbf{r}^{(\Omega)}$ as a vector of concentrated loads applied to the nodes of the element assemblage, and applying the equations B.5 and B.7

$$\sum_i \delta\mathbf{u}_i^T\mathbf{r}_i = \left[\delta\mathbf{a}^{(\Omega)}\right]^T\mathbf{r}^{(\Omega)}; \qquad \delta\mathbf{u}^T = \left[\delta\mathbf{a}^{(\Omega)}\right]^T\mathbf{N}^T; \qquad \delta\varepsilon^T = \left[\delta\mathbf{a}^{(\Omega)}\right]^T\mathbf{B}^T$$

Substituting,

$$\left[\delta\mathbf{a}^{(\Omega)}\right]^T\left[\sum_\Omega\int_{V^{(\Omega)}}\mathbf{B}^T\sigma dV\right] = \left[\delta\mathbf{a}^{(\Omega)}\right]^T\left[\sum_\Omega\int_{V^{(\Omega)}}\mathbf{N}^T\mathbf{f}^b\sigma dV + \sum_\Omega\int_{\Sigma S^{(\Omega)}}\mathbf{N}^T\mathbf{f}^S\sigma dS + \mathbf{r}^{(\Omega)}\right]$$

Choosing an arbitrary virtual displacement $\left[\delta\mathbf{a}^{(\Omega)}\right]^T$ it can be,

$$\sum_\Omega\int_{V^{(\Omega)}}\mathbf{B}^T\sigma dV = \sum_\Omega\int_{V^{(\Omega)}}\mathbf{N}^T\mathbf{f}^b\sigma dV + \sum_\Omega\int_{\Sigma S^{(\Omega)}}\mathbf{N}^T\mathbf{f}^S\sigma dS + \mathbf{r}^{(\Omega)}$$

This equation states the balance between the nodal forces, the strain of the element, the mass forces and the surface forces. We can change the stress vector,

$$\sum_\Omega\int_{V^{(\Omega)}}\mathbf{B}^T\sigma dV = \sum_\Omega\int_{V^{(\Omega)}}\mathbf{B}^T\mathbf{D}\mathbf{B}\mathbf{a}dV$$

This equation can be written as a matrix system of equations. Knowing that the sum of different elements Ω, is the assemblage of the matrix and the vectors, and grouping together all the forces in $\mathbf{q}$

$$\mathbf{K}\mathbf{a} = \mathbf{q} \tag{B.9}$$

The matrix $\mathbf{K}$ is the stiffness matrix of the element assemblage

$$\mathbf{K} = \sum_\Omega\mathbf{K}^{(\Omega)} = \sum_\Omega\int_{V^{(\Omega)}}\mathbf{B}^T\mathbf{D}\mathbf{B}dV$$

and the vector load $\mathbf{q}$ includes the effect of the element body forces $\mathbf{f}^B$, the element surface forces $\mathbf{f}^S$ and the nodal concentrated loads $\mathbf{r}$

$$\mathbf{q} = \mathbf{q}^S + \mathbf{q}^B + \mathbf{r}$$

$$\mathbf{q}^S = \sum_\Omega\mathbf{q}^{S(\Omega)} = \sum_\Omega\int_{\Sigma S^{(\Omega)}}\mathbf{N}^T\mathbf{f}^S dS; \quad \mathbf{q}^B = \sum_\Omega\mathbf{q}^{B(\Omega)} = \sum_\Omega\int_{V^{(\Omega)}}\mathbf{N}^T\mathbf{f}^b dV$$

In practice, the element stiffness matrix may first be calculated corresponding to local element with the degrees of freedom, not aligned with the global assemblage degrees of freedom, in which case a transformation is necessary prior to the assemblage.

The equation B.9 is a statement of the static equilibrium of the assemblage. In these equilibrium considerations, the applied forces may vary with time, in which case the displacements also vary with time and equation B.9 is a statement of equilibrium for any specific point in time. If the loads are really applied fast enough, measured on the natural frequencies of the system, inertia forces need to be considered and consequently, a truly dynamic problem needs to be solved. Using d'Alembert's principle, we can simply include the element inertia forces as part of the body forces.

Assuming that the element accelerations are approximated in the same way as the element displacements, the contribution from total body forces to the vector load $\mathbf{q}^B$ is

$$\mathbf{q}^B = \sum_{\Omega} \int_{V^{(\Omega)}} \mathbf{N}^T [\mathbf{f}^B - \rho \mathbf{N}\ddot{\mathbf{a}}] dV$$

where $\mathbf{q}^B$ no longer includes inertia forces, $\ddot{\mathbf{a}}$ lists the nodal point accelerations and ρ is the mass density. The equilibrium equations are, in this case $\mathbf{M}\ddot{\mathbf{a}} + \mathbf{K}\mathbf{a} = \mathbf{q}$ where $\mathbf{q}$ and $\mathbf{a}$ are time-dependent. The matrix $\mathbf{M}$ is the mass matrix of the structure,

$$\mathbf{M} = \sum_{\Omega} \mathbf{M}^{(\Omega)} = \sum_{\Omega} \int_{V^{(\Omega)}} \rho \mathbf{N}^T \mathbf{N} dV$$

Actually, for measured dynamic responses of structures it is observed that energy is dissipated during vibration analysis, therefore it is usual to introduce velocity-dependent damping forces. Introducing the damping forces as additional contributions to the body forces, we obtain a new term corresponding

$$\mathbf{q}^B = \sum_{\Omega} \int_{V^{(\Omega)}} \mathbf{N}^T [\mathbf{f}^B - \rho \mathbf{N}\ddot{\mathbf{a}} - c\mathbf{N}\dot{\mathbf{a}}] dV$$

In this case the vectors $\mathbf{q}^B$ no longer include inertia and velocity-dependent damping vector forces, $\dot{\mathbf{a}}$ is a vector of the nodal point velocities and c is the damping parameter of element Ω. The equilibrium equations are in this case,

$$\mathbf{M}\ddot{\mathbf{a}} + \mathbf{C}\dot{\mathbf{a}} + \mathbf{K}\mathbf{a} = \mathbf{q} \tag{B.10}$$

where $\mathbf{C}$ is the damping matrix of the structure,

$$\mathbf{C} = \sum_{\Omega} \mathbf{C}^{(\Omega)} = \sum_{\Omega} \int_{V^{(\Omega)}} c\mathbf{N}^T \mathbf{N} dV$$

B.3 Isoparametric Formulation for the Hexaedrical Elements

The basic procedure in the isoparametric finite element formulation is to express the element coordinates and the elemental displacements in the form of interpolations, using the natural coordinate system of the element. For the description of the hexahedric element is adopted a natural coordinate system $\{\xi, \eta, \zeta\}$ in which the faces of the element are in the planes $\xi = \pm 1$, $\eta = \pm 1$ and $\zeta = \pm 1$, as it is shown in the figure B.1.

And to integrate any function $f(x, y, z)$ on the element, the following transformation can be effected on the natural coordinate system

$$\int_{V^{(\Omega)}} f(x, y, z) dV = \int_{-1}^{+1} \int_{-1}^{+1} \int_{-1}^{+1} f(\xi, \eta\zeta) \cdot abc \cdot d\xi d\eta d\zeta$$

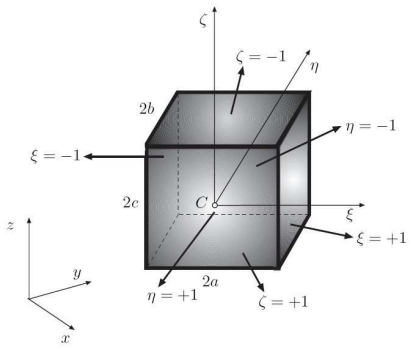

Figure B.1: Natural coordinate system for an regular hexahedric element

In this case, the derivatives of the interpolation functions of the straight hexahedric element needed for the matrix **B** can be calculated easily

$$\frac{\partial N_i}{\partial x} = \frac{1}{a}\frac{\partial N_i}{\partial \xi}; \qquad \frac{\partial N_i}{\partial y} = \frac{1}{b}\frac{\partial N_i}{\partial \eta}; \qquad \frac{\partial N_i}{\partial z} = \frac{1}{c}\frac{\partial N_i}{\partial \zeta};$$

The interpolation functions must satisfy

$$N_i(\xi_j, \eta_j, \zeta_j) = \begin{cases} 1 & if \quad i = j \\ 0 & if \quad i \neq j \end{cases}; \quad and \quad \sum_{i=1}^{n} N_i(\xi, \eta, \zeta) = 1 \quad for \quad each \quad (\xi, \eta, \zeta)$$

The element chosen to model the passive part of the muscle, it is a hexahedrical element of eight nodes. Is the simplest hexahedrical element and is common in the Lagrangian and Serendipity families. The interpolation functions are obtained using the product of the three functions corresponding to each direction, and the general expression of the interpolation function for any node i is,

$$N_i(\xi, \eta, \zeta) = \frac{1}{8}(1 + \xi_i\xi)(1 + \eta_i\eta)(1 + \zeta_i\zeta) \tag{B.11}$$

where ξ_i, η_i i ζ_i are ± 1 because the polynomial have to take the nodal value, for each one, and we have

$$\mathbf{x}^{(\Omega)} = \begin{pmatrix} \mathbf{x}_1^{(\Omega)} \\ \vdots \\ \mathbf{x}_8^{(\Omega)} \end{pmatrix}; \qquad \mathbf{x}_i^{(\Omega)} = \begin{pmatrix} x_i \\ y_i \\ z_i \end{pmatrix}$$

the displacements vector in each point.

B.4 Isoparametric Hexahedric Element

The isoparametric formulation permits to use irregulars hexahedric elements. The definition of the element is made with the real coordinates and use the isoparametric transformation to refer all the integrations to the normalized geometry of the element.

The coordinates x, y and z of any point in the n-nodes element Ω can be written as.

$$\mathbf{x} = \begin{pmatrix} x \\ y \\ z \end{pmatrix} = \begin{pmatrix} N_1x_1 + N_2x_2 + \ldots + N_8x_8 \\ N_1y_1 + N_2y_2 + \ldots + N_8y_8 \\ N_1z_1 + N_2z_2 + \ldots + N_8z_8 \end{pmatrix} = \sum_{i=1}^{8} \mathbf{N}_i\mathbf{x}_i^{(\Omega)} = \mathbf{N}\mathbf{x}^{(\Omega)} \tag{B.12}$$

Where N_i is the same function used in the interpolation of displacements field. These equations relate the cartesian coordinates of a point with the natural coordinates of the same point. This relationship is a direct automorphism if the Jacobian $\mathbf{J}^{(\Omega)}$ of the transformation is positive in all the points of the element (direct transformation). Then we have

$$\mathbf{J}^{(\Omega)} = \sum_{i=1}^{8} \begin{pmatrix} \frac{\partial N_i}{\partial \xi}x_i & \frac{\partial N_i}{\partial \xi}y_i & \frac{\partial N_i}{\partial \xi}z_i \\ \frac{\partial N_i}{\partial \eta}x_i & \frac{\partial N_i}{\partial \eta}y_i & \frac{\partial N_i}{\partial \eta}z_i \\ \frac{\partial N_i}{\partial \zeta}x_i & \frac{\partial N_i}{\partial \zeta}y_i & \frac{\partial N_i}{\partial \zeta}z_i \end{pmatrix}$$

And the relationship between the derivatives of the interpolation functions as

$$\begin{pmatrix} \frac{\partial N_i}{\partial x} \\ \frac{\partial N_i}{\partial y} \\ \frac{\partial N_i}{\partial z} \end{pmatrix} = \left(\mathbf{J}^{(\Omega)}\right)^{-1} \begin{pmatrix} \frac{\partial N_i}{\partial \xi} \\ \frac{\partial N_i}{\partial \eta} \\ \frac{\partial N_i}{\partial \zeta} \end{pmatrix}$$

where (x_i, y_i, z_i) are global coordinates and $(\frac{\partial N_i}{\partial \xi}, \frac{\partial N_i}{\partial \eta}, \frac{\partial N_i}{\partial \zeta})$ are evaluated in the nodes of the element with local coordinates.

B.5 Computing the Strain-displacements Matrix

When we use the equations B.7 and B.12, we obtain the displacement vector for each one of the generic elements with 8 nodes:

$$\varepsilon = \sum_{i=1}^{8} \begin{pmatrix} \frac{\partial N_i}{\partial x}u_i \\ \frac{\partial N_i}{\partial y}v_i \\ \frac{\partial N_i}{\partial z}w_i \\ \frac{\partial N_i}{\partial y}u_i + \frac{\partial N_i}{\partial x}v_i \\ \frac{\partial N_i}{\partial z}u_i + \frac{\partial N_i}{\partial x}w_i \\ \frac{\partial N_i}{\partial z}v_i + \frac{\partial N_i}{\partial y}w_i \end{pmatrix} = \sum_{i=1}^{8} \mathbf{B}_i\mathbf{a}_i^{(\Omega)} = \mathbf{B}\mathbf{a}^{(\Omega)}$$

where $\mathbf{B}$ is the strain-displacements matrix for the element with $\mathbf{B} = [\mathbf{B}_1, \mathbf{B}_2, \ldots, \mathbf{B}_8]$ and $\mathbf{B}_i$ is the strain-displacements matrix for the node i, with

$$\mathbf{B}_i = \begin{pmatrix} \frac{\partial N_i}{\partial x} & 0 & 0 \\ 0 & \frac{\partial N_i}{\partial y} & 0 \\ 0 & 0 & \frac{\partial N_i}{\partial z} \\ \frac{\partial N_i}{\partial y} & \frac{\partial N_i}{\partial x} & 0 \\ \frac{\partial N_i}{\partial z} & 0 & \frac{\partial N_i}{\partial x} \\ 0 & \frac{\partial N_i}{\partial z} & \frac{\partial N_i}{\partial y} \end{pmatrix}$$

The vectors $(\frac{\partial N_i}{\partial x}, \frac{\partial N_i}{\partial y}, \frac{\partial N_i}{\partial z})$ can be computed with the previous section indications, using the inverse Jacobian $\left(\mathbf{J}^{(\Omega)}\right)^{-1}$.

B.6 Computing the Stiffness Matrix K

To compute the stiffness matrix we are going to use the virtual work principia, but we need to do some previous considerations. We are to call $\mathbf{x}^{(\Omega)}$ the nodal displacements for a point in reference each node for a three dimensional element d'un element, then we have $\mathbf{x}^{(\Omega)} = (x_1, y_1, z_1, x_2, \ldots, z_8)$ and we can rewrite these nodal displacements in global coordinates as $\mathbf{u} = \mathbf{N}\mathbf{x}^{(\Omega)}$ In a similar way, we can compute the displacements in global coordinates using the strain-displacements matrix as $\varepsilon = \mathbf{B}\mathbf{x}^{(\Omega)}$. And we are going to say virtual displacement vector is the following vector $\delta\mathbf{x}^{(\Omega)} = (\delta x_1, \delta y_1, \delta z_1, \delta x_2, \ldots, \delta z_8)^T$ where $\delta x_i, \delta y_i, \delta z_i$ are the nodal virtual displacements for the i element. On the other hand, the vector of nodal forces can be defined as: $\mathbf{q}^{(\Omega)} = (X_1, Y_1, Z_1, X_2, \ldots, Z_8)^T$ where X_i, Y_i, Z_i are the virtual nodal forces in equilibrium state corresponding to the i element.

Now, we can establish $\delta\mathbf{u}^T = \delta\left(\mathbf{x}^{(\Omega)}\right)^T\mathbf{N}^T; \qquad \delta\varepsilon^T = \delta\left(\mathbf{x}^{(\Omega)}\right)^T\mathbf{B}^T$ and now, using the Virtual Displacements Principle B.4, we have:

$$\int_V \delta\left(\mathbf{x}^{(\Omega)}\right)^T\mathbf{B}^T\sigma dV = \int_V \delta\left(\mathbf{x}^{(\Omega)}\right)^T\mathbf{N}^T\mathbf{f}^B dV + \int_{\Sigma S^{(\Omega)}} \delta\left(\mathbf{x}^{(\Omega)}\right)^T\mathbf{N}^T\mathbf{f}^S dS + \delta\left(\mathbf{x}^{(\Omega)}\right)^T\mathbf{q}^{(\Omega)}$$

and we obtain

$$\int_V \mathbf{B}^T\sigma dV - \int_V \mathbf{N}^T\mathbf{f}^B dV - \int_{\Sigma S^{(\Omega)}} \mathbf{N}^T\mathbf{f}^S dS = \mathbf{q}^{(\Omega)}$$

Now, using B.3 we obtain

$$\int_V \mathbf{B}^T\left(\mathbf{D}\mathbf{B}\mathbf{x}^{(\Omega)} - \mathbf{D}\varepsilon^0 + \sigma^0\right)dV - \int_V \mathbf{N}^T\mathbf{f}^B dV - \int_{\Sigma S^{(\Omega)}} \mathbf{N}^T\mathbf{f}^S dS = \mathbf{q}^{(\Omega)}$$

$$\mathbf{x}^{(\Omega)}\int_V \mathbf{B}^T\mathbf{D}\mathbf{B}dV - \int_V \mathbf{B}^T\mathbf{D}\varepsilon^0 dV + \int_V \mathbf{B}^T\sigma^0 dV - \int_V \mathbf{N}^T\mathbf{f}^B dV - \int_{\Sigma S^{(\Omega)}} \mathbf{N}^T\mathbf{f}^S dS = \mathbf{q}^{(\Omega)}$$

that we can rewrite as

$$\mathbf{K}^{(\Omega)}\mathbf{x}^{(\Omega)} - \mathbf{f}^{(\Omega)} = \mathbf{q}^{(\Omega)}; \quad where \quad \mathbf{K}^{(\Omega)} = \int_V \mathbf{B}^T\mathbf{D}\mathbf{B}dV$$

the stiffness matrix for Ω. And, we can define:

$$\mathbf{f}^{(\Omega)} = \mathbf{f}_\varepsilon^{(\Omega)} + \mathbf{f}_\sigma^{(\Omega)} + \mathbf{f}_B^{(\Omega)} + \mathbf{f}_S^{(\Omega)} \tag{B.13}$$

as the nodal equivalent force vector for an element, where

$$\mathbf{f}_\varepsilon^{(\Omega)} = \int_V \mathbf{B}^T\mathbf{D}\varepsilon^0 dV; \qquad \mathbf{f}_\sigma^{(\Omega)} = -\int_V \mathbf{B}^T\sigma^0 dV; \qquad \mathbf{f}_B^{(\Omega)} = \int_V \mathbf{N}^T\mathbf{f}^B dV; \qquad \mathbf{f}_S^{(\Omega)} = \int_{\Sigma S^{(\Omega)}} \mathbf{N}^T\mathbf{f}^S dS$$

Now, we want to compute the coefficients for the stiffness matrix. We have defined the stiffness matrix for each element, and we need to do the effective calculus. According to the previous developments, we need to compute this matrix for each element, and we can not compute analytically this matrix

$$\mathbf{K}_{ij}^{(\Omega)} = \int_V \mathbf{B}_i^T\mathbf{D}\mathbf{B}_j dV$$

To compute that integral, we are going to use Gaussian integration to compute their volume in $n_p \times n_q \times n_r$ dots, and we have

$$\mathbf{K}_{ij}^{(\Omega)} = \int_{V^{(\Omega)}} \mathbf{B}_i^T\mathbf{D}\mathbf{B}_j dV = \int_{-1}^{1}\int_{-1}^{1}\int_{-1}^{1} \mathbf{B}_i^T\mathbf{D}\mathbf{B}_j \left|\mathbf{J}^{(\Omega)}\right| d\xi d\eta d\zeta =$$

$$= \sum_{p=1}^{n_p} \sum_{q=1}^{n_q} \sum_{r=1}^{n_r} \left(\mathbf{B}_i^T \mathbf{D} \mathbf{B}_j \left| \mathbf{J}^{(\Omega)} \right| \right) (\xi_p, \eta_q, \zeta_r) \, W_p W_q W_r$$

where (ξ_p, η_q, ζ_r) are the points where we evaluate the function or integration points and W_p, W_q and W_r are the weights of integration.

To elaborate the simulation, we are going to use the Gaussian integration with eight nodes, where the weights have the value $W_p = W_q = W_r = 1.$ and the eight nodes are fixed by the roots of the Legendre second order polynomial, so that if we took $\alpha = 0.5773502692$ then the eight nodes are $(\pm\alpha, \pm\alpha, \pm\alpha)$.

B.7 Computing the Mass Matrix M

The calculation of the mass matrix **M** using an isoparametric formulation and using the same numerical integration

$$\mathbf{M}_{ij}^{(\Omega)} = \int_{V^{(\Omega)}} \rho \mathbf{N}_i^T \mathbf{N}_j dV = \int_{-1}^{1} \int_{-1}^{1} \int_{-1}^{1} \rho \mathbf{N}_i^T \mathbf{N}_j \left| \mathbf{J}^{(\Omega)} \right| d\xi d\eta d\zeta =$$

$$= \sum_{p=1}^{n_p} \sum_{q=1}^{n_q} \sum_{r=1}^{n_r} \left(\rho \mathbf{N}_i^T \mathbf{N}_j \left| \mathbf{J}^{(\Omega)} \right| \right) (\xi_p, \eta_q, \zeta_r) \, W_p W_q W_r$$

B.8 Computing the Damping Matrix C

In the direct integration approach of the dynamic equation (B.10) a damping matrix is also required, but the development of this matrix is not straightforward because there is no physical counterpart for the assumed viscous damping. While there is no requirement that the damping matrix used in direct integration, it will be used Rayleigh damping, which is the most accepted method [13].

In Rayleigh damping, it is assumed that the damping matrix is proportional to mass stiffness, as $\mathbf{C} = \mathbf{C}_M + \mathbf{C}_K = a_0 \mathbf{M} + a_1 \mathbf{K}$ where the scalar coefficients a_0 and a_1 have units $1/sec$ and sec, respectively. The usual approach with Rayleigh damping is to specify the a_0 and a_1 values for the entire system, in which case damping matrix is calculated internally by the source code.

B.9 Model for the Pressure

In the case of forces acting on one of the faces of the element, there is little difference with the previous explanation. To explain the process, we will consider that an orthogonal force t_n is applied on the face in $\zeta = +1$. For the calculation of the vector of surface forces, we need necessarily to know the term t dA (see $f_t^{(e)}$), where dA is the differential one of area in this face, and t is the vector of forces in global coordinates, that it operates on the above mentioned surface. In this way, to project correctly the vector

force, we need to know n_x, n_y and n_z which are the cosines of the normal one to the surface, in this way we have that $\mathbf{t} = t_n\mathbf{n}$. The normal vector $\mathbf{n}$ is obtained as vectorial product of the tangent vectors $\eta = cte$ and $\xi = cte$ are contained in the surface. In this way,

$$\mathbf{u} = \left(\frac{\partial x}{\partial \xi}, \frac{\partial y}{\partial \xi}, \frac{\partial z}{\partial \xi}\right)_{\zeta=+1} d\xi; \quad \mathbf{v} = \left(\frac{\partial x}{\partial \eta}, \frac{\partial y}{\partial \eta}, \frac{\partial z}{\partial \eta}\right)_{\zeta=+1} d\eta$$

Of this is deduced that the components of the vectors $\mathbf{u}$ and $\mathbf{v}$ we can obtain easily of the Jacobian $\mathbf{J}^{(\Omega)}$, and since $dA = \|\mathbf{u} \wedge \mathbf{v}\|$, we have:

$$\mathbf{n} = \frac{1}{dA} \left\{ \begin{array}{c} J_{12}J_{23} - J_{22}J_{13} \\ J_{21}J_{13} - J_{11}J_{23} \\ J_{11}J_{32} - J_{21}J_{12} \end{array} \right\}^{(\Omega)}_{\zeta=+1} d\xi d\zeta = \frac{1}{dA}\mathbf{j}^{(\Omega)} d\xi d\zeta$$

where the $J_{ij}^{(\Omega)}$ are the elements of $\mathbf{J}^{(\Omega)}$. So that, the final expression of the vector of forces on the surface is

$$\mathbf{f}_{t_i}^{(\Omega)} = \int_{A^{(\Omega)}} \mathbf{N}_i t_n \mathbf{n} dA = \int_{-1}^{+1}\int_{-1}^{+1} \mathbf{N}_i t_n \mathbf{j}^{(\Omega)} d\xi d\zeta = \sum_{p=1}^{n_p}\sum_{q=1}^{n_q} \left(\mathbf{N}_i t_n |\mathbf{J}^{(\Omega)}|\right)(\xi_p, \eta_q, +1)\, W_p W_q$$

where the weight is those that correspond to the formula of Gaussian squaring in dimension two.

B.10 Weight of the Own Element

The forces of the own weight are equivalent to a mass force operating for unit of surface/volume in direction of the gravity. For simplicity, we are going to suppose that it is vertical, in parallel direction to the z axis. In this way, the forces of the own weight for different elements are obtained by:

$$\mathbf{f}_i^{(\Omega)} = -\int_{V^{(\Omega)}} \mathbf{N}_i^T \rho g \mathbf{c} dV = -\sum_{p=1}^{n_p}\sum_{q=1}^{n_q}\sum_{r=1}^{n_r} \left(\mathbf{N}_i^T \rho g \mathbf{c} |\mathbf{J}^{(\Omega)}|\right)(\xi_p, \eta_q, \zeta_r)\, W_p W_q W_r$$

where $\mathbf{c} = [1, 0, 0]^T$ and the weight is the same, that the one used for the integration of the counterfoil of inflexibility in equation B.13. In our simulation we will consider the usual values of density and we presupposes that it will have a scanty repercussion in the local dynamics for small variations.

Appendix C

Non Linear Formulation

C.1 Equilibrium

In order to derive the differential static equilibrium equations, consider the spatial configuration of a general deformable body defined by a volume v with boundary area ∂v. We can assume that the body is under the action of body forces f per unit volume and traction forces t per unit area acting on the boundary (da).

For simplicity, however, inertia forces will be ignored, and therefore translational equilibrium implies that the sum of all forces acting on the body vanishes. This gives,

$$\int_{\partial v} t da + \int_v f dv = 0 \tag{C.1}$$

Using the Cauchy stress tensor, that relates the relation between the normal vector n to the traction vector t as,

$$t(n) = \sum_{i,j=1}^{3} \sigma_{ij}(e_j \cdot n)e_i = \left[\sum_{i,j=1}^{3} \sigma_{ij}(e_i \otimes e_j)\right] n = \sigma n \tag{C.2}$$

for the traction vector enables equation C.1 to be expressed in terms of the Cauchy stresses as,

$$\int_{\partial v} \sigma n da + \int_v f dv = 0$$

The first term in this equation can be transformed into a volume integral by using the Gauss theorem given in

$$\int_{\partial V} SndA = \int_V \div S dV = 0 \quad where \quad \div S = \nabla S : \mathbf{I} = \sum_{i,j=1}^{3} \frac{\partial S_{ij}}{\partial x_j} e_i$$

with $\mathbf{I}$ is the identity matrix. Now,

$$\int_v (\div \sigma + f) dv = 0$$

The fact that the above equation can be equally applied to any enclosed region of the body implies that the integrand function must vanish, that is, $\div\sigma + f = 0$. This equation is known as the local (that is, pointwise) spatial equilibrium equation for a deformable body. In anticipation of situations during a solution procedure in which equilibrium is not yet satisfied, the above equation defines the pointwise out-of-balance or residual force per unit volume r as,

$$\div\sigma + f = r \tag{C.3}$$

C.2 Principle of Virtual Work

Generally, the finite element formulation is established in terms of a weak form of the differential equations under consideration. In the context of solid mechanics this implies the use of the virtual work equation. For this purpose, let δv denote an arbitrary virtual velocity from the current position of the body. The virtual work, δw, per unit volume and time done by the residual force r during this virtual motion is $r \cdot \delta v$, and equilibrium implies $\delta w = r \cdot \delta v = 0$. Note that the above scalar equation is fully equivalent to the vector equation $r = 0$. This is due to the fact that v is arbitrary, and hence by choosing $\delta v = [1, 0, 0]^T$, followed by $\delta v = [0, 1, 0]^T$ and $\delta v = [0, 0, 1]^T$, the three components of the equation $r = 0$ are retrieved. We can now use equation C.3 for the residual vector and integrate over the volume of the body to give a weak statement of the static equilibrium of the body as,

$$\delta W = \int_v (\div\sigma + f)\delta v dv = 0 \tag{C.4}$$

A more common and useful expression can be derived by recalling property

$$\div(S^T v) = S : \nabla v + v \cdot \div S$$

to give the divergence of the vector $\sigma\delta v$ as,

$$\div(\sigma\delta v) = (\div\sigma) \cdot \delta v + \sigma : \nabla\delta v \tag{C.5}$$

Using this equation together with the Gauss theorem enables equation C.4 to be rewritten as,

$$\int_{\partial v} n \cdot \delta v da - \int_v \sigma : \nabla\delta v dv + \int_v f \cdot \delta v dv = 0 \tag{C.6}$$

The gradient of δv is, by definition, the virtual velocity gradient δl. Additionally, we can use equation C.2 for the traction vector and the symmetry of σ to rewrite $n \cdot \sigma\delta v$ as $\delta v \cdot t$, and consequently equation C.6 becomes,

$$\int_v \sigma : \delta l dv = \int_v f\delta v dv + \int_{\partial v} t \cdot \delta v da$$

Finally, expressing the virtual velocity gradient in terms of the symmetric virtual rate of deformation δd and the antisymmetric virtual spin tensor δw and taking into account again the symmetry of σ gives the spatial virtual work equation as,

$$\delta W = \int_v \sigma : \delta d dv - \int_v f\delta v dv - \int_{\partial v} t \cdot \delta v da = 0 \tag{C.7}$$

This fundamental scalar equation states the equilibrium of a deformable body and will become the basis for the finite element discretization.

C.3 The Kirchhoff Stress Tensors

In equation C.7 the internal virtual work done by the stresses is expressed as,

$$\delta W_\epsilon = \int_v \sigma : \delta d dv \tag{C.8}$$

Pairs such as σ and D in this equation are said to be work conjugate with respect to the current deformed volume in the sense that their product gives work per unit current volume. Expressing the virtual work equation in the material coordinate system, alternative work conjugate pairs of stresses and strain rates will emerge. To achieve this objective, the spatial virtual work equation C.7 is first expressed with respect to the initial volume and area by transforming the integrals using

$$dv = dx_1 \cdot (dx_2 \times dx_3) = \frac{\partial \phi}{\partial X_1} \cdot \left(\frac{\partial \phi}{\partial X_2} \times \frac{\partial \phi}{\partial X_3} \right) dX_1 dX_2 dX_3$$

or

$$dv = detF dV = J dV$$

to give,

$$\int_V J\sigma : \delta D dV = \int_V f_0 \cdot \delta v dV + \int_{\partial V} t_0 \cdot \delta v dA \tag{C.9}$$

where $f_0 = Jf$ is the body force per unit undeformed volume and $t_0 = t(da/dA)$ is the traction vector per unit initial area, where the area ratio can be obtained after some algebra from the volume element

$$dV = dLdA; \quad and \quad dv = dlda$$

Relating the current and initial volumes in terms of the Jacobian J and recalling that $dl = FdL$ gives,

$$JdL\dot{d}A = (FdL) \cdot da; \quad da = JF^T dA$$

as,

$$\frac{da}{dA} = \frac{J}{\sqrt{n \cdot bn}}$$

The internal virtual work given by the left-hand side of equation C.9 can be expressed in terms of the Kirchhoff stress tensor or τ as,

$$\delta W_\epsilon = \int_v \tau : \delta D dV; \quad \tau = J\sigma$$

This equation reveals that the Kirchhoff stress tensor τ is work conjugate to the rate of deformation tensor with respect to the initial volume. Note that the work per unit current volume is not equal to the work per unit initial volume. However, equation C.3 and the relationship $\rho = \rho_0/J$ ensure that the work per unit mass is invariant and can be equally written in the current or initial configuration as:

$$\frac{1}{\rho}\sigma : d = \frac{1}{\rho_0}\tau : d$$

C.3.1 The First Piola-Kirchhoff Stress Tensor

The transformation that resulted in the internal virtual work given above is not entirely satisfactory because it still relies on the spatial quantities τ and d. Velocity expressed as a function of the spatial coordinates as v(x, t), we obtain the derivative of this expression with respect to the spatial coordinates defines the velocity gradient tensor l as

$$l = \frac{\partial v(x,t)}{\partial x} = \nabla v$$

This is clearly a spatial tensor, which, gives the relative velocity of a particle currently at point q with respect to a particle currently at p as $dv = ldx$. The tensor l enables the time derivative of the deformation gradient to be more usefully written as,

$$\dot{\mathbf{F}} = \frac{\partial v}{\partial X} = \frac{\partial v}{\partial x}\frac{\partial \phi}{\partial X} = lF$$

from which an alternative expression for l emerges as,

$$l = \dot{\mathbf{F}}\mathbf{F}^{-1} \tag{C.10}$$

To alleviate this lack of consistency, note that the symmetry of σ together with equation C.10 for l in terms of $\dot{\mathbf{F}}$ and the properties of the trace give,

$$\delta W_\epsilon = \int_v J\sigma : \delta l dV = \int_v J\sigma : (\delta\dot{\mathbf{F}}\mathbf{F}^{-1})dV$$

$$\int_v tr(J\mathbf{F}^{-1}\sigma\delta\dot{\mathbf{F}})dV = \int_v (J\sigma\mathbf{F}^T) : \delta\dot{\mathbf{F}})dV$$

We observe from this equality that the stress tensor work conjugate to the rate of the deformation gradient $\dot{\mathbf{F}}$ is the so-called first Piola-Kirchhoff stress tensor given as,

$$\mathbf{P} = J\sigma\mathbf{F}^T \tag{C.11}$$

Note that like $\mathbf{F}$, the first Piola-Kirchhoff tensor is an unsymmetric two-point tensor with components given as,

$$\mathbf{P} = \sum_{i,I=1}^{3} P_{iI}(e_i \otimes E_I); \qquad P_{iI} = \sum_{j=1}^{3} J\sigma_{ij}(\mathbf{F}^{-1})_{Ij}$$

We can now rewrite the equation for the principle of virtual work in terms of the first Piola-Kirchhoff tensor as,

$$\int_V \mathbf{P} : \delta\dot{\mathbf{F}}dV = \int_V f_0 \cdot \delta v dV + \int_{\partial V} t_0 \cdot \delta v dA$$

Additionally, if the procedure employed to obtain the virtual work equation C.7 from the spatial differential equilibrium equation C.5 is reversed, an equivalent version of the differential equilibrium equation is obtained in terms of the first Piola-Kirchhoff stress tensor as $r_0 = Jr = \mathbf{DIV}(\mathbf{P}) + f_0 = 0$ where $\mathbf{DIVP}$ is the divergence of $\mathbf{P}$ with respect to the initial coordinate system given as,

$$\mathbf{DIV}(\mathbf{P}) = \nabla_0\mathbf{P} : \mathbf{I}; \qquad \nabla_0\mathbf{P} = \frac{\partial \mathbf{P}}{\partial \mathbf{X}}$$

It is instructive to re-examine the physical meaning of the Cauchy stresses and thence the first Piola–Kirchhoff stress tensor. An element of force dp acting on an element of area $da = nda$ in the spatial configuration can be written as $dp = tda = \sigma da$.

Broadly speaking, the Cauchy stresses give the current force per unit deformed area, which is the familiar description of stress. Consider an element of area in the initial configuration $d\mathbf{A} = dA\mathbf{N}$ which after deformation becomes $d\mathbf{a} = da\mathbf{n}$. For the purpose of obtaining a relationship between these two vectors, consider an arbitrary material vector $d\mathbf{L}$, which after deformation pushes forward to $d\mathbf{l}$. The corresponding initial and current volume elements are $dV = d\mathbf{L} \cdot d\mathbf{A}$ and $dv = d\mathbf{l} \cdot d\mathbf{a}$. Relating the current and initial volumes in terms of the Jacobian J and recalling that $d\mathbf{l} = \mathbf{F}d\mathbf{L}$ gives,

$$Jd\mathbf{L} \cdot d\mathbf{A} = (\mathbf{F}d\mathbf{L}) \cdot da$$

The fact that the above expression is valid for any vector $d\mathbf{L}$ enables the elements of area to be related as $d\mathbf{a} = J\mathbf{F}^{-T}d\mathbf{A}$. Using that information for the spatial area vector, dp can be rewritten in terms of the undeformed area corresponding to da to give an expression involving the first Piola–Kirchhoff stresses as,

$$dp = J\sigma\mathbf{F}^{T}dA = \mathbf{P}dA \tag{C.12}$$

This equation reveals that $\mathbf{P}$, like $\mathbf{F}$, is a two-point tensor that relates an area vector in the initial configuration to the corresponding force vector in the current configuration. Consequently, the first Piola–Kirchhoff stresses can be loosely interpreted as the current force per unit of undeformed area.

C.3.2 The Second Piola-Kirchhoff Stress Tensor

The first Piola-Kirchhoff tensor $\mathbf{P}$ is an unsymmetric two-point tensor and as such is not completely related to the material configuration. It is possible to contrive a totally material symmetric stress tensor, known as the second Piola-Kirchhoff stress $\mathbf{S}$, by pulling back the spatial element of force dp from equation C.12 to give a material force vector dP as,

$$dP = \phi_{*}^{-1}[dp] = \mathbf{F}^{-1}dp \tag{C.13}$$

Substituting from Equation C.12 for dp gives the transformed force in terms of the second Piola-Kirchhoff stress tensor $\mathbf{S}$ and the material element of area dA as $dP = \mathbf{S}dA$ and $\mathbf{S} = J\mathbf{F}^{-1}\sigma\mathbf{F}^{T}$. It is now necessary to derive the strain rate work conjugate to the second Piola-Kirchhoff stress in the following manner. From the rate of deformation tensor d given as $d = \phi_{*}[\dot{\mathbf{E}}] = \mathbf{F}^{-T}\dot{\mathbf{E}}\mathbf{F}^{-1}$, $\dot{\mathbf{E}} = \phi_{*}^{-1}[d]\mathbf{F}^{-T}d\mathbf{F}$ it follows that the material and spatial virtual rates of deformation are related as $\delta d = \mathbf{F}^{T}\delta\dot{\mathbf{E}}\mathbf{F}^{-1}$. Substituting this relationship into the internal virtual work equation C.8 gives,

$$\delta W_{int} = \int_{v} \sigma : \delta d dv = \int_{V} J\sigma : (\mathbf{F}^{T}\delta\dot{\mathbf{E}}\mathbf{F}^{-1})dV$$

$$\int_{V} tr(\mathbf{F}^{-1}J\sigma\mathbf{F}^{T}\delta\dot{\mathbf{E}})dV = \int_{V} \mathbf{S} : \delta\dot{\mathbf{E}})dV$$

which shows that $\mathbf{S}$ is work conjugate to $\dot{\mathbf{E}}$ and enables the material virtual work equation to be alternatively written in terms of the second Piola-Kirchhoff tensor as,

$$\int_{V} \mathbf{S} : \delta\dot{\mathbf{E}}dV = \int_{V} f_0 \cdot \delta v dV + \int_{\partial V} t_0 \cdot \delta v dA$$

For completeness the inverse of equations C.11 and C.13 are given as $\sigma = J^{-1}\mathbf{P}\mathbf{F}^T$ and $\sigma = J^{-1}\mathbf{F}\mathbf{S}\mathbf{F}^T$.

Applying the pull back and push forward concepts to the Kirchhoff and second Piola–Kirchhoff tensors yields,

$$\mathbf{S} = \mathbf{F}^{-1}\tau\mathbf{F}^{-T} = \phi_*^{-1}[\tau]; \qquad \tau = \mathbf{F}\mathbf{S}\mathbf{F}^T = \phi_*[\phi]$$

from which the second Piola–Kirchhoff and the Cauchy stresses are related as,

$$\mathbf{S} = J\phi_*^{-1}[\sigma]; \qquad \sigma = J^{-1}\phi_*[\tau]$$

In the above equation $\mathbf{S}$ and σ are related by the so-called Piola transformation which involves a push forward or pull back operation combined with the volume scaling J.

A useful interpretation of the second Piola–Kirchhoff stress can be obtained by observing that in the case of rigid body motion the polar decomposition given as the tensor F is expressed as the product of a rotation tensor $\mathbf{R}$ times a stretch tensor $\mathbf{U}$ to define the polar decomposition as $\mathbf{F} = \mathbf{R}\mathbf{U}$ indicates that $\mathbf{F} = \mathbf{R}$ and $J = 1$. Consequently, the second Piola–Kirchhoff stress tensor becomes $\mathbf{S} = \mathbf{R}^T\sigma\mathbf{R}$. This equation shows that the second Piola–Kirchhoff stress components coincide with the components of the Cauchy stress tensor expressed in the local set of orthogonal axes that results from rotating the global Cartesian directions according to $\mathbf{R}$.

Appendix D

Publications

- G. Fortuny and A. Susín. A mechanical model for the lower abdominal wall. Proceedings of the 2007 Summer Workshop of the European Society of Biomechanics, pp. 199-200. Dublin 2007 *Poster presented in the second ESBiomech Summer Workshop, it was hosted by the Trinity Centre for Bioengineering in Dublin on 26-28 August 2007. The theme for this Workshop was 'Finite Element Modelling in Biomechanics and Mechanobiology'.*
- G. Fortuny, A. Susín and M. Lopez-Cano. Effects young modulus of muscular tissue in the simulation with FEM of the inguinal area. Proceeding of the 8th International Symposium on Computer Methods in Biomechanics and Biomedical Engineering, CMBBE 2008, Porto, 2008. *To appear in Computer Methods in Biomechanics and Biomedical Engineering.*
- G. Fortuny, A. Susín, M. López-Cano and J. Marcé. Simulation with FEM to describe the dynamic of the inguinal area: The shutter mechanism. Journal of Biomechanics, Volume 41, Supplement 1, July 2008, pp. S375. *Poster presented in the 16th Congress of the European Society of Biomechanics, Lucerne ,Switzerland , 2008. Journal of Biomechanics, Volume 41, Supplement 1, July 2008, pp. S375.*
- G. Fortuny, J. Rodríguez-Navarro, A. Susín, M. Armengol-Carrasco and M. López-Cano. A Simulation Finite Element Model for the Mechanics of the Internal Oblique Muscle: A Defense Mechanism against Inguinal Hernia Formation?. Submitted to Computers in Biology and Medicine. *Submitted since 17-04-2008.*
- G. Fortuny, J. Rodríguez-Navarro, A. Susín and M. López-Cano. Dynamical Model for the Defence Mechanisms in the Inguinal Area. Submitted to Computer Methods and Programs in Biomedicine. *Submitted since 3-07-2008.*
- G. Fortuny, J. Rodríguez-Navarro, A. Susín and M. López-Cano. Simulation and Study of the Behaviour of the Tranversalis Fascia in Protecting against the Genesis of Inguinal Hernias. Submitted to Journal of Biomechanics. *Submitted since 13-07-2008.*

Bibliography

[1] R.Z. Abdalla, W.E. Mittelstaedt. The importance of the Hessert's triangle in the etiology of inguinal hernia. *Hernia 2001; 5, pp 119-123.*

[2] J. Abrahamson. Mechanisms of hernia formation. In: Bendavid R, Abrahamson J, Arregui ME, Flament JB, Phillips EH (eds). Abdominal wall hernias: principles and management. *Springer-Verlag, New York, 2001; pp 133-137.*

[3] M.A. Ajabnoor, A.M. Mokhtar, A.A. Rafee, A.M. Taha. Defective collagen matabolism in Saudi patients with hernia. *Annals of Clinical Biochemistry 1992; 29, pp 430-436.*

[4] M.L. Ajmani, K. Ajmani. The anatomical basis for the inguinal hernia. *Anat. Anz. 1983; 153, pp 245-248.*

[5] V. Alastrué, M.A. Martínez, M. Doblaré. Modelling adaptative volumetric finite growth in patient-specific residually stressed arteries. *Journal of Biomechanics 2008; 41, pp 1773-1781.*

[6] A. Alonso, A. Ramirez, B. Calvo, M. Doblaré. Towards a 3D finite element model of skeletal muscle concentric and eccentric contraction. *Journal of Biomechanics 2008; 41 (s1), pp S367*

[7] C. Avisse, J. Delattre and J. Flament. The inguinal rings. *Surgical Clinics of North America 2000; 80 (1), pp 49-69.*

[8] R. Burns, M. Donald Cave. Rapid Review Histology and Cell Biology. *Elseiver, 2007.*

[9] Burkitt, H.G. Young, B. Health, J.W. Wheater. Histología funcional. Texto y atlas en color. *Harcourt S.A. 3a ed., Madrid, 2000.*

[10] J. Bestel. Modelè diffèntiel de la contraction muscularie contrôlée. Aplication au système cardio-vasculaire. *PhD thesis, Univesité Paris IX Dauphine, 2000.*

[11] D. Chapelle, F. Clément, F. Génot, P.Tallec, M. Sorine and J.M. Urquiza. A physiologically-based model for the active cardiac muscle contraction. *T.Katila et al.:FIMH 2001, LNCS 2230, Springer-Verlang Heidelberg, 2001; pp 128-133.*

[12] G. Chauvet. Traité de Phusiologie théorique: De la cellule à l'homme. *Masson Edition, 1987.*

[13] F.A. Charney. Consequences of using Raylegh damping in inelastic response history analysis. *Technical report, Department of Civil and Environmental Engineering. Virginia Tech, 2005.*

[14] D.T.Chen, D. Zelter. Pump it up: Computer animation of Biomechanically based model of muscle using the finite element method. *Computer graphics, SIGGRAPH'92 1992; 26.*

[15] C.J.Choung, Y.C. Fung. Residual stress in arteries, in: Frontiers in Biomechanics. *Springer-Verlang, New York, 1986.*

[16] R.E. Condon. The Biology and Anatomy if Inguinofemural Hernia. *Seminars in Laparoscopic Surgery 1994; 1 (2).*

[17] S.C. Cowin, S.B. Doty. Tissue Mechanics.*Ed. Springer Science. New York, 2007.*

[18] A.D. McCulloch. The Biomedical Engineering Handbook.*CRC Press, New York 1995.*

[19] G. Drobinsky, J.M.Eugène. Exploration hémodynamique cardiovaculaire. *Masson Edition, 1982.*

[20] B. J. Ellis, R. E. Debski, S. M. Moore, P. J. McMahon, J. A. Weiss. Methodology and sensitivity studies for finite element modeling of the inferior glenohumeral ligament complex *Journal of Biomechanics 2007; 40, pp 603-612.*

[21] Don W. Fawcett. Tratado de histologia. *McGraw Hill Interamericana. 12 ed. Madrid 1995.*

[22] J.D. Folley, A. van Dam, S.K. Feiner, J.F. Hughes. Computer graphics, principles and practice. *Ed. Addison-Wesley publishing company, New York, 1996.*

[23] M.G. Franz. The biology of hernias and the abdominal wall. *Hernia 2006; 10 pp 462-471.*

[24] H. Fruchaud. The effect of the upright position proper to man upon the anatomy of the inguinal region: surgical consequences; anatomic bases of surgical treatment of inguinal hernia. *Mem. Acad. Chir. 1953; 63 pp 652-661.*

[25] Y.C. Fung. Biomechanics: Mecanical properties of living tissues. *Springer-Verlag, New York 1993.*

[26] Y.C. Fung. Elasticity of soft tissues in simple elongation. *Am. J. Physiol. 1967; 213 pp 1532-1544.*

[27] L.P. Gartner et al. Cell Biology and Histology. *Lippincott Williams and Wilkins, 5th Ed. 2005.*

[28] A.E. Green, J.E. Adkins. Large Elastic Deformations. *Ed. Oxford University Press, 2nd Edition, 1970.*

[29] F.I. Harris, A.S. White. The lenght of the inguinal ligament in the differentiation between direct and indirect hernia. *JAMA 1937; 109 pp 1900-1903.*

[30] B. Herrera. Splines, curvas y superficies. *Artyplan, 2007.*

[31] P.W. Hodges, S.C. Gandevia. Changes in intra-abdominal pressure during postural and respiratory activation of the human diaphragm. *J. Appl. Physiol. 2000; 89 pp 967-976.*

[32] G.A. Holzapfel. Nonlinear Solid Mechanics, a continuum approch for engineering.*John Wiley and Sons, LTD, 2007.*

[33] G.A. Holzapfel. Mechanics of biological tissue. IUTAM Symposium on Mechanics of Biological Tissue : Graz, Austria 2004.*Springer Berlin, 2006.*

[34] G.A. Holzapfel, T.C Gasser. A viscoelastic model for fiber-reinforced composites at finite strains: Continuum basis, computational aspects and aplications.*Comput. Mathods Appl. Mach. Engrg. 2000; 190 pp 4379-4403.*

[35] A. Horowitz, I. Sheinman, Y. Lanir. Nonlinear incompressible finite element for simulating cardiac tissue - Part II: Three-dimensional formulation for thick ventricular wall segments. *ASME J. Biomechanics Engrg. 1988; 110.*

[36] J.D. Humphrey, R. Strumpf and F.C.P. Yin. Determination of a constitutive relation for passive myocardium: A new functional form. *Journal of Biomechanics Engineering 1990; 112, pp 333-339.*

[37] J.D. Humphrey. Cardiovascular Solid Mechanics: cells tissues and organs.*Springer-Verlag, 2002.*

[38] A.F. Huxley. Muscle structure and theory of contraction. *Progress in biophysics and biological chemistry. Pergamon Press, 1957.*

[39] A.F. Huxley. Muscular Contraction. *J. Physiology 1974; 243 (1), pp 1-43.*

[40] A. Keith. On the origin and nature of hernia. *Br J Surg 1923; 11, pp 455-475.*

[41] A. Keith. The sacular theory of hernia. *Lancet 1938; 2, pp 1906.*

[42] D. Kernell. Motoneurone and its muscle fibres. *Oxford University Press, 2006.*

[43] M. Ledinsky, A. Matejcic, De Syo D, Doko M. Some structural characteristics of the inguinal region in the Northern Croatia. *Coll. Antropol. 1998; 22, pp 515-524.*

[44] M. Lopez-Cano, J. Rodriguez-Navarro, A. Rodriguez-Baeza, M. Armengol-Carrascoa, A. Susin. A real-time dynamic 3D model of the human inguinal region for surgical education. *Computers in Biology and Medicine, 2007; 39-9, pp 1321-1326.*

[45] W.J. Lytle. The internal inguinal ring. *Br J Surg 1945; 128, pp 441-446.*

[46] J. Marcé. Aplica cio mitjan cant el Mètode dels Elements Finits del model de la banda miocàrdica en la mecànica cardiàca de lárquitectura ventricular. *Prj. thesis, 2005.*

[47] A. Maciel, R. Boulic, D. Thalmann. Deformable tissue parameterized by propietes of real biological tissue. *In. 5th IFAC 2003 Symposium on Modelling and Control in Biomedical Systems (including Biological Systems), Melbourne. Elsevier Ltd., Oxford, 2003; pp 235-240.*

[48] R.B. Martin, D.B. Burr, N.A. Sharkey. Skeletal Tissue Mechanics.*Ed. Springer Verlag. New York, 1998.*

[49] W. Maurel. 3D Modeling of the human upper limb including the biomechanics of joints, muscles and soft tissues.*PhD thesis, Ecole Polytechnique Federale de Laussane, 1999.*

[50] J. Menck, W. Lierse. The fascia of the inguinal canal ring. *Chirurgy 1991; 62 (2), pp 117-120.*

[51] I. Mirsky and W.W. Parmley. Assessment of passive elastic stiffness for isolated heart muscle and the intact heart. *Circulation Research, XXXIII, 1973.*

[52] R. Monroe Vignes. Modeling muscle fatigue in digital humans. *PhD thesis, University of Iowa, 2004.*

[53] M. Mooley. A theory of large elastic deformation. *J. Appl. Phys. 1940; 11, pp 582-592.*

[54] E. Munhequete. Estudio de las estructuras anatómicas relacionadas con la formación de hernias inguinales. *PhD thesis, Universitat Autonoma de Barcelona, 2003.*

[55] L.M. Nyhus, M.S. Klein, F.B Rogers. Inguinal hernia. *Current Problems in Surgery 1991; 6, pp 406-418.*

[56] J.L. Emmery, J.H. Omens and A.D. McCulloch. Biaxial mechanics of the passively overstreched left ventricle. *Am. J. Physol. 1997; 272, pp H2299-H2305.*

[57] C. Ogilvie. Prognosis of inguinal hernia. *Lancet 1936; 2.*

[58] E. Oñate. Cálculo de estructuras por el método de elementos finitos. Análisis estático lineal. *Centro Internacional de Métodos Numéricos en Ingenieria, Barcelona 1995.*

[59] A. Pans, G.E. Pierard, A. ALbert. Adult groin hernias: New insight into their biochemical characteristics. *European Journal of Clinical Investigation 1997; 27, pp 863.*

[60] E. Peña, B. Calvo, M.A. Martinez, M. Doblaré. Computer simulation of damage on distal femoral articular cartilage after meniscectomies. *Computers in Biology and Medicine 2007; 38, pp 69-81.*

[61] A. Pérez, B. Calvo, M. Doblaré. An accurate finite element model of the cervical spine under quasistatic loading. *Journal of Biomechanics 2008; 41, pp 523-531.*

[62] M. V. Razumova, A. E. Bukatina, and K. B. Campbell. Stiffness-distortion sarcomere model for muscle simulation.*PhD thesis, University of Toronto, 1998.*

[63] R.C. Read. Why do human beings develop groin hernias? *Ed. Fitzgibbons RJ Jr., Greenburg AG (eds) Nyhus and Condon's hernia, 5th edn. Lippincott, Philadelphia, pp 1-8.*

[64] Recurrent Hernia. Several authors. *Ed. Springer Berlin Heidelberg 2007.*

[65] D.F. Rogers, J.A. Adams. Mathematical elements for Computer grafics. *Ed. McGraw-Hill, New York 1990.*

[66] N.C. Sanchez, P.L. Tenofsky, J.M. Dort, L.Y. Shen, S.D. Helmer, R.S. Smith. What is normal Intra-Abdominal Presure? *The American Surgeron, (Health Module) 2001; 67-3.*

[67] R. Schwab, U. Klinge, O.Schumacher, M.Binnebosel, K. Junge. Biomechanical Data -"Hernia Mechanics": Hernia Size, Overlap and Mesh Fixation. *Ed. Springer Berlin, Heidelberg, 2007.*

[68] M. Sermesant. Modelè électromécanique du coeur pour lánalyse dímage et la simulation. *PhD thesis, Institut National de Recherche en Informatique et Automatique, 2003.*

[69] M. Sermesant, P. Moireau, O. Camara, J. Sainte-Marie, R. Andriantsimiavona, R. Cimrman, D.L.G. Hill, D. Chapelle, R. Razavi. Cardiac function estimation from MRI using a heart model and data assimilation: Advances and difficulties . *Med. Image Analysis 2006; 10, pp. 642-656.*

[70] J.C. Simo, T.J.R. Hughes. Computational Inelasticity. *New York 1998.*

[71] J.E. Skandalakis, S.W. Gray, L.J. Skandalakis, G.L. Colborn, L.B. Pemberton. Surgical anatomy of the inguinal area. *World J. Surg. 1989; 13, pp 490-498.*

[72] G.F. Smith, R.S. Rivlin. Integrity bases for vectors. the crystal classes*Arch. Rat. Mech. Anal. 1994; 15, pp 169-221.*

[73] A.J.M. Spencer. Continuum Theory of the Mechanics of Fibre-Reinforced Composites*Springer-Verlag, New York, 1984.*

[74] J. Stalhand, A.Klarbring, G.A.Holzapel. Smooth muscle contraction: Mechanochemical formulation for homogeneous finite strains. *Progress in Biophysics and Molecular Biology 2008; 96, pp 465-481*

[75] M. Stutek, M. van Griensven, J.Zeichen, N. Brauer, U. Bosch. Cyclic mechanical stretching modulates secretion pattern of growth factors in human tendon fibroblasts. *Eur. J. Appl. Physiol. 2001; 86(1), pp 48-52.*

[76] J.D. Talbot. Accurate characterization of skin deformationss using range data. *PhD thesis, University of Toronto, 1998.*

[77] J. Teran, E. Sifakis, S. Blemker, Victor Ng-Thow-Hing, Cynthia Lau, Ronald Fedkiw. Creating and Simulating Skeletal Muscle from the Visible Human Data Set. *IEEE Transactions on visualization and computer graphics, 2005; 11 3.*

[78] J. Teran, S. Blemker, V. Ng Thow Hing, R. Fedkiw. Finite Volume Methods for the Simulation of Skeletal Muscle. *Eurographics/SIGGRAPH Symposium on Computer Animation, 2003.*

[79] B.J.J.J. van der Linde. Mechanical modeling of skeletal muscle functioning. *PhD thesis, Universieit Twente, 1998.*

[80] J.A. Weiss, B.J. Maakestad. Permeability of human medial collateral ligament in compression transverse to the collagen fiber direction. *Journal of Biomechanics, 2004.*

[81] J.A. Weiss, B.N. Maker, S. Govindjee. Finite element implementation of incompressible, transversely isotropic hyperelasticity. *Comput. Methods Appl. Mech. Engrg. 1996; 135, pp 107-128.*

[82] T. Wolloscheck, A. Gaumann, A. Terzic, A. Heintz, Th. Junginger, M.A. Konerding. Ingunal hernia: Measurament of the biomechanics of the lower abdominal wall and the inguinal canal. *Hernia 2004; 8, 233-241.*

[83] G.I. Zahalak and S.P. Ma. Muscle actication and contraction -constitutive relations based directly on cross-bridge kinetics. *Journal of biomechanical Engineering 1990; 112(1), pp 52-62.*

[84] G.I. Zahalak and S.P. Ma. A Distribution-Moment Model of Energetics in Skeletal Muscle. *Journal of Biomechanics 1991; 24 1, pp 21-35.*

[85] F.E. Zajac. Muscle and Tendon: Properties, Models, Scaling, and Application to Biomechanics and Motor Control. *Crit. Revs. Biomed. Eng. 1989; 17-14, pp 359-411.*

[86] O.C. Zienkiewicz, R.L. Taylor. El método de los elementos finitos. Mecánica de Sólidos. Vol. II .*Ed. CIMNE. Barcelona, 2004*

[87] O.C. Zienkiewicz, R.L. Taylor. El método de los elementos finitos. Las bases. Vol. I .*Ed. CIMNE. Barcelona, 2004*

[88] L.M. Zimmermann, B.J. Anson. Anatomy and surgery of hernia. *2nd edition. Williams and Wilkins, Baltimore, 1967; pp 136-140*